GIS4PV

A technological impact assessment of the application of GIS for Photovoltaic Solar Energy

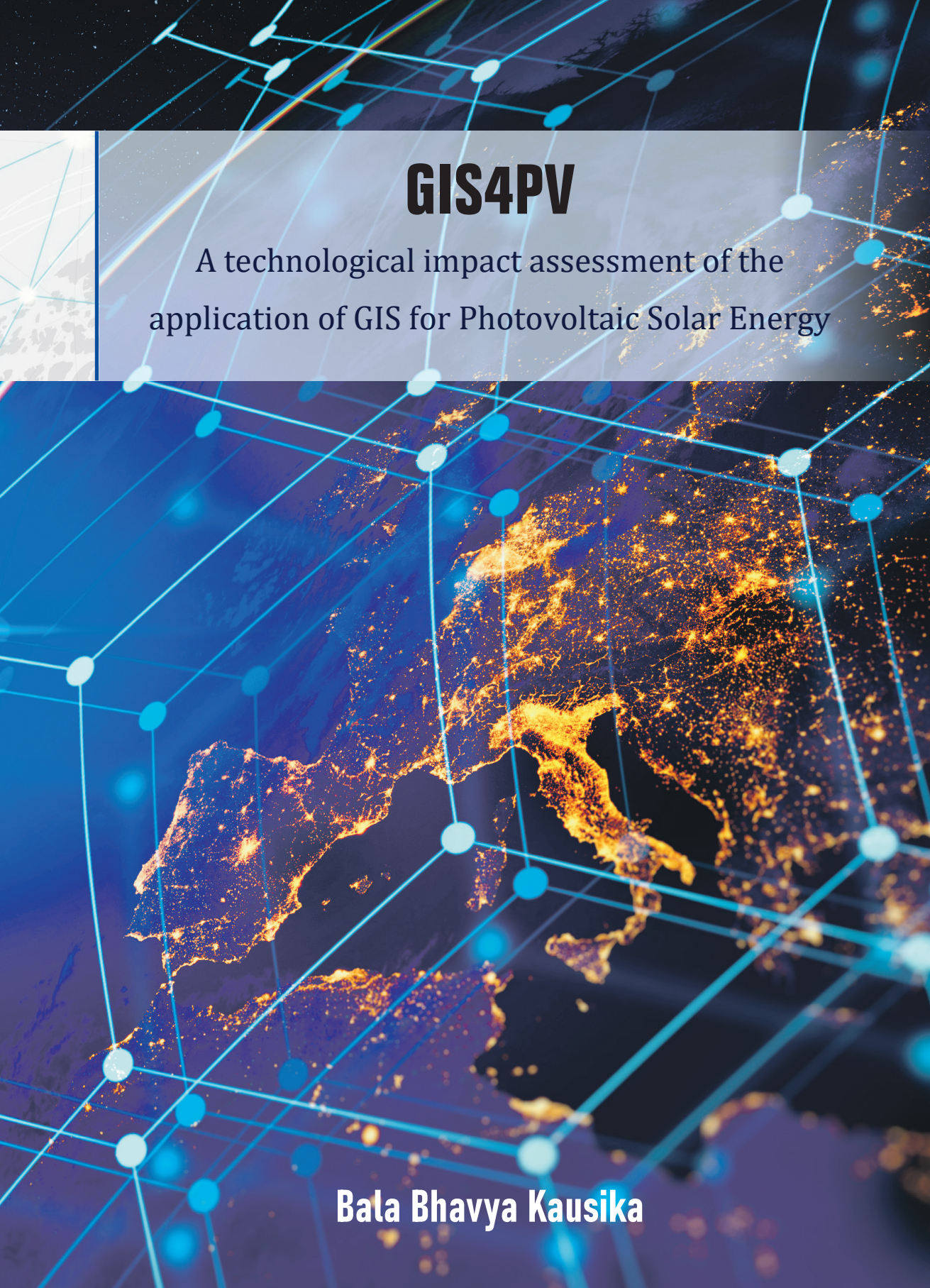

Bala Bhavya Kausika

GIS4PV

A technological impact assessment of the application of GIS for Photovoltaic Solar Energy.

Bala Bhavya Kausika

GIS4PV

A technological impact assessment of the application of GIS for Photovoltaic Solar Energy.

Bala Bhavya Kausika
Copernicus Institute of Sustainable Development, Utrecht University

ISBN : 978-94-6458-290-1
Print: Ridderprint B.V. |www.ridderprint.nl
Cover photo: Rawpixel and User12683362, Freepik.com
Cover design: José Stroo

GIS4PV

A technological impact assessment of the application of GIS for Photovoltaic Solar Energy.

GIS4PV – Een technologische impact evaluatie van de toepassing van GIS voor fotovoltaïsche zonne-energie

(met een samenvatting in het Nederlands)

Proefschrift

ter verkrijging van de graad van doctor aan de
Universiteit Utrecht
op gezag van de
rector magnificus, prof.dr. H.R.B.M. Kummeling,
ingevolge het besluit van het college voor promoties
in het openbaar te verdedigen op
vrijdag 3 juni 2022 des middags te 4.15 uur

door

Bala Bhavya Kausika

geboren op 30 april 1989 te Visakhapatnam, India

Promotor:

Prof. dr. W.G.J.H.M. van Sark

Part of this work was carried out within the framework of the ASM-1 (Advanced Solar Monitoring - phase 1) and ASM-2 projects (Advanced Scenario Management - phase 2), made possible by TKI-Solar and TKI-Urban Energy as part of the Topsector Energy."

Summary

Photovoltaic solar energy is one of the fastest growing renewable energy resources which is being adopted by households and large organizations alike. Encouraging citizens to switch to this renewable energy source requires an understanding of the factors that influence this phenomenon. Technology hereby plays an important role to comprehend the complex process and present it in a way that is straightforward for both policymakers and citizens to recognize and realize. Moreover, integration of this energy source into the existing power grid, implies the need for strategies aimed at identifying new routes that minimize visual and environmental impact, cost and social concerns related to new infrastructures. Addressing all these aspects requires an interdisciplinary approach. In this context, the impact of using Geographic Information Systems (GIS) for evaluating the present status, solar potential, policy implications and future tools is investigated in this thesis.

Chapter 2 presents a method to evaluate the present status of small and medium scale rooftop solar photovoltaic (PV) installations in the Netherlands. Artificial Intelligence (AI) specifically, Deep Learning (DL) algorithms and geo-spatial techniques are applied on very high-resolution aerial imagery to detect PV installations. The information that is currently missing from the national PV register could be supported with data gathered from this method to complete the database. It is shown that the use of Deep Learning algorithms alone is not sufficient to produce reliable results but in combination with geo-spatial analysis, the results are more consistent. The method therefore is termed GeoAI. The effect of variations in aerial images used in the process along with the quality of ancillary data is discussed. The precision and recall rates of the DL model were evaluated at an average of 0.93 and 0.92 respectively. Use of post-processing techniques was found to be integral to detect and allocate panels to the corresponding roofs and was instrumental in improving the results by at least 50%. Overall, GeoAI methods produce fast and consistent results which can give an overview of the present status of rooftop PV installations which can then be quickly scaled-up to create nation-wide datasets.

In addition to the currently installed capacity, another important factor is the solar potential. It useful to access the maximum possible deployable rooftop solar capacity which means that it can help immensely in urban planning for building energy neutral buildings, or even energy generating buildings in the future. A GIS based method to estimate solar potential is presented in Chapter 3. This method is quite useful for estimating solar potential on existing buildings or future building plans and it can be used to also calculate the potential on building façades. In this method rooftops are classified based on amount of irradiation received and potential capacities have been calculated accordingly using different production capacities. Rooftop solar potential for the city of Apeldoorn was estimated at 319 MWp, with a potential energy yield of 283.9 GWh for the year 2015. In combination with the results from Chapter 2, the left-over or unused potential on buildings can be estimated.

The potential estimation is based on the ArcGIS based solar radiation model, which uses various assumptions which thus needs to be validated. Atmospheric parameters that can be controlled within this model are diffusivity and transmissivity. These values need to be calibrated and validated to produce results closer to reality. Chapter 4 shows how this has been conducted for the Netherlands using the ArcGIS solar radiation tool. GIS based solar radiation models offer flexibility in terms of level of detail in the analysis which is dependent on the resolution of the input data. The results show that the default values of diffusivity and transmissivity used by the model lead to substantial underestimation or overestimation of solar insolation. Monthly calibration leads to higher accuracies and is useful for high-resolution (spatial and temporal) energy profile generation. The effect of spatial resolution on the results of radiation modelling within the tool was explored and related to processing time and quality of the output. The estimated irradiation values could be improved up to 20% depending on the time scales used in the model

In Chapter 5 the most fundamental component of GIS, i.e., “visualization” has been explored. PV system data gathered through crowd sourcing over multiple years has been processed, mapped, and analysed using various visualization techniques to evaluate their performance and monitor them. Effects of data stretching during visualization has been addressed and discussed. Data stretching during visualisation

could lead to different interpretation of the results. Specific yields and performance ratios of the systems from five countries have been mapped creating a seamless transition of data visualization. Variations in yield and performance ratios over the years were observed with higher values in 2015 compared to 2014 and 2016 due to higher irradiation values.

The theoretical estimation on solar potential is obviously good to have. However, the usefulness and reliability of such data in aiding and regulating policies takes precedence. On the other hand, understanding the effectiveness of current policies in driving the diffusion of this technology further, is another question that is helpful in visualizing the driving factors behind adoption and for adjusting the future policies accordingly. GIS when incorporated to evaluate the effectiveness of policies can determine the realistic potential of the technology. One such policy, i.e., the Postal Code Rose policy, which was in effect till April 2021 was evaluated using economic and geographic parameters in Chapter 6. Multicriteria decision analysis was implemented in a GIS environment for the city of Apeldoorn with information regarding the technical potential and social factors such as income, value of the house, electricity demand and neighbours with solar installation. It was observed that by fully applying the Postal Code Rose policy ~77% of the total electricity demand of Apeldoorn could be covered by solar PV under the assumptions specified in the chapter. The chapter demonstrates the potential of GIS for use in such complex analysis. With the availability of more data on other factors contributing to the diffusion, the model can be adapted to incorporate new data and knowledge in order to re-assess the effect of policy potential.

Chapter 7 shows the capability of GIS in modelling and mapping of scenario studies in the context of self-consumption and greenhouse gas (GHG) reduction potential. Scenarios relating to PV rooftop utilization, battery storage systems, energy demand and electric vehicle demand were evaluated for 88 neighbourhoods in the city of Utrecht, The Netherlands. The results have been mapped to visualize the PV integration capabilities within the neighbourhoods. Large variations were observed with self-consumption ranging between 34% and 100%, which in turn is highly dependent on available rooftop for PV siting. This could be further increased with electric vehicles (12%) and batteries (25%) Furthermore, avoided life cycle GHG

emissions were on an average about 17 tCO_2-eq per household. The visualization of potential areas for PV integration clearly shows the power of spatial models. The results therefore can be used for targeting area specific investments and policies.

To summarize, the different spatial-data science techniques that are inherent to GIS have been applied in photovoltaic solar energy. In particular, GIS-based studies for practical implementation in support of the energy transition have been explored. In addition, the bottlenecks with regards to this multi-disciplinary approach, the gap between technology and policy is addressed in this thesis. To conclude, the prospective of using spatial science is imperative to be able to answer questions related to the energy transition leading to a sustainable future.

Samenvatting

Fotovoltaïsche energie (PV) is één van de snelst groeiende bronnen van duurzame energie die steeds meer wordt toegepast, zowel binnen huishoudens als grote organisaties. Om burgers aan te kunnen moedigen om over te gaan op deze bron van duurzame energie, is begrip van de factoren die dit fenomeen beïnvloeden noodzakelijk. Technologie speelt hierbij een grote rol om het complexe proces te kunnen begrijpen en dit te kunnen presenteren aan beleidsmakers en burgers op een manier die voor hun herkenbaar en behapbaar is. Bovendien vereist de inpassing van deze energiebron binnen het bestaande elektriciteitsnet het gebruik van strategieën die gericht zijn op het identificeren van nieuwe routes die de impact beperken op het milieu, visuele beleving, kosten en maatschappelijke zorgen wat betreft deze nieuwe infrastructuur. Om rekening te kunnen houden met al deze aspecten is een interdisciplinaire benadering nodig. Daarom is in dit proefschrift onderzocht wat de impact is van het gebruik van Geografische Informatie Systemen (GIS) voor de evaluatie van de huidige installaties, zonnepotentie, beleidsimplicaties en toekomstige hulpmiddelen.

In Hoofdstuk 2 wordt een methode gepresenteerd om de huidige status van kleine tot middelgrote fotovoltaïsche (zon-PV) installaties op daken in Nederland te evalueren. Kunstmatige Intelligentie (AI) – in het bijzonder Deep Learning (DL) algoritmes – en GIS analyse zijn toegepast op zeer hoge resolutie luchtfoto's om zon-PV installaties te detecteren. Informatie die momenteel nog mist binnen het nationale zon-PV register zou op deze manier kunnen worden aangevuld. Het gebruik van alleen Deep Learning algoritmes is nog niet voldoende om tot betrouwbare resultaten te komen, maar in combinatie met GIS analyse zijn de resultaten consistenter. De methode wordt daarom GeoAI genoemd. Zowel het effect van variaties binnen de gebruikte luchtfoto's, als de kwaliteit van aanvullend materiaal worden besproken. De precision en recall-rates van het DL model werden beoordeeld op een gemiddelde van respectievelijk 0,93 en 0,92. Het gebruik van GIS analyse bleek een integraal onderdeel te zijn van het detecteren en toewijzen van

panelen aan de juiste daken en droeg bij aan het verbeteren van de resultaten met ten minste 50%.In het algemeen levert GeoAI snelle en consistente resultaten die een overzicht kunnen geven van de huidige status van zon-PV installaties op daken. De methode kan ook snel worden opgeschaald voor het maken van een nationale dataset.

Naast de huidige capaciteit van gerealiseerde installaties is zonnepotentie een andere belangrijke factor. Het is belangrijk om te weten wat de maximum mogelijke capaciteit van zon-PV op daken is. Dit is essentieel bij planologische vraagstukken over de bouw van energieneutrale woningen of toekomstige gebouwen die energie kunnen opwekken. Een GIS methode om zonnepotentie in te kunnen schatten wordt beschreven in Hoofdstuk 3. Met deze methode kan de zonnepotentie goed ingeschat worden van bestaande woningen of toekomstige bouwplannen. Het kan ook gebruikt worden om de zonnepotentie te berekenen van façades van gebouwen. Bij deze methode worden rooftops geclassificeerd op basis van de ontvangen zoninstraling en zijn potentiële capaciteiten dienovereenkomstig berekend met behulp van verschillende productiecapaciteiten. Voor de jaar 2015, was het zonnepotentie op het dak voor de stad Apeldoorn op 319 MWp geschat, met een potentiële energieopbrengst van 283,9 GWh. Samen met de resultaten van Hoofdstuk 2 kan zo een schatting worden gemaakt van de ongebruikte zonnepotentie van gebouwen.

De zonnepotentie berekening is gebaseerd op het zoninstralingsmodel dat ingebouwd is in ArcGIS. Deze maakt gebruik van enkele aannames. De atmosferische parameters diffusie en transmissie in de atmosfeer moeten hiervoor gekalibreerd en gevalideerd worden om realistische resultaten te krijgen. Hoofdstuk 4 laat zien hoe deze controle is uitgevoerd voor Nederland met behulp van ArcGIS. Zoninstralingsmodellen in GIS applicaties zijn flexibel afhankelijk van de ruimtelijke resolutie van de input. De resultaten laten zien dat de standaardwaarden van diffusie en transmissie die door het model worden gebruikt, leiden tot een aanzienlijke onder- of overschatting van de zoninstraling. Maandelijkse kalibratie leidt tot hogere nauwkeurigheid en is nuttig voor het genereren van energieprofielen met een hoge resolutie (ruimtelijk en tijdelijk). Er is onderzocht wat het effect van de gebruikte ruimtelijke resolutie op het stralingsmodel van de tool is, gerelateerd aan de rekentijd en de kwaliteit van de output. De geschatte bestralingswaarden kunnen

worden verbeterd tot 20%, afhankelijk van de tijdschalen die in het model worden gebruikt.

In Hoofdstuk 5 wordt het belangrijkste aspect van GIS verkend: “visualisatie”. Data van zon-PV systemen, verzameld door crowdsourcing over enkele jaren, was verwerkt, gekarteerd en geanalyseerd met verschillende visualisatie technieken. Het effect van het oprekken van waarden voor visualisatie wordt besproken, evenals hoe dit kan leiden tot verschillende interpretaties van dezelfde resultaten. Specifieke opbrengst en performance ratio’s van de systemen van vijf landen zijn in kaart gebracht als demonstratie van data visualisatie. Variaties in opbrengst en performance ratio’s door de jaren heen werden waargenomen met hogere waarden in 2015 in vergelijking met 2014 en 2016 als gevolg van hogere instralingswaarden.

Het beschikbaar hebben van een theoretische inschatting van zonnepotentie is handig. De data moet bovenal bruikbaar en betrouwbaar zijn om beleid te kunnen reguleren en ondersteunen. Aan de andere kant is het nuttig om het effect van huidig beleid te begrijpen bij de verdere ondersteuning van zon-PV technologie. Op deze manier kunnen de achterliggende mechanismes van diffusie van zon-PV worden geïdentificeerd, waarop toekomstig beleid ook op kan worden aangepast. Wanneer GIS wordt ingezet om het effect van reguleringen te evalueren, kan de realistische potentie van de bijbehorende technologie ook bepaald worden. Eén van deze reguleringen was de Postcoderoosregeling, die van kracht was tot april 2021. In Hoofdstuk 6 wordt deze regeling geëvalueerd met behulp van economische en geografische parameters. Hiervoor is met behulp van GIS een multicriteria-analyse geïmplementeerd voor de stad Apeldoorn. Hierbij is informatie over de technische potentie en sociale factoren gebruikt zoals inkomen, WOZ-waarde, energiebehoefte en buren met zon-PV installaties. Uit de analyse bleek dat als de Postcoderoosregeling overal zou zijn toegepast, ongeveer 77% van de totale elektriciteitsvraag opgewekt zou kunnen worden met zon-PV installaties. Het hoofdstuk laat de potentie van GIS zien in een complexe beleidsanalyse. Wanneer er meer data beschikbaar komt, of andere factoren rond zon-PV diffusie bekend zijn, kan het model worden aangepast om deze nieuwe data en kennis te gebruiken voor revaluatie.

Hoofdstuk 7 presenteert de potentie van GIS bij het modelleren en in kaart brengen van scenariostudies in de context van eigen verbruik van PV systemen en het reductiepotentieel van broeikasgasemissies (GHG). Scenario's met betrekking tot het gebruik van PV-daken, batterijopslagsystemen, de energievraag en de vraag naar elektrische voertuigen werden geëvalueerd voor 88 buurten in de stad Utrecht in Nederland. De resultaten zijn in kaart gebracht om de mogelijkheden van PV-integratie in de wijken te visualiseren. Er werden grote variaties waargenomen van eigen verbruik tussen 34% en 100%, welke voornamelijk afhankelijk zijn van het beschikbare dakoppervlak voor zon-PV installaties. Elektrische auto's kunnen het aandeel eigenverbruik verhogen met 12% en batterijen met 25%. De vermeden broeikasgasemissies over de levenscyclus zijn gemiddeld 17 tCO2-eq per woning. Het op deze manier visualiseren van potentiële gebieden voor PV-integratie laat de kracht zien van ruimtelijke modellen. De resultaten kunnen gebruikt worden voor gerichte gebiedsspecifiek investeringen en ondersteunend beleid.

Samenvattend zijn er verschillende GIS technieken toegepast op het gebied van fotovoltaïsche zonne-energie. In het bijzonder is GIS onderzoek gedaan om de praktische implementatie van de energie transitie te ondersteunen. In het proefschrift worden de knelpunten van een multidisciplinaire aanpak en de kloof tussen technologie en beleidsvorming blootgelegd. Tenslotte, het inzetten van GIS analyse is essentieel voor het beantwoorden van vraagstukken rond de energie transitie dat nodig is voor een duurzame toekomst.

Nomenclature

Abbreviation	Description
AHN	Actueel Hoogtebestand Nederland
AHP	Analytical Hierarchy Process
AI	Artificial Intelligence
BAG	Basisregistratie Adressen en Gebouwen
BIPV	Building Integrated Photovoltaics
BRT	Basisregistratie Topografie
BSRN	Baseline Surface Radiation Network
CNN	Convolution Neural Network
CO_2-eq	Carbon dioxide equivalent
COP	Conference of Parties
DEM	Digital Elevation Model
DL	Deep Learning
DT	Digital Twins
DTM	Digital Terrain Models
EFE	Emission factor of electricity
EV	Electric Vehicles
FCN	Fully Convolution Network
FN	False negative
FP	False positive
GBPV	Ground-based Photovoltaics
GHG	Greenhouse gas

Abbreviation	Description
GIS	Geographic Information Systems
GIS4PV	Geographic Information Systems for Photovoltaics
IEA	International Energy Agency
IoT	Internet of Things
KNMI	Royal Netherlands Meteorological Institute
LiDAR	Light Detection and Ranging
LOD	Level of detail
MCDA	Multi-criteria decision analysis
nDSM	Normalized Digital Surface Model
OGC	Open Geospatial Consortium
PC4	Postal code 4
PC6	Postal code 6
PIR	Productie-installatieregister
POA	Plane of array
PR	Performance ratio
PV	Photovoltaics
RES	Regional Energy Strategy
SCR	Self-consumption ratio
SDE	Stimulering Duurzame Energieproductie
SOC	State of charge
SSR	Self-sufficiency ratio
TN	True negative
TP	True positive
UNFCCC	United Nations Framework Convention on Climate Change
VGI	Volunteered Geographic Information

Abbreviation	Description
VIVET	Verbetering van de Informatievoorziening voor de Energietransitie

Symbol	Notation	Unit
D_{BESS}	battery storage capacity degradation	%
E_{demand}	electricity demand	Wh
GHG_{mfg}	emissions from manufacturing the total system	CO_2-eq
$GHG_{neighb.}$	life cycle GHG emiss. from a neighbourhood perspective	CO_2-eq
GHG_{system}	life cycle GHG emissions from an elec. sys. perspective	CO_2-eq
GHI_{meas}	Measured Global Horizontal Irradiation	Wh/m^2
GHI_{mod}	Modelled Global Horizontal Irradiation	Wh/m^2
MBE	Mean bias error	
$P_{direct\text{-}consumed}$	direct self-consumed PV power	W
$P_{B\ charge}$	power charged to battery	W
$P_{B\ discharge}$	power discharged from battery	W
PD	Percentage difference	%
P_{demand}	power demand	W
P_{PV}	PV produced power	W
$P_{PV\ neighb.}$	used PV power from a neighbourhood perspective	W
$P_{PV\ system}$	used PV power from an elec. sys. perspective	W
t	time step	
Y_f	final system yield	kWh/kWp
Y_r	Reference yield	kWh/kWp
Δt	time step of 5 min	min

Contents

List of Figures

List of Tables

1.

Introduction

1.1. Motivation

The world of energy is changing. A marked shift in the way we produce and consume energy is becoming evident [1]. Until the 18th century renewable energy was the only form of energy resource but with the industrial revolution, the exploitation of fossil fuels began. While already noticed at the beginning of the 20th century that CO_2 emission would potentially lead to a temperature increase of the planet, it took 50 years before people began to realize that fossil fuels are not going to last forever, and are damaging the environment causing adverse effects as climate change [2].

After the Paris agreement of 2015 at the United Nations Framework Convention on Climate Change (UNFCCC) Conference of Parties (COP), many countries have started investing heavily in renewable energy technologies. European Union's (EU) initial strategy to keep global warming below 2°C was to cut greenhouse gas emissions by 20%, increase the total energy consumption from renewable energy by 20% along with 20% increase in energy efficiency, all by 2020 [3]. In spite of many efforts in this direction, data suggests that global energy related carbon-dioxide emissions rose by 1.6% in 2017 which is not on par with the climate goals [4]. With increasing urgency to meet climate challenges, recently EU committed to climate neutrality by 2050 and a more ambitious target of emissions reduction of at least 55% compared to 1990 [5]. A recent report by the International Energy Agency (IEA) explored the requirements to nudge the world on a path to net-zero emissions stating that numerous amendments must be realized simultaneously across all parts of the energy sector [6]. This calls for more efficient and rapid deployment of technologies and appropriate policies especially, to tackle issues with energy transitions [7].

1.2. Solar PV – Driving future electricity supply

Photovoltaic (PV) solar energy is one of the fastest growing renewable technologies to supply sustainable energy and decarbonize the power sector. PV systems generate electricity using solar cells which convert energy from the sun (photons) into a flow of electrons by the photovoltaic effect. The electricity thus produced can be used

directly, fed into the electricity grid, or for charging a battery for later use. PV technology is modular and thus can be deployed from the lowest scale, i.e., household level, to a very large scale, i.e., utility power plants. Improvements in the production process and efficiency have lowered the costs of solar panels enormously. Residential PV systems are the most common and these small-scale (up to 15kW) installations are all mostly connected to the grid. Building Integrated Photovoltaic (BIPV) systems are now starting to replace conventional building materials [8,9] in parts like roofs [10], facades [11] and windows with PV in spite of challenges [12].

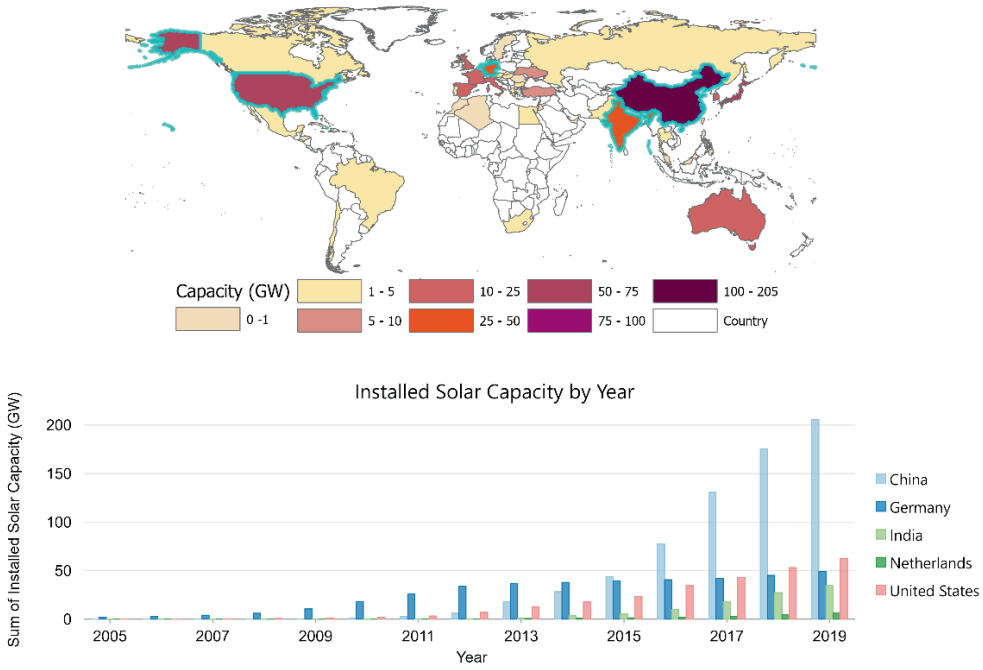

Figure 1-1– Cumulative installed solar capacity in GW for five countries from 2010-2019. Data source BP [13].

Globally, installed PV capacity reached about 758 gigawatts (GW) by the end of 2020 [14]. In the Netherlands, the capacity stands at 10 GW by the end of 2020, 2.9 GW alone accounting for 2020 in spite of the outbreak of the global pandemic [15]. The World Energy Outlook 2020 report by the IEA declares PV as the forerunner in renewable energy [6]. In countries like China, India, the Netherlands, and the United States this growth has been remarkable in the past decade (Figure 1-1) and PV installations are still on the rise. Moreover, forecasts predict that with the right policy measures, there could be a further large growth for PV. However, for PV to expand to its full potential it might be required to combine policy and technology in an efficient manner.

1.3. Geographic Information Systems – Driving future analytics

Geography is the interaction between people and the environment, and their relationship with places. In addition, physical processes that occur on Earth and which influence climate are heavily dependent on geography. But how can we understand and visualize these complex interactions? In addition, in today's world, which is so closely connected and yet has many uncharted boundaries relating to demography, environment, climate businesses, governments etc., there is huge amount of data at play. Here, spatial analysis plays an important role, revolutionizing the way we think about location, aiding decision-making and in delivering location-based services.

Over the past decades, mapping has evolved from finding one's way to one's destination to a completely new way on how we look at location. The first simple spatial analysis started from paper maps in 1854, when John Snow mapped out the locations of deaths caused due to cholera and found that they were clustered around public wells; this was the beginning of a new study known as epidemiology [16]. Now, with digital maps we are able to do incredibly much more. Instead of dealing with papers, we can store maps, visualize them and switch between layers of data in these

maps with ease. This layer handling to mapping approach is an integral part of Geographic Information Systems (GIS).

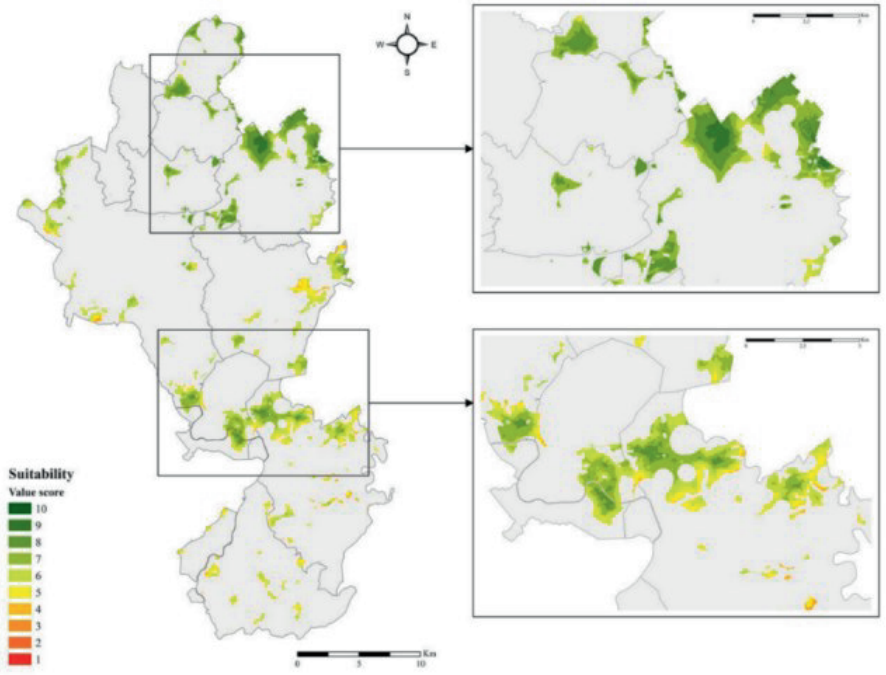

Figure 1-2: Example of site suitability analysis for installation of wind turbines, conducted by grading various criteria such as wind energy potential, distance from natural environments, distance from urban areas, distance from places of interest, distance from electricity grid, distance from road network, landscape architecture, land cover type, and slope of terrain. The map shows suitability on a scale of 1 to 10, with 1 being least suitable and 10 denoting most suitable areas for wind turbine installation. Source: E.O.N [17]

GIS is a framework or system for capturing, storing, managing, analyzing and visualizing geographic or spatial data from simple locations to complex information [18]. Data can be stored in map layers, for example roads, political boundaries, building footprints, satellite imagery, terrain, utility lines, weather station data etc.,

With spatial data, one knows “what” information is present along with “where” it is, which is essential for rational decision making.

GIS has evolved from merely a map making or a decision support tool to a sophisticated combination of spatial science and technology. For example, GIS can be used for locating suitable sites for installation of wind turbines [17] as shown in Figure 1-2 or for estimating the environmental or economic effects of policy on technology adoption.

1.4. Integrating GIS and PV

Analyses like finding the right market for solar PV, suitable locations for deployment of PV, effects of PV integration with the grid in real time, PV forecasting, economic, environmental or policy effects on PV diffusion, etc., are highly data driven. Data needed for these types of analyses is very diverse, decentralized, huge and sometimes comes with privacy issues. Proper data storage, management, analysis, and visualization techniques are needed to deal with such data and analysis. In addition, if the data can incorporate spatial components besides the temporal context, new insights can be explored. For example, Van der Kam et al. show the significance of including geographical context in studying the diffusion of PV and Electric Vehicles (EV) and its implications for the energy transition [19]. In another study, the performance of PV modules based on irradiance time series data was analyzed in combination with life cycle assessment studies to map the environmental footprint of the modules over large geographic areas and observed spatial variations in module performance and environmental impact [20]. Location-based data in combination with powerful analytics is the key to smart decision making: one can perform scenario analysis to investigate spatial consequences or restrictions of policy decisions. For example PV performance indicators in combination with spatial analysis in GIS revealed that performance losses corelate to urban compactness indicators and seasonality [21]. Trend analysis is being used in combination with spatial patterns to build predictive models to help address various issues related to data collection, climate change [22,23], PV adoption, etc. This type of information

can easily be adapted to study various scenarios for the growth of PV technology, make changes in governance and policy for faster diffusion of PV.

Generally, integrating GIS and energy system modelling can provide a picture of the total energy system also incorporating future energy landscapes [23]. But, to understand spatio-temporal dynamics of aspects like energy demand, capacity and demand patterns of energy or return on investments or even environmental impacts, it is important to fully integrate space and time into an energy system modelling process instead of simply using them as additional parameters [24]. Therefore, this thesis focuses on four aspects of employing GIS techniques for PV: 1) present PV status, 2) potential estimation, 3) Monitoring and Analysis and 4) Policy integration and scenario management. These are discussed below.

1.4.1. Present PV status

Transition to sustainable energy does not stop at a country border and hence needs to be implemented at various geographic levels; global, European, regional, national and local [25]. This calls for data and information related to energy to be available and accessible to everyone involved in energy transition to resolve the bottlenecks [26].

Information pertaining to installed capacity with locations helps in making necessary changes to the grid infrastructure for the future. So far in the Netherlands, only Statistics Netherlands (Centraal Bureau voor de Statistiek) publishes this information at a regional level with the help of various registers. However, information regarding installations at small-scale consumers is not complete due to registration of PV systems not being a norm [27].

GIS is particularly useful in these cases for detecting PV installations from rooftops with the help of satellite and/or aerial images or with the help of volunteered geographic information (VGI) to aid in supplementing information of the registers or to monitor the status of these installations automatically. With technical advancements in machine learning image recognition tasks are very fast and accurate. Until now, this has been static information. Furthermore, data from smart

meters also help in monitoring the energy system. Most network companies in the Netherlands have already or are busy with digitizing their infrastructure and are incorporating the spatial component to detect faults and provide quick and precise support to increase network operational efficiency and reduce costs.

A realistic picture of the present PV status at various spatial levels (neighborhood, municipality, province, etc.) aids in rolling out customized policies to achieve the energy transition goals. Moreover, this information is also useful to create awareness, promote sustainable energy and allows for transparency and a robust energy monitoring system.

1.4.2. Potential estimation

Potential estimation studies are important to evaluate the scope of PV penetration. Besides the realized installed capacity, estimation of as of yet unused potential helps in utility planning, formulating future adaptive energy policies, arranging financial schemes, etc. A recent report evaluated the PV potential studies conducted till date in the Netherlands and presented the spatial potential for PV installations based on key registers. This study provides an extensive survey of the potential on different land use types along with a technical evaluation on potential energy generation based on system typologies [28]. However, only an estimate of roof obstructions was considered in this study. If detailed terrain modelling was incorporated, the results could have been less uncertain.

GIS based solar radiation mapping using spatial interpolation techniques can be useful where ground measurements are unavailable [29] or for accurately estimating rooftop solar potential [30]. In recent times with the availability of high-resolution data (10 cm) GIS is being extensively employed for solar radiation modelling on rooftops [31] apart from site suitability analysis [32]. 3D models incorporating complex roof structures and surroundings to account for shade are being modelled to generate realistic scenarios for PV energy production [33–36]. Although these techniques can produce good results, problems relating to scaling, data enormity and homogeneity still exist. Data, methods, assumptions, and level of analysis determine

the quality and type of potential estimation. In addition, these methods have been tested on smaller areas and have not been upscaled to national levels.

1.4.3. Monitoring and Analysis

GIS provides very dynamic and powerful visualization techniques to view and analyze data. The set of cartographic and spatial analysis tools within GIS offers numerous possibilities for data visualization, management, assessment, and predictions. Data imported in a GIS environment has the capability to provide insights based on spatial relationships between the data objects, see Figure 1-3.

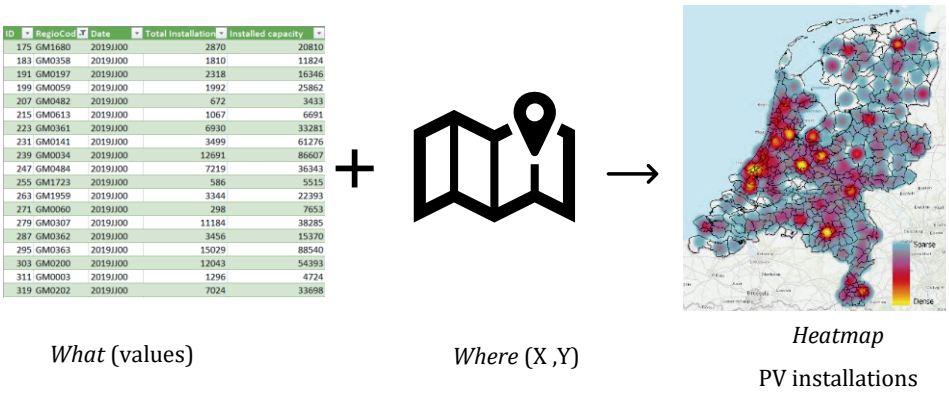

Figure 1-3– Tabular data combined with location information illustrating spatial patterns. Data displayed is PV installations per municipality for 2019 as a density map. Data source [37]

For example, if locations of PV installations along with demographic information is fed into a GIS environment, one can determine if spatial patterns exist and investigate why certain regions have more PV installations than others based on underlying demographic data. Moreover, adding temporal dimension to this data enriches this dataset further and one can perform trend analysis and predictions.

This information is of particular use businesses for market expansion or assessment of grid capacities.

1.4.4. Policy integration and scenario management

With the recent report on climate change [38], the need for stronger policies cannot be reiterated. Scalable new technologies and solutions that allow and aid in mitigation of the accelerating climate crisis especially in urban areas is the need of the hour. A step further from visualizing present status and tracking the progress of energy transition is modelling complex scenarios related to energy transition and policy implementation that provide concrete answers and help in taking the right steps. GIS has long been used to provide information tailored to stakeholder preferences especially in questions related to land-suitability analysis. However, a combination of spatially explicit data in combination with qualitative stakeholder considerations has not been performed. Spatial Transition Analysis proposed by Oudes and Stremke addresses this issue with an integrated approach and presents the variables that influence the transition targets and the time needed to energy neutrality in addition to exploring alternate transition paths [39].

GIS based tools can facilitate simulation of efficiency of planned actions and therefore display the cost/benefit analysis. This can lead to environmental friendly, low-carbon policy making be it for intermodal transport [40], supporting local energy and environmental policies [41], or aid in creating a targeted energy policy [42]. With advances in technology and availability of spatially explicit data, there is now room for innovative solutions to energy transition problems. Artificial Intelligence (AI), Internet of Things (IoT), and Digital Twins (DT) have the leverage to provide integrated solutions both locally and globally, taking geo-spatial analysis to a whole different level. At the same time, it is also necessary to be aware of the limitations of these technologies to use them in a safe, ethical manner for sustainable development.

Research Question

This thesis addresses the topics described above by answering the following main research question:

To what extent is GIS instrumental in the field of Solar PV?

In addition, the following research questions are used to further streamline the topic:

Q1. How can data regarding current PV installations and solar potential be enriched using geospatial techniques?

Q2. How can GIS mapping and visualization techniques be harnessed for monitoring and identifying trends in PV diffusion and performance?

Q3. How can spatial or spatio-temporal analysis be used in evaluating policy effectiveness or for modelling future scenarios for energy transition?

In order to fully evaluate the efficacy of a technology, one has to have an understanding of the present status, its potential, a method to access its resilience to policy and a means to track its progress with improving technological advancements. In this thesis, the potential of using GIS for various applications related to solar PV technology will be presented. All the case studies have been conducted in the Netherlands.

1.5. Thesis Outline

An overview of the chapters and the details which research question it addresses is shown in Table 1.1.

Table 1.1 – Overview of chapters

Chapter	Title	Q1	Q2	Q3
2	GeoAI for detection of Solar Photovoltaic installations in the Netherlands	•	•	
3	Bottom-up analysis of the solar photovoltaic potential for a city in the Netherlands: A working model for calculating the potential using high resolution LiDAR data	•		
4	Calibration and Validation of ArcGIS Solar Radiation Tool for Photovoltaic Potential Determination in the Netherlands	•	•	
5	Visualization of Operational Performance of Grid-Connected PV Systems in Selected European Countries	•	•	•
6	Assessment of policy based residential solar PV potential using GIS-based multicriteria decision analysis: A case study of Apeldoorn, The Netherlands		•	•
7	A spatio-temporal city-scale assessment of residential photovoltaic power integration scenarios		•	•
8	Synthesis and perspectives	•	•	•

Chapter 2 of this thesis presents the application of one of the latest technologies: GeoAI for the detection of solar PV installations from high resolution aerial images. This method is currently being used at the Kadaster[1] to provide information to the Regional Energy Strategy (RES) regions to aid in energy transition planning. GeoAI utilizes machine learning with spatial information to perform object detection tasks. The developed model has successfully been scaled up to process aerial images for the entire country to detect solar PV installations. Post-processing techniques have been employed to refine the results. In addition, the results have been compared with the existing PV system registry from CBS and finally caveats regarding this method and recommendations have been discussed.

In Chapter 3, a GIS based solar PV potential model is presented. This is a bottom-up raster model where a very high-resolution height information model derived from Light Detection and Ranging (LiDAR) data has been used as a key input and modelling has been performed using ArcGIS software. The model is used to classify residential rooftops as suitable or not for PV installations based on factors like irradiation, slope, and orientation, along with potential roof area and capacity. In Chapter 4, the sensitivity of the model to variable inputs of the model like atmospheric parameters, input image resolution and temporal resolution are discussed. Moreover, calibration and validation of the model based on the atmospheric parameters is conducted with the help of ground measurements.

Chapter 5 focuses on data capture and management for remote monitoring and visualization. The importance of cartographic principles and the usage of right types of visualization for presenting information is discussed along with the advantages of quick data visualizations for understanding data to perform the appropriate analysis.

Chapter 6 addresses a case of the Dutch Postal Code Rose policy, which was in force until 1 April 2021, by developing a GIS based multi-criteria decision analysis (MCDA), which allows determining the solar PV potential when fully applying this policy. The research evaluates the technical potential of the city and then applies it to the Postal Code Rose framework by using social criteria. The social criteria

[1] Kadaster is the National mapping agency of the Netherlands.

comprise of the most important factors that play a role in the adoption of solar PV. It also shows how multi-criteria analysis and GIS can make it easier to understand and analyze policy incentives for decision makers that target local PV adoption. Different sensitivity tests have been conducted to show how to effectively design policies to have maximum impact.

In Chapter 7, a spatio-temporal framework to assess the self-consumption and avoided GHG emissions potential has been developed. Scenarios relating to available rooftop for PV production, storage battery capacities, energy demand and future electric vehicle demand for 88 neighbourhoods within the city of Utrecht have been analysed. The mapped results show spatial insights that are useful to understand where the greatest potential for PV integration lies and which solutions are suitable for specific neighbourhoods.

The results of the thesis are synthesized in Chapter 8. This chapter strives to answer the research questions and presents the authors' perspectives on GIS technology for future exploitation.

2.

Present PV status

This chapter is based on the publication:

B. B. Kausika, D. Nijmeijer, I. Reimerink, P. Brouwer, and V. Liem, "GeoAI for detection of solar photovoltaic installations in the Netherlands," *Energy and AI*, vol. 6, p. 100111, Dec. 2021, DOI: 10.1016/j.egyai.2021.100111.

Abstract

National mapping agencies are responsible for creating and maintaining country wide geospatial datasets that are highly accurate and homogenous. The Netherlands' Cadastre, Land Registry and Mapping Agency, in short, the Kadaster, has created a database of information related to solar installations, using GeoAI. Deep Learning techniques were employed to detect small and medium-scale solar installations on buildings from very high-resolution aerial images for the whole of the Netherlands. The impact of data pre-processing and post-processing are addressed and evaluated. The process was automatized to deal with enormous data and the method was scaled-up nation-wide with the help of cloud solutions. In order to make this information visible, consistent and usable, we built-upon the existing TernausNet; a convolution neural network (CNN) architecture. Model metrics were evaluated after post-processing. The algorithm when used in combination with automated or custom post-processing improves the results. The precision and recall rates of the model for 3 different regions were evaluated and are on average about 0.93 and 0.92 respectively after implementation of post-processing. Use of custom post-processing improves the results by removing the false positives by at least 50%. The final results were compared with the existing national PV register. Overall, the results are not only useful for policy makers to assist them to take the necessary steps in achieving the energy transition goals but also serves as a register for infrastructure planning.

2.1. Introduction

In recent years, GeoAI has moved from being a buzzword to reality. GeoAI incorporates artificial intelligence (AI) techniques with methods in geospatial science to extract meaningful information. GeoAI has the capability to address, understand, discover and solve geospatial problems in a fast, consistent and accurate manner [43]. Advances in this domain include object detection and/or classification [44,45], automatic large-scale mapping [46], change detection, risk and damage assessment [47,48] to name a few. The ease of handling and mining through volumes of data in a relatively short time and aiding in automatic mapping of features makes GeoAI very useful to national mapping agencies [49]. With this technique updating and maintaining the key registers which otherwise is a manual job that is time and cost intensive, becomes relatively easy.

Solar Photovoltaic (PV) is becoming very popular due to its reducing costs and its positive impact on the environment. Over the last few years, the Netherlands has seen a rapid increase in the number of PV installations, leading to cumulative capacity of 10 GWp by the end of 2020 [50]. Although the small-scale (upto 15kWp) consumers in the Netherlands are required to register their PV panels in a national PV register (PIR: Productie-installatieregister), this is however not reinforced. Therefore, information regarding the specifics of the installations such as installed capacity, locations and energy generated is not complete and sometimes even unavailable. This might give a false impression of the present capacity leading to misguided assumptions and ineffective policies. On a functional level this could lead to difficulty in planning, operating and monitoring the grid network for the network operators.

With the intention to reduce greenhouse gas emissions by 49% in 2030 [51], the government of the Netherlands formed 30 Regional Energy Strategy (RES) regions each of which are responsible for realizing the goals stated in the Climate Agreement relating to energy transition [52]. These RES regions are currently investigating where and how best to generate renewable electricity. Currently, Statistics Netherlands (CBS) is the only organization that estimates the national figures on an

annual basis which have an uncertainty of 20% [53]. However, in order to explore and allow a smoother energy transition, data on a regional scale are needed. Verbetering van de Informatievoorziening voor de Energietransitie (VIVET, improvement of information supply for the energy transition) is one such program aimed at creating visible and structured information related to energy transition [26]. Measuring and mapping the energy transition at different levels and at different time scales can give insight into the present and future energy scenarios which can prove to be helpful in planning climate resilient (urban) energy systems and even short-term solar PV forecasting [54]. Information on present PV installations is one such dataset that could improve the existing database.

Although, with traditional image processing techniques like image segmentation, object-based image analysis and template matching techniques detection of solar installations achievable, implementation of such algorithms is computationally intensive. Malof et al., were the first to propose a technique of automatically collecting solar PV information from high resolution aerial images using a combination of traditional image processing algorithms [55] and later others [56–59] proposed semi-automated methods. These studies perform well in terms of pixel classifications or capturing the location of the installation in general. However, they are not effective in estimating or delineating the shape of the detected object. These algorithms also fall short when dealing with huge amounts of data especially at national scale especially in terms of processing time and automation.

Deep learning on the other hand utilizes convolutional neural networks; a class of machine learning algorithms which use a multi-layer approach to extract high level features from raw unstructured data [46,60,61]. Convolutional Neural Networks (CNN) can also detect the shapes of the objects efficiently as these algorithms are trained to distinguish features at the most basic level [57]. Deep convolution networks (ConvNets) [62], SegNets [63], U-Net based networks [64–66], have been tested for the application of detecting solar panels from either satellite or aerial images. These studies employed CNN or Fully Convolution Network (FCN) approaches which improved the results to a great extent showing the potential of the technique. However, these studies were either based on limited testing (smaller test

areas) or have used 30 cm resolution data for detection of large PV parks or plants, which do not capture the small-scale installations effectively. An evaluation of different deep learning algorithms, with data from the Netherlands revealed the challenges accompanied with capturing, modelling and using deep learning algorithms on cross-border data [67], which gives insights on varying image specifications. A recent study also showed the resourcefulness of CNN's by mapping solar and green roofs and combining them with building from OpenStreetMap to create a geospatial registry at building level [68].

In this chapter, a semantic segmentation method that can detect the location of rooftop solar PV installations and estimate their shapes and sizes is presented. For this purpose, very high-resolution aerial images (10 cm) have been used. Additionally, post-processing steps and the process used for scaling up the method for the whole country along results from a comparative study with the national PV register is presented. The information thus retrieved when combined with solar potential and building information, could provide valuable insights into the energy dynamics within neighbourhoods. A nation-wide dataset can subsequently present realistic and accurate information about PV installations which is currently missing on a regional level [27]. Moreover, it could be the potential solution to generate the required regional level information related to energy statistics that is consistent and homogeneous for the whole country thus, useful to policy makers to understand and implement policies related to energy transition. Therefore, we develop a fast, accurate feature capturing system which allows automatic mapping and subsequently help in monitoring of PV installations.

2.2. Data

Data is integral in GeoAI given that deep learning models need a large amount of training data. The case of "garbage in, garbage out" cannot be truer for deep learning, where the quality of the model is highly dependent on the quality of the training data. Fundamental data required for deep learning is transitioning from being resources used for mining, to being an integral part of the tools [69]. To create deep learning

models that are consistent, reproducible and repeatable, data used should be consistent and well managed. This section provides an overview of the data that has been used in this study.

2.2.1. Aerial Imagery

The Kadaster has a repository of aerial photographs[2], captured twice every year starting from 2011, with resolutions ranging from 10 cm in winter months to 25 cm during the summer. There are two variations of these aerial photographs captured during winter: orthophotos (Orthos) and true orthophotos (TO). Orthos are aerial images which are true to scale but might contain distortions or displacement, while TO's are corrected for these image distortions with the help of digital elevation models (DEM) or terrain models (DTM), (Figure 2-1).

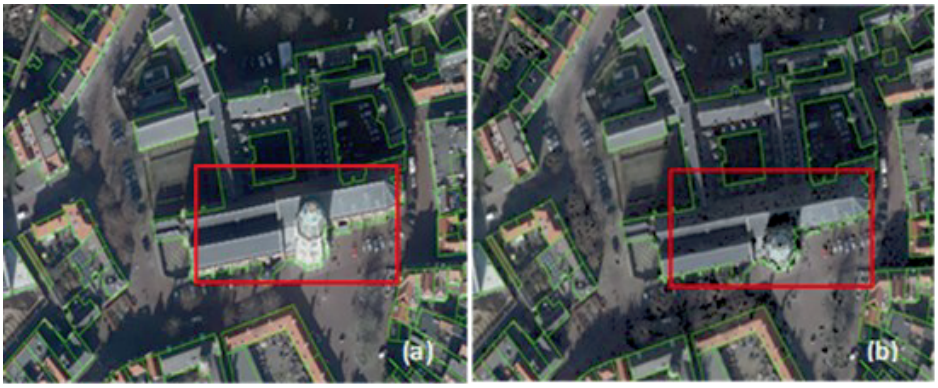

Figure 2-1: (a) Ortho and b) TO [70]. Displacement or image distortion is evident from Ortho while this has been corrected in TO. No data points (black) are clearly visible in TO, where trees, shadows or tall buildings are present.

[2] Aerial photographs are captured twice every year by different companies with varying resolutions: in winter and in summer. Winter aerial imagery has RGB channels while summer imagery has RGB and near infrared chanels. For the purpose of detecting solar panels, winter aerial photographs have been used. These photographs are usually captured over a period of two-three months, thus having different reference moments.

Dense image matching techniques [71,72] specifically semi-global image matching [73] from stereo image point clouds was used to create these TO's. Although, TO's are refined and adjusted to reflect reality, they may have no data points or image quality is affected due to insufficient data points during the DEM reconstruction. This is especially observed where trees, shadows and tall buildings are concerned as shown in Figure 2-1b. Both Orthos and TO's with image resolutions of 10 cm have been used in this project. It is to be noted that the TO's from the image matching technique have an image resolution of 20 cm, which have been resampled to 10 cm for further use in this process.

2.2.2. Ancillary Data

In addition to the aerial images, building footprint data (BAG: Basisregistratie Adressen en Gebouwen) of the Netherlands which contains information relating to approximately 9.7 million buildings and the topographic register (BRT: Basisregistratie Topografie) which contains the topographic features at various scales were used in the post-processing to refine the results. The BAG dataset comprises of building attributes such as year of construction, a unique ID which can be coupled to an address, area and purpose of use, in addition to the building shape and location [74]. BAG extract from 1st of April, 2019 was used in this study, to match with the acquisition time of the aerial images.

Top10NL are digital object-oriented topographic files that belong to the Key Register of Topography (BRT) [75]. The products are uniform and consistent for the whole of the Netherlands. The TopNL products are distinguished by the scale levels and Top10NL can be used on a 1:5000 to 1:25,000 scale. Figure 2-2 shows an overview of these datasets.

Figure 2-2: (a) An example of BAG data [74]. Building polygons in grey with building functional information in points and (b) BRT Top10NL data extract with rich attribute information on detailed land-use cover classes [75].

2.3. Deep Learning Model

The CNN which was used in this use case is known as TernausNet; a modified version incorporating U-Net architecture with VGG16 encoding [76]. U-Net architecture is widely used in image segmentation problems, because it can be trained with few images. TernausNet is open and is publicly available [77]. The network architecture in shown in Figure 2-3. The architecture consists of a contracting path where image patches are downsampled, aimed to capture context. In the expanding path, output is upsampled. With the help of skip connections, high resolution features from the contracting path are combined with the upsampled output to enable precise localization. We use this pretrained model with an image size of 1024×1024 pixels for training as this captures the features of interest (PV panels) and also the surrounding (buildings) effectively. With pixel sizes of 10 cm, the image tiles correspond to 102.4 m on the ground. The output from the model is a probability image which is then converted to a binary result using a threshold.

2.4. Implementation

2.4.1. Ground truth and training

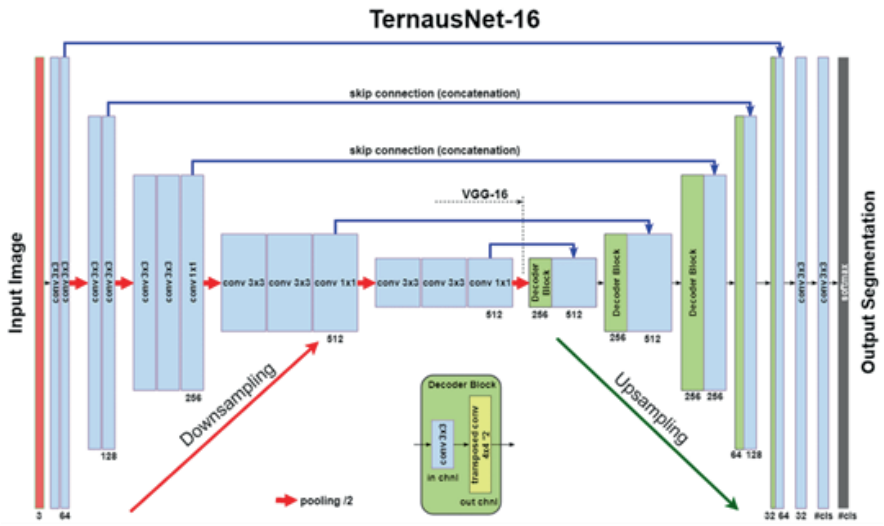

Figure 2-3: TernausNet architecture [76].

The workflow of the project is shown in Figure 2-4. Ground truth was prepared by manually drawing the panels on the images and then converting the vector polygons to raster image tiles. Initially, about 5000 panel locations were hand drawn for the city of Zwolle, which were then converted into raster masks for use in training (Figure 2-5b). Figure 2-5a shows the locations where training data has been captured and the partitioning of this data into training and validation sets.

In total about 800 image tiles with annotations have been used for training the models. The data was split into training and validation sets with a ratio of 80%, 20% respectively. TernausNet has an in-built data augmentation function which increases the training samples after the dataset has been split into training, validation and test sets. Once the model has been trained, it was implemented on the province of Zeeland and the municipality of Almere (province of Flevoland). False positives

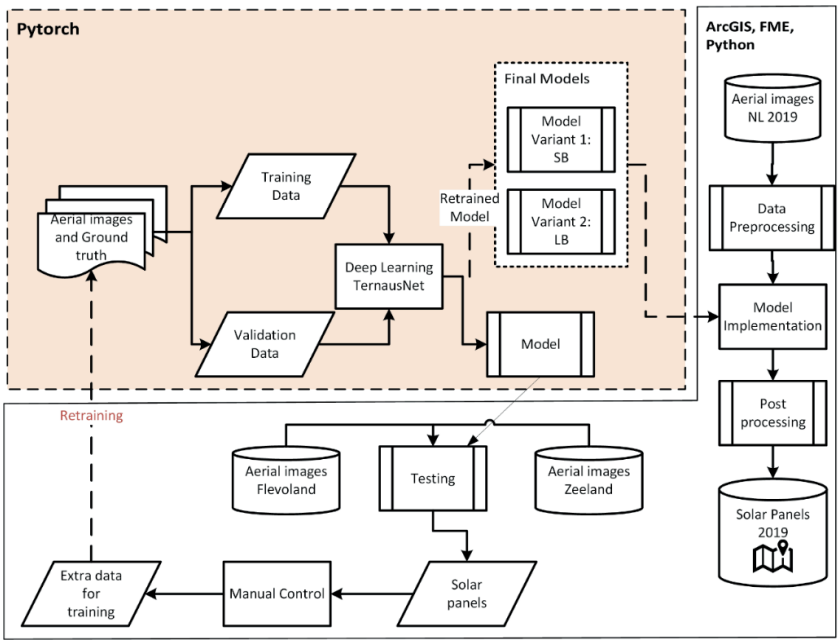

Figure 2-4: Workflow of the project implemented using cloud infrastructure to optimize and scale the process efficiently.

(FPs) were identified on greenhouses and tanks which were not of interest. In addition, the model also missed identifying many panels. It was also observed that the model was performing better on residential buildings or rather smaller buildings than on larger industrial buildings. This was attributed to imbalance in and lack of sufficient training dataset.

Consequently, to ensure that the model and the training data are unbiased and valid for the whole country, training data was expanded, and the model was retrained. Manual controls were performed, and more training samples were collected from the test areas of Flevoland and Zeeland. This introduced uniformity in the training data classes and the model was exposed to diverse panel types, spatial background and image types from different data providers. The new training samples and the original training data were pooled and split into two categories to retrain the model. Ultimately, two model variants were created; one for detecting PV on small buildings

(SB) (<200 m2) and the other for large buildings (LB) (area > 200 m2), with different hyperparameters. In total, 16 models were trained and tested using various combinations of training data, layers (RGB and CIELAB), batch sizes and normalization techniques.

(a)

(b)

Figure 2-5: (a) Training data locations in the Netherlands; Initial training data location in orange, additional data locations in red and pink (large buildings) added after testing and (b) example of training data and associated label information fed into the model.

For the final models, the learning rate was set at 0.0001, batch size at 8 and 3 layers (RGB) with standard normalization was used. The data used in the final models and the associated performance scores are presented in Table 2-1.

Table 2-1: Model hyperparameters for the two model variants.

Model	Training data	Epoch	Jaccard score	Valid loss
Small buildings (SB)	Zwolle (TO) + Flevoland (Ortho)	49/50	0.75	0.10
Large buildings (LB)	Zwolle (TO) + Zeeland (TO)	41/50	0.67	0.11

2.4.2. Post-processing

Processing huge amounts of spatially varying data using deep learning algorithms has limitations, especially when very high-resolution data is used. Numerous FPs were identified on greenhouses and outside building footprints. In order to improve the results by minimizing the FPs, post-processing techniques have been employed.

The direct output from the deep learning algorithms is a binary raster with detected PV installations. These raster files have been converted to vector features using FME software, and geo-location is reassigned to the vector files facilitate geo-spatial analysis. To account for noise in the dataset all features with area less than 0.6 m2 have been removed. Features detected outside BAG polygons have been removed. However, due to displacement in Orthos, the detected features sometimes fall outside the building footprint. This also creates problems when allocating the panels to the buildings. This has been illustrated in Figure 2-6(a). Therefore, step 1 of post-processing handles this by negatively buffering the building footprints by half a meter ensuring that the detected features are indeed solar installations and not shadows or FP's. In addition, features detected within greenhouses and tanks were deleted using the Top10NL dataset. Then, the remaining features were assigned to the buildings using the BAG dataset.

Figure 2-6: (a) Displacement problems causing confusion in panel assignment to a building, solved using post-processing. In this case the panel has been assigned to the building represented in green, (b) identified false positives on green houses, (c) panels detected from TOs and (d) panels detected from Orthos.

BAG polygons were used to clip the panels when using TOs, while a slightly different approach was adopted to deal with predictions from Orthos. Sometimes the detected panels extend over more than one building or fall slightly outside the building due to displacement. Step 2 of the post-processing was developed in order to deal with this issue and to assign the panels to the corresponding building. Panels that are partly outside building have been added to that building as a whole. Panels that are located over several buildings are initially split by the building footprint. If the area of the detected panel in such a case is smaller than $\frac{100}{(1+x)}$ % of the whole, where x is number of buildings the panel is located on, then the panel is not assigned to that building

(Figure 2-6a). Furthermore, if the total area of the detected panels within a building is less than 1.5 m^2, it was also removed considering minimum panel sizes pertaining to the market standards.

Finally, the results from both Orthos and TO's were analyzed to create a single dataset to compensate for the true negatives and false positives. This was accomplished by running queries after visually analyzing the results after post-processing step 2 from Orthos and TO's. This final step is a customized approach to improve the results was performed on three different regions using different geospatial queries some of which are as follows

- Selection of features present in both datasets also accounting for displacement in Orthos.
- Adding features from Orthos to TO dataset if significant number of features are missing from TO dataset by using spatial queries and performing visual inspections to find missing features.
- Removing features if the area is less than 1% of the building area.

2.4.3. Evaluation metrics

In order to evaluate the model performance, standard model metrics [78,79]; precision, recall and F1 score have been used. These can be defined with the help of four terms namely TP's, true negative (TN), FP's and false negative (FN). Precision is the number of true positive predictions divided by the total number of positive predictions which gives a sense of the classifiers exactness as given in equation 2.1.

$$\text{Precision} = \frac{TP}{TP + FP} \tag{2.1}$$

Recall is the number of true positive predictions divided by the number of all (relevant) predictions that should have been identified as positive. Recall measures

the accuracy of the model to identify relevant data also known as sensitivity or TP rate and is calculated using equation 2.2.

$$\text{Recall} = \frac{TP}{TP + \text{FN}} \tag{2.2}$$

Finally, F1 score is an overall measure of a model's accuracy defined by the harmonic mean of precision and recall as shown in equation 2.3. This score gives an impression of the precision of the classifier as well as its robustness. Greater the F1 score, better is the performance of the model.

$$F1 = 2 \times \frac{Precision \times Recall}{Precision + Recall} \tag{2.3}$$

2.4.4. Scaling-up the process

The most substantial part in this whole process is scaling the method to handle the enormous volume of images for the whole of the Netherlands. The data that has been processed for 2019, was approximately 4 TB, which needed to be reorganized, resampled to 10 cm and tiled to image sizes of 1024×1024 pixels. Cloud storage and computing was utilized to create tooling to manage and run the whole setup in a fast and efficient manner. The tooling was optimized so that it can be reused when new data is available. Every run with new data for a particular location, produces image tiles that are consistent with the previous runs. In other words, there is no location mismatch among image tiles produced in one year to another, which is quite useful when performing monitoring tasks.

This scaling-up tooling comprises of different tasks, the first of which is to read the bounding boxes of the raw images and segregation of the data accordingly into subsets or working blocks to continue with the rest of the tasks. The creation of these working blocks is based on a seed point (X, Y location), located at the center of the Netherlands. Nation-wide about 8,236 working blocks were created, and each

working block produces 625 image tiles and in total about 5.1 million image tiles. The working blocks are created on the basis of the image resolution of 10 cm; hence, the boundaries of the tiles remain consistent (Figure 2-7b). The rest of the tasks comprise of processing the images within these working blocks by combining, resampling and tiling them into required image sizes and saving them in ".png" format. Furthermore, processing times were improved by parallelly processing the tasks.

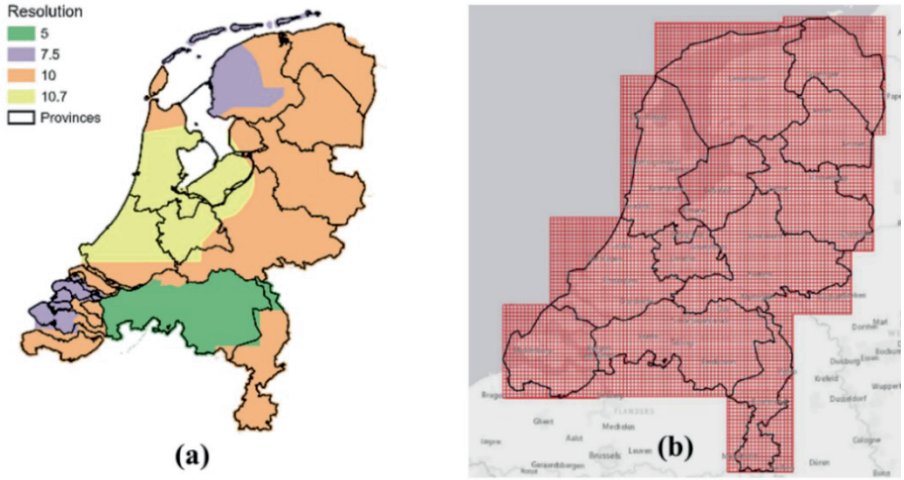

Figure 2-7: (a) Aerial image acquisition in 2019 with varying resolutions in cm, (b) working blocks to process and create the image tiles from the base images.

Efficient storage solutions were explored to reduce costs and data handling time. Docker [80] and Azure storage [81] were utilized for seamless data transfer and processing. The whole process has been automated with manual controls in between to stop the processes or adjust the parameters if needed. In-between results are also stored for analysis and reference purpose. Docker images were primarily used to deploy software and models efficiently to multiple Linux machines with 4 GPUs, for training and prediction. The machines were connected to the blob storage from Azure for seamless transfer of input and output data.

Figure 2-8: Results of the DL algorithms on different building types. Solar panels have been detected with location and shape accuracy. These results are the combination of two modes variants described in Section 2.4.1.

2.5. Results and Discussions

In this section the outcomes of the deep learning algorithms are presented, and the observations and shortcomings of the method are discussed.

2.5.1. Results

A few examples of the final results of method are shown in Figure 2-8. The vector layer displaying the detected panels in red is a combination of the Small Building (SB) and Large Building (LB) variants after post-processing. Figure 2-8 also shows how the algorithm performs in different areas and conditions. Under most circumstances the algorithm functions adequately as it detects most of the panels. Orthos have better accuracy in detecting the shape of the panel correctly while TOs had better location accuracy.

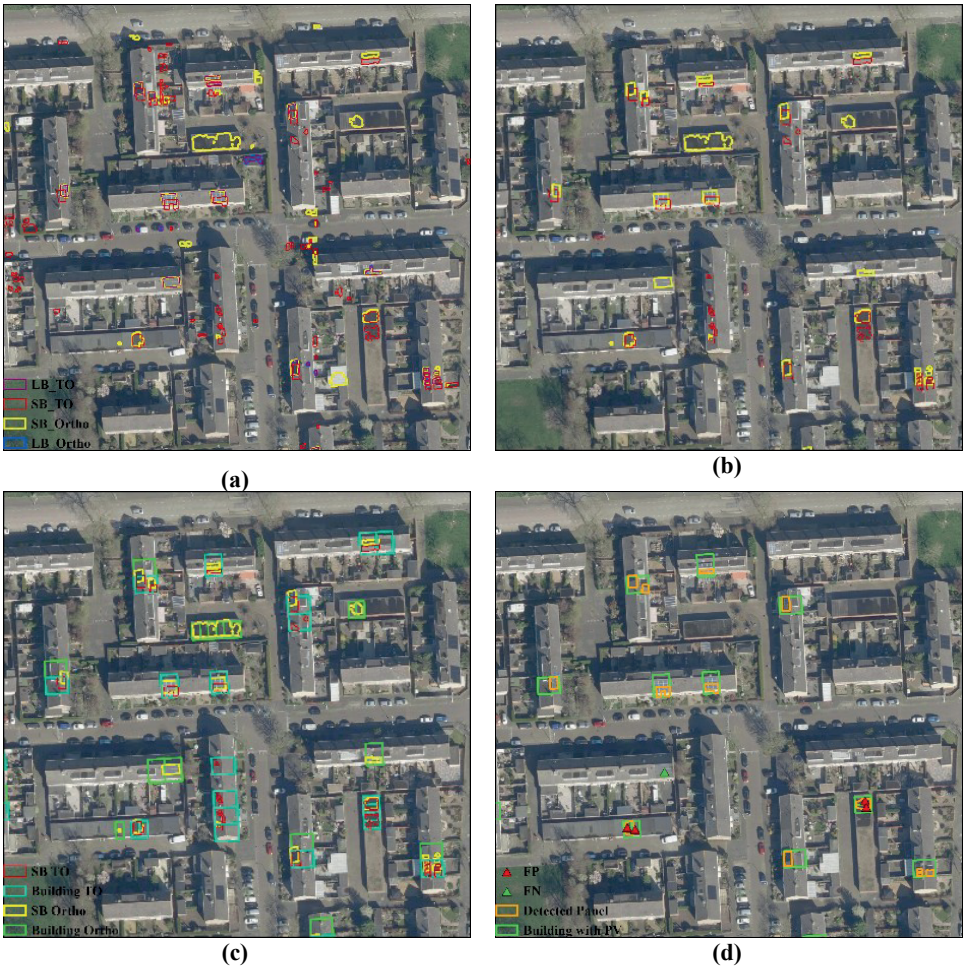

Figure 2-9: Results from both the model versions displayed on ortho photos (a) results before post-processing, (b) results after post-processing step 1, where most of the FP's outside the buildings are removed, (c) detected features are allocated to the building in post-processing step 2 and (d) final result after customized post-processing.

Subsequently, results from Orthos had many FP's while TO results missed quite a few features. Therefore, by combining both these datasets we were able to produce a final dataset encompassing both improved location accuracy and shapes. From Figure 2-9, one can observe the extent to which results are refined when using both automatic and customized post-processing described in Section 2.4.2. A closer look at the panel allocation from ortho results is shown in Figure 2-10, where the panel

allocation has been well executed, despite of uncertainty caused due to ortho image displacement. We observed that FPs occur mostly on green houses or large commercial buildings with glass domes or roofs. Removing the greenhouses in the post-processing steps seemed logical and improved the results to a great extent. However, due to the image artifacts within TO's the shapes of the detected panels were not always good and due to no data pixels, many features were undetected. Therefore, Orthos were used for correcting and improving the results.

Figure 2-10: Results of the post-processing steps to compensate for FP's, missing panels and to assign panels to the right building with Orthos.

Despite many improvements with post-processing, FP's pertaining to certain building styles were reoccurring in the results. A few of these examples are presented in Figure 2-11. One such case of reoccurring FP's was on buildings with rooftop dormers. (Figure 2-11b). The model detects dormers as panels in most of the cases. When the area of these dormers is less than 1.5 m2 they can successfully be removed from the results during post-processing. Another issue is wet patches on rooftops as shown in Figure 2-11a. The reason as to why the model detects these as solar panels in some cases is unidentified. LB model variant has shown promising results where it is very accurate with complex shapes and multiple array detection (Figure 2-8) but in a few cases, it detects only parts of the solar array (Figure 2-11d).

Figure 2-11: Observed issues with results (a) wet or shadows detected as panels, (b) dormers detected as panels, (c) unexplainable FP's, (d) parts of panels detected from panel arrays, e) example of false negative and f) panels not detected properly due to distortion.

Having a common post-processing for the whole country has its advantages and disadvantages. On the one hand it is easy to implement one set of standard tools for the whole country while on the other hand, true positives may be removed. Therefore, a customized approach might be required based on spatial contiguity and associated feature types to improve the results. The computation time for post-processing country wide took 24 hours and can go faster with parallel processing on more nodes. On the other hand, custom post-processing is highly dependent on the intuition visual controller and can vary from the size of the area under processing and the quality of the ortho and true ortho images. The smaller the region of custom post-processing the better the quality of the final results

2.5.2. Quality controls

Model performance evaluation was conducted by human controller visually i.e., by manually scanning through the results and marking FPs, FNs, and TPs. Results from three regions, varying in location and area were assessed at every step of the method, before and after the implementation of post-processing. Tile blocks of 1×1 km were randomly selected from these regions for the quality controls. The areas where these controls were conducted, and the corresponding inspection performed is shown in Figure 2-12.

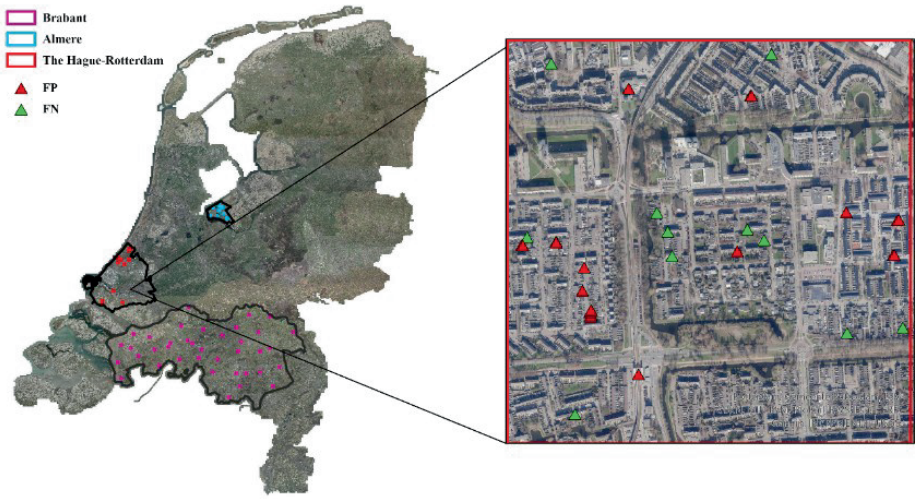

Figure 2-12: Regions where controls were performed to assess model performance. Tile blocks in pink, blue and red were manually controlled for FP, FN and TP.

The effect of post-processing has been assessed stepwise based and is presented in Table 2-2 and Figure 2-13. Almost all the panels were detected after step 2, but the data still had as many FP which reduces the overall accuracy. Therefore, customized post-processing was used even though a few TP are removed during this process (Figure 2-13). For example, the ortho results for the region of The Hague-Rotterdam included 2957 TP and 116 FN after post-processing step 2, but the dataset also contained 2168 FP. The FP were reduced to 173, but the FN increased by 165 features after customized post-processing. This is a small setback compared to positive gains to due reduction in FP.

Table 2-2: Table showing the effect of post-processing per step for three regions for Small Building (SB) and Large Building (LB) model variants. The reduction in the number of false positives after each step of post-processing is evident.

Region		**The Hague-Rotterdam**		**Almere**		**Brabant**	
Image		**Ortho**	**TO**	**Ortho**	**TO**	**Ortho**	**TO**
Features within control area (output after vectorization)	SB	12,145	19,624	4968	4921	17,188	16,038
	LB	7145	6779	3970	3218	1066	9154
Post-processing step 1 (features detected within buildings)	SB	6022	7487	3032	2771	7846	6824
	LB	3470	1817	918	851	117	3337
Post-processing step 2 (buildings with solar installations)	SB	4608	5544	1948	1593	5860	4327
	LB	280	214	121	85	40	420
Customized postprocessing	Final dataset	2965		1945		4123	

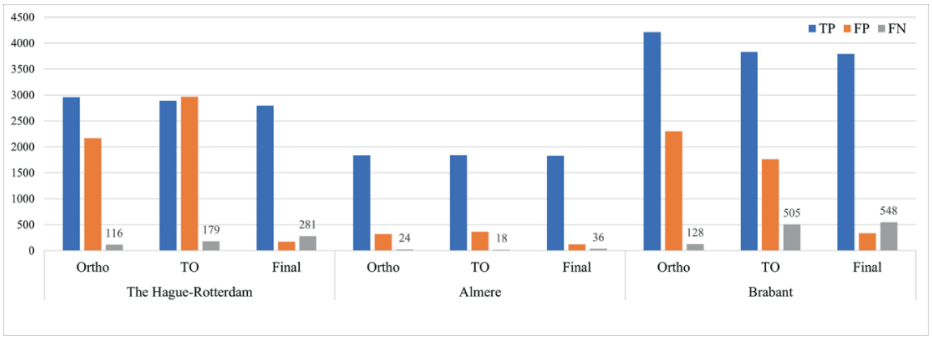

Figure 2-13: The number of identified TP, FP and FN on Ortho and TO photos after post-processing step 2 and the final dataset after custom post-processing for the three regions. Use of custom post-processing reduces the FP by at least 50% from the previous step. TO were observed to have more FN than Orthos which can be attributed to the TO image quality.

The use of classification accuracy as an evaluation metric in this case of detecting solar installations gives a false sense of achieving high accuracy due to the imbalance in the dataset. Classification accuracy is the ratio of correct predictions to the total number of input samples. In this case, the number of buildings without PV are considerably more than those with PV. 15.4%, 5.8% and 6% of the buildings have PV installations within the controlled regions of Almere, The Hague-Rotterdam and Brabant respectively. This means that even if all the buildings were predicted as not having an installation, the classification accuracy would be 84.6%, 94.2%, and 94% correspondingly. Thus, classification accuracy is not the right metric to evaluate the robustness of this model.

Metrics described in section 2.4.3, on building level using TPs, FPs FNs and TNs were calculated after post-processing and are presented in Table 2-3. In addition, shapes of the detected features were also evaluated. The algorithm performs better in the regions of Almere and The Hague-Rotterdam than in Brabant. From Table 2-3, it is also evident that the precision of the model improves greatly if post-processing is included in the workflow. The Recall rate for the Hague-Rotterdam and Brabant

is low compared to Almere, which means that the even after post-processing there are still several false negatives in Brabant and The Hague-Rotterdam. This is also reflected in the overall accuracy of the model (F1) score which is high for Almere and low for Brabant. The reason for this being the quality of the TO images from Brabant and The Hague-Rotterdam. In addition, Brabant is also twice as large as compared to The Hague-Rotterdam and thus also difficult to implement custom post-processing to refine the results on visual basis. On visual inspection of the feature shapes during the control process for The Hague-Rotterdam, it was observed that shapes of the detected features (TP) were 94.7% accurate.

Table 2-3: Manually controlled statistics from three test areas after post-processing the results.

Metrics	**The Hague-Rotterdam**	**Almere**	**Brabant**
Total no. buildings	954,566	109,954	1,727,384
Detected no. of buildings with PV	45,870	11,119	99,648
No. of buildings checked	52,566	12,055	71,080
Percentage of buildings checked	5.50%	11.00%	4.10%
TP	2792	1824	3790
FP	173	121	333
FN	281	36	548
Precision	0.94	0.94	0.92
Recall	0.91	0.98	0.87
F1 score	**0.93**	**0.96**	**0.90**

2.5.3. Comparative study

A study was conducted, comparing the methods and results from this research with the PV register database at CBS [82]. The results from both the methods provide a low regional scale indication on the number of installed solar panels at different time periods (reference data registrations and acquisition time of aerial imagery). On closer observation, it was evident that the difference in methodology for identifying solar panels leads to completely different results. The study summarizes the results of the comparison of the two data files along with an explanation regarding the cause of discrepancies between the two datasets [82]. Data from the municipalities of Arnhem, Heerlen, Het Hogeland and Utrecht were compared and the differences in the results were attributed to the following:

- Time of data acquisition: while the method presented in this chapter is subjective to the aerial images acquired in spring 2019 (ranging from March to June), CBS complies their registry at the end of every year in December. This led to a difference in the datasets used for comparison. Two time periods (end of 2018 and end of 2019) from CBS PV register were used to account for this extra data or lack thereof.
- Level of detail: The output from the current model is mapped at building level, while CBS collects data at address level. There can be more than one address in a building, and this causes some ambiguity in accessing and mapping the addresses to the corresponding building.
- Quality of the source data: As demonstrated, the dataset is not free from FPs and FNs. The same is true with the PV installation register as well. Not everyone registers their panels and at times pre-registrations are the source of the problem.

For detailed analysis and numbers one can refer to the published report available on the CBS website[3]. Additional research is also needed to find out how both sources

[3] The report was a result of the study conducted with the results from this method and the PV register from CBS. This report is in Dutch. https://www.cbs.nl/nl-nl/achtergrond/2021/04/verkenning-samenhang-regionale-zonnestroomcijfers

can complement each other for a more complete mapping of solar power at a low regional level. The fact that the two can complement each other was noted (Figure 2-14), however the best methodological implementation needs to be investigated. Only in Utrecht Kadaster has found more panels than CBS while considering data over 2019 while in Heerlen CBS registers more panels even though data over 2019 is not considered. The first can be attributed either false positives or the effect of custom post-processing while the reason for the later needs to be investigated.

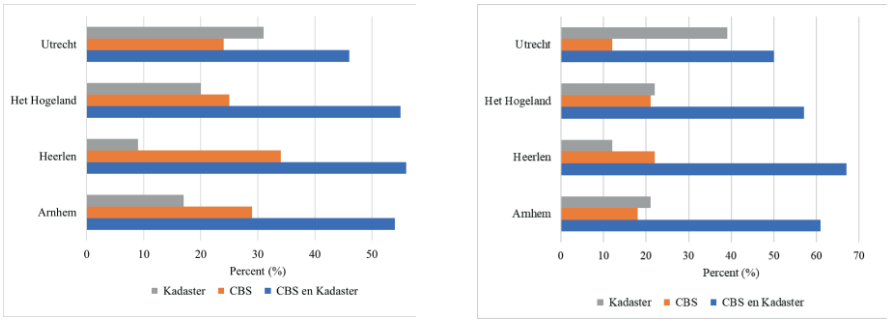

(a) **(b)**

Figure 2-14: The result from the comparison study considering (a) data over 2019 from CBS and (b) data until end of 2018 from CBS. Data from Kadaster is until April 2019, the time of acquisition of the aerial photos. More than half of the identified panels are included in both the databases of CBS and Kadaster. Data source [82]

2.5.4. Image quality and homogeneity

Image quality is an important factor that also determines the quality of the output. The aerial images in the Netherlands are captured by different companies with varying spatial resolutions (Figure 2-7a). The model is highly sensitive to the differences in image quality and the fact that these images are processed using different sensors and techniques by different companies makes this task challenging.

This leads to discrepancies in the results and therefore requires customized post-processing techniques for different regions. It is also hard to determine beforehand which regions have better quality without implementing the algorithm as it is difficult to mine through volumes of this imagery database. It therefore becomes necessary to create a balanced training dataset which accounts for this factor.

Digital elevation models (DEM) were also used as an extra layer for training during the development phase. However, it was an intensive process to create the normalized DSM (nDSM); the quality was insufficient and using this data as an extra layer in training did not show significant effect on the results. Nevertheless, nDSMs could still be used during post-processing along with slope layer to improve the results.

2.5.5. Quality of ancillary data

Figure 2-15: Issues with BAG data.

The BAG database is manually updated by different source holders along which leads to variations in styles and recorded attribute values. Data filtering based on BAG attributes was performed to select only those buildings which are currently in use. During the testing phase, we came across instances where ancillary data was incomplete or incorrect. This contributed to the quality of the end result. Quantifying

the contributing factor for these errors is often difficult to estimate. Sometimes, buildings extensions might take longer to update (Figure 2-15) causing a mismatch between the image used for predictions and the BAG used in post-processing. Even though, features are detected during implementation of the algorithm, these might be removed during the post-processing where only features intersecting with the BAG are selected. Similarly, Top10NL is updated once every year and therefore certain updates visible on images might not be included in the database.

2.6. Conclusions

This chapter presented the current method adopted at the Kadaster for automatic detection of solar PV panels using deep learning techniques. Data, methods and their corresponding issues were discussed. A comparative study with the results from the presented method was introduced which reiterates the need for a homogenous dataset with PV installation information for smooth energy transition. Post-processing techniques both automatic and custom, are integral to this method and improve the results drastically. Although, custom post-processing refines the results, the task itself if intensive and depends largely on the instincts of visual interpreter.

3D models could be used to improve post-processing especially if the models can capture dormers and height jumps effectively (LOD 2.2). In addition, with good 3D models, slope and orientation can be used as extra factors either in training or during post-processing. To obtain consistent and accurate results, constant improvement and development of the techniques is essential. Since the aerial images are acquired by different companies it is hard to maintain similar levels of consistency. In addition, the inherent image artifacts make it challenging to deal with all the images in a similar manner. K means clustering techniques which aims to categorize observations (images) into specified number of categories based on similarities in the images can be utilized to realize the goal of creating a balanced training dataset by differentiating between different classes of image tiles before implementing the model. We are investigating if the use of this technique can improve the process. In

addition, the use of random forest classifier to improve post-processing is also being explored in order to bypass the custom post-processing.

Finally, this method is quite useful for detecting existing PV installations and allocating the appropriate share of PV potential or detected PV. Moreover, it can also be used for short-term forecasting which is useful for grid-operators. The installation data when combined with information relating to purpose of the building or type of owner can be useful analyzing the present PV status along with potential sectors for PV diffusion. Furthermore, with monitoring, trend analysis can reveal spatial insights useful to policy makers to target the right audience.

3.

PV Potential estimation

This chapter is based on the publication:

B. B. Kausika, O. Dolla, W. Folkerts, B. Siebenga, P. Hermans and W. G. J. H. M. van Sark, "Bottom-up analysis of the solar photovoltaic potential for a city in the Netherlands: A working model for calculating the potential using high resolution LiDAR data," 2015 International Conference on Smart Cities and Green ICT Systems (SMARTGREENS), 2015, pp. 1-7. DOI: 10.5220/0005431401290135.

Abstract

This chapter presents a working model to estimate the solar photovoltaic potential using high-resolution LiDAR data and Geographic Information Systems. This bottom-up approach method has been selected to arrive at the potential as this gives a better estimate than a top-down approach. The novelty of the study lies in estimating the potential at high resolution and classifying the rooftop as suitable or not for solar photovoltaic installations based on factors like irradiation, slope and orientation. The city of Apeldoorn in the Netherlands has been selected as the study area. The model was able to successfully locate suitable sites for photovoltaic installations at rooftop level. In addition, the area feasible for the installations and the potential power output has also been calculated. We conclude that the city has a potential of 319 MWp capacity, which would yield 283.9 GWh/yr in relation to the 304 GWh/yr consumption from residential buildings in the area.

3.1. Introduction

Photovoltaic (PV) solar energy in Europe has been increasing rapidly in the past few years. Technological developments and research efforts have brought PV in the renewable energy sector to a new level. Estimation of the actual potential of PV in the residential sector creates various business opportunities and would assist in policy making. In addition, consumers are also increasingly aware of how PV could benefit them, as in many countries retail grid parity is present [83]. Several top-down studies have been performed on solar PV potential in the Netherlands, sometimes in conjunction with potential studies for Europe [84–87]. Some of these studies also mention different capacities based on different top-down approaches. [84,85,87]. De Noord *et al.* re-assessed these potential estimates and presented the realistic potential of solar PV in the Netherlands to be 400 km² (80-120 GWp) for building integrated PV (BIPV) and 200 km² (40-60 GWp) for ground-based PV (GBPV) [86]. The latest figure for PV potential is presented by Lemmens et al., at 150 GWp and is based on the present electricity consumption in the Netherlands of 120 TWh [88].

To summarize present top-down estimates for BIPV potential, in the Netherlands it ranges from 200-400 km², or 40-80 GWp. Land based PV installations would perhaps add another 200 km². Total country potential thus ranges from 80-120 GWp. At the end of 2013, the total amount of installed PV was estimated at 722 MWp [89]. It is predicted that in the year 2020 an amount of 4 GWp will be installed in the Netherlands [90]. With present annual growth rates, this may be a conservative estimate.

Since the top-down assessment values are difficult to rely upon these should be validated using bottom-up assessments that now are possible, using tools such as “Solar Atlas”, in Dutch Zonatlas [91], which are based on aerial photographs and solar irradiation. But determining the actual solar potential of BIPV using high-resolution data can be very challenging due to the complexity of the urban areas.

High-resolution rooftop potential studies are relatively new and not much has been done in this area at rooftop level for estimating the technical and geographical

potential for PV deployment. Izquierdo *et al.,* estimated the technical potential of roof integrated PV systems using easily available data and stratified-samples of Geographical Information Systems (GIS) maps at a regional level [92]. Based on this work, PV solar energy potential estimations at municipal to regional level was conducted in Italy with the help of global solar radiation maps taken from the Joint Research Centre of the European Commission [93]. Hofierka and Kanuk proposed a methodology for PV potential estimation in urban areas based on the open-source solar radiation tool r.sun (developed by [94]) and 3-D city model in GIS [95]. Furthermore, models to estimate solar potential on building rooftops using GIS and statistical approaches to create roof-top solar radiation maps were explored by [96,97]. Redweik *et al.*, developed a model to calculate the solar energy potential of the buildings taking into account both the roofs and the facades using high resolution LiDAR (Laser Imaging Detection And Ranging) data and applied the model to the campus of university of Lisbon [98]. However, all the mentioned studies fall short in estimating the potential at individual rooftop level.

In the present study, we estimate the rooftop PV potential in Apeldoorn, a city in the Netherlands using high resolution LiDAR data and GIS techniques. Only roof integrated PV is addressed here. With the use of Solar Analyst [99] of ArcGIS solar irradiation over large geographic areas is computed accounting for atmospheric effects, sun angle, elevation and effects of shadows by buildings, elevation and orientation. Classification of the solar irradiation map was done to differentiate between optimum and less optimum suitable sites. These were the basis of potential estimation, where further energy potential calculations are made taking into account the slope and orientation information. These estimations would help in looking at the trend of PV diffusion, create business opportunities and additionally provide an insight for policy implementations.

3.2. Methodology

The area chosen for the study was the city of Apeldoorn (52° 13′ N, 5° 57′ E), in the Gelderland province of the Netherlands. For locating the potential PV sites and for

calculating the PV potential the digital elevation model (DEM) was derived from LiDAR data, obtained from Actueel Hoogtebestand Nederlands (AHN)[100]. The DEM as the key input has a resolution of 50 cm (point spacing of 9 points per m^2, which is well suited for estimation of solar radiation at roof-tops. The DEM for the city of Apeldoorn is shown in Figure 3-1. The city itself is at low elevation, while in the West one recognizes a hilly region called De Veluwe. Another important dataset was a vector file of footprints of residential buildings in the study area. In this chapter we focus on the residential sector. The recent building footprint layer was obtained from Basisregistratie Adressen en Gebouwen (BAG), which is a part of the government cadastre system.

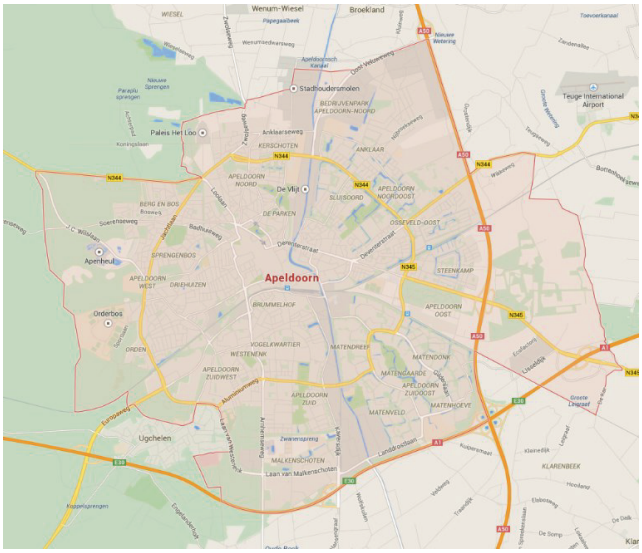

Figure 3-1:City of Apeldoorn which is taken as the study area in this research.

The estimation of solar potential in this study was calculated in two steps. First, suitable locations for roof-top PV were singled out, and then potential estimation calculations were performed based on GIS data analysis. We specified some requirements in order to characterize suitable locations; and performed all the calculations using ArcGIS.

The criteria chosen for locating suitable PV sites were solar irradiation, slope and orientation. This has been adopted from the work of Chaves and Bahill [101]. The Area Solar Radiation Tool of the ArcGIS Spatial Analyst automatically performs the solar irradiation calculation based on the model by Fu and Rich[102]. This model takes DEM as the main input and other parameters relating to slope, shade and transmissivity of the atmosphere and calculates the solar irradiance during the time specified and produces an output image having pixel values in units of Wh/m^2.

The other inputs for the model were slope and orientation, which were also created by the Spatial Analyst tool in ArcGIS. All the three images were masked to show only residential buildings and were converted into binary raster images taking the following criteria:

- Feasible Slope: less than or equal to 38 degrees
- Feasible Solar Irradiation: greater than 70% of the annual maximum received in the area which has been taken at 600 kWh/m^2 according to the modelled irradiance
- Feasible Orientation: (a) South facing and (b) other orientations.

South facing slopes have been considered as optimum while the other slopes have been taken as less optimum in this study. The binary rasters were then combined together to create a final binary image, which was then filtered to create a smooth and continuous image.

A raster to polygon tool was used to convert the suitable areas into a vector polygon layer. Attributes like area, potential capacity and power were then attached to these polygons. A value of 150 Wp/m^2 has been taken as the PV power density that can be installed. Therefore, the final output has been classified as follows

- 0: for unsuitable areas shown in red
- 1: partially suitable areas (with high solar irradiance and orientations other than south) shown in yellow and
- 2: optimally suited areas (high irradiation and south facing slopes) in green.

In addition, the production from the estimated capacity was determined using values determined by [103]. This study states that the annual production of a PV system in the Netherlands can be estimated at 875 kWh/kWp. Therefore, for optimum (south facing) oriented areas 950 kWh/kWp has been chosen and for other, less optimal orientations 750 kWh/kWp has been taken.

3.3. Results

The results are explained in the following subsections. The first subsection shows the model inputs and in the second subsection binary outputs after the application of criteria are shown. The third subsection shows the final output, which is the result of a binary (AND) operation followed by a raster to polygon transformation and addition of attributes and finally the potential estimations.

3.3.1. Model Inputs

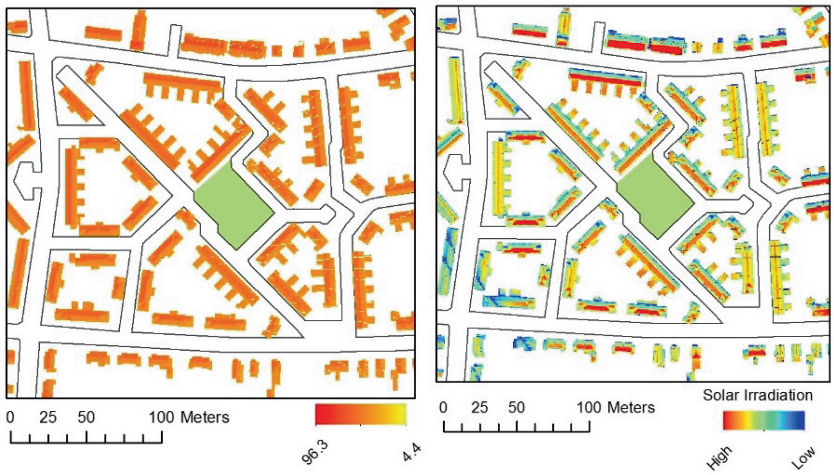

Figure 3-2: AHN height information derived for residential buildings. Height information is in meters (left) and solar irradiation image derived for building by running the Solar radiation tool. South facing slopes are seen to receive greater irradiation (right).

In this subsection the inputs taken in the model are displayed. Figure 3-2 shows the height map of the buildings and the annual solar radiation image in kWh/m² on the left and right respectively. The area receives an annual maximum of 960 kWh/m² in a year according to the model-based calculations. Figure 3-3 shows the orientation image or the direction of the slope, followed by a slope image where a distinction between flat and sloping roofs is vivid.

Figure 3-3: Orientation image showing the direction of slope of the rooftops (left). Slope image classified in classes to distinguish between flat and sloping roofs (right).

3.3.2. Binary outputs

Binary outputs after applying the mentioned criteria for slope, solar irradiation and orientation have been applied determined and are presented here. Figure 3-4 shows the optimum radiation map showing areas receiving greater than 600 kWh/m2 per year in green. We see that most of the building rooftops are selected along with a few roads or empty areas. The image on the right in Figure 3-4 shows the feasible slope areas in green, which are 38° and below. The white areas show unfeasible areas, which we can identify mostly as facades or vegetation. Images in Figure 3-5 are the optimum orientation map, which shows south facing slopes in green (left image) and other orientations map (right image).

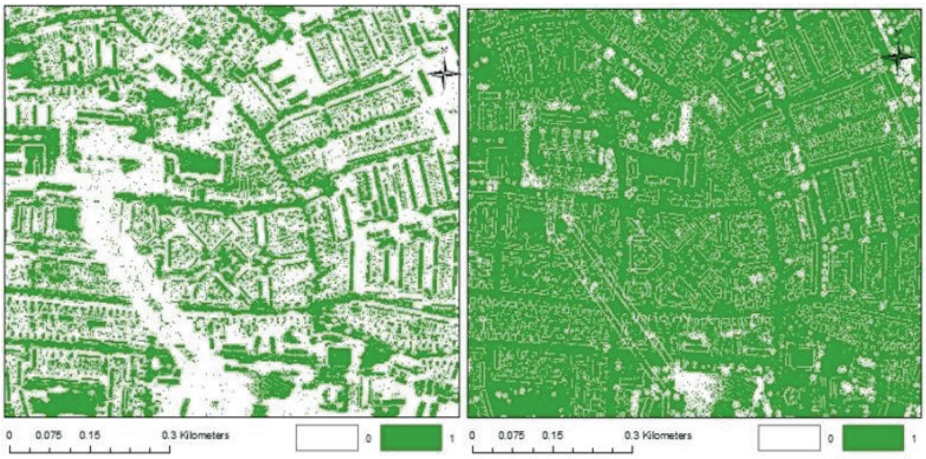

Figure 3-4: Optimum irradiation image (left) and feasible slope image (right).

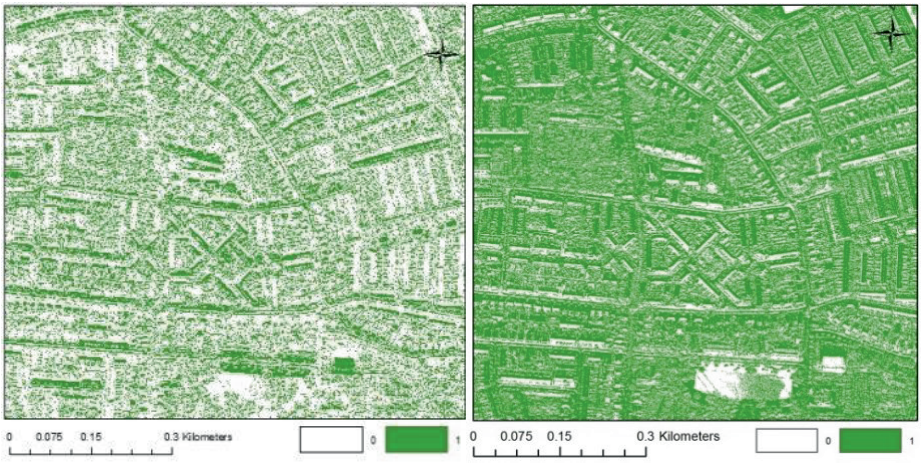

Figure 3-5: Optimum orientation image (left) showing south facing slopes and other orientations image (right)

3.3.3. Final Output

The final output is a polygon layer that shows 3 classes (Figure 3-6). Areas in green are optimally best-suited locations for PV. These areas receive maximum amount of solar irradiation and have an optimum slope and south orientation. South facing slopes in the Northern hemisphere receive maximum amount of solar irradiation.

The areas in yellow are partially optimum or the other orientation, which still receive on an average about more than 70% of solar irradiation in the region. These areas are suitable for PV but may not show high energy yields, as they do not receive maximum solar irradiation throughout the year. The red areas are categorised as totally unsuitable areas. These regions receive either minimum amount of solar radiation or have unfeasible slopes (facades or steep slopes) or are either shaded from trees or nearby buildings.

Figure 3-6:Final output showing the geographic potential. Grid code 0 shows unfeasible areas, 1 represents partially suitable area and 2 shows best suits areas for the deployment of PV

The final output presented is the result of a smoothing filter on a raster, which was then converted into a polygon shapefile. These polygons were then intersected with the building information from BAG so that the final output has address information along with the building properties as shown in.Figure 3-87 shows the attribute table associated with the final map. Each record corresponds to an address and each address is further categorised based on the grid code, which is 0, 1 or 2.

Figure 3-7:Final map with information on address, potential capacity, and power.

3.3.4. Potential Estimation

Potential estimations for the city of Apeldoorn have been calculated using the field calculator of ArcGIS for each of the final polygons as can been seen from the table in Figure 3-8. Figure 3-9 shows the rooftop area in relation to grid code. Total area is about 3.9 km^2. A constant power density of 150 Wp has been used to estimate the potential capacity per square meter. This value has been multiplied with the total area available. Potential estimation has not been performed for grid code values of 0.

The potential PV capacity for the city of Apeldoorn thus was estimated at 319.9 MWp for the residential buildings (Figure 3-9). This would mean a power production of 283.94 GWh. Note that the present PV capacity installed in the region is 3.4 MWp and the annual demand is around 230 GWh at the rate of 3500 kWh/yr per household. Using an annual average household consumption, PV would be able to provide the annual energy demand of 65,730 households, which is more than 100% of the total households in Apeldoorn.

Table

resbuild_inter_dissolve

FID	Shape	GRIDCODE	Address	Area	capacity kWp	Power_kwh
1	Polygon ZM	0	1e Beukenlaan 1 7313AH Apeldoorn	155.598	0	0
4138	Polygon ZM	1	1e Beukenlaan 1 7313AH Apeldoorn	6.69555	0.669555	502.166
7584	Polygon ZM	2	1e Beukenlaan 1 7313AH Apeldoorn	45.8384	6.87576	6531.97
2	Polygon ZM	0	1e Beukenlaan 1 A 7313AH Apeldoorn	6.93131	0	0
4138	Polygon ZM	1	1e Beukenlaan 1 A 7313AH Apeldoorn	77.6978	7.76978	5827.33
7584	Polygon ZM	2	1e Beukenlaan 1 A 7313AH Apeldoorn	106.567	15.9851	15185.8
3	Polygon ZM	0	1e Beukenlaan 10 7313AJ Apeldoorn	78.9644	0	0
4138	Polygon ZM	1	1e Beukenlaan 10 7313AJ Apeldoorn	24.3852	2.43852	1828.89
7584	Polygon ZM	2	1e Beukenlaan 10 7313AJ Apeldoorn	2.25	0.3375	320.625
4	Polygon ZM	0	1e Beukenlaan 11 7313AJ Apeldoorn	82.4278	0	0
4138	Polygon ZM	1	1e Beukenlaan 11 7313AJ Apeldoorn	5.88867	0.588867	441.65
7585	Polygon ZM	2	1e Beukenlaan 11 7313AJ Apeldoorn	18.8675	2.83013	2688.62
5	Polygon ZM	0	1e Beukenlaan 12 7313AJ Apeldoorn	49.6556	0	0
4139	Polygon ZM	1	1e Beukenlaan 12 7313AJ Apeldoorn	12.9069	1.29069	968.018
7585	Polygon ZM	2	1e Beukenlaan 12 7313AJ Apeldoorn	41.2643	6.18964	5880.16
6	Polygon ZM	0	1e Beukenlaan 13 7313AJ Apeldoorn	59.7151	0	0
7585	Polygon ZM	2	1e Beukenlaan 13 7313AJ Apeldoorn	48.0723	7.21084	6850.3
7	Polygon ZM	0	1e Beukenlaan 14 7313AJ Apeldoorn	82.7415	0	0
4139	Polygon ZM	1	1e Beukenlaan 14 7313AJ Apeldoorn	3.35988	0.335988	251.991
8	Polygon ZM	0	1e Beukenlaan 16 7313AJ Apeldoorn	72.0345	0	0
4139	Polygon ZM	1	1e Beukenlaan 16 7313AJ Apeldoorn	3.82378	0.382378	286.784
7585	Polygon ZM	2	1e Beukenlaan 16 7313AJ Apeldoorn	29.4144	4.41216	4191.55
9	Polygon ZM	0	1e Beukenlaan 17 7313AJ Apeldoorn	75.1865	0	0
7585	Polygon ZM	2	1e Beukenlaan 17 7313AJ Apeldoorn	29.5764	4.43646	4214.64

Figure 3-8: Attribute table for the final output.

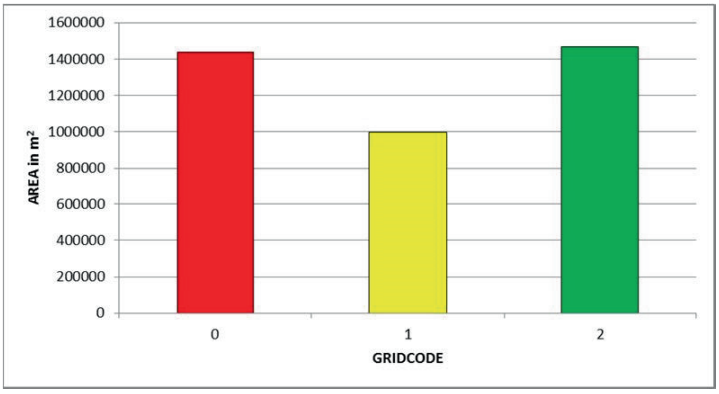

Figure 3-9: Graph showing rooftop area covered under each class after analysis. The total of these classes corresponds to the total roof area of the residential buildings in Apeldoorn.

3.4. Conclusions

In this chapter a working model for the estimation of solar PV potential using high-resolution LiDAR data and GIS techniques has been presented. Detailed PV potential

estimation studies require high-resolution height information models. The model presented in this chapter shows great potential and is easy to implement. The calculations showed that the city of Apeldoorn has great PV potential in its residential sector. Based on an average electricity consumption of residential houses in Apeldoorn of 3500 kWh/yr, the potential electricity that could be generated would be able to cover the electricity demand of the city completely and even produce more.

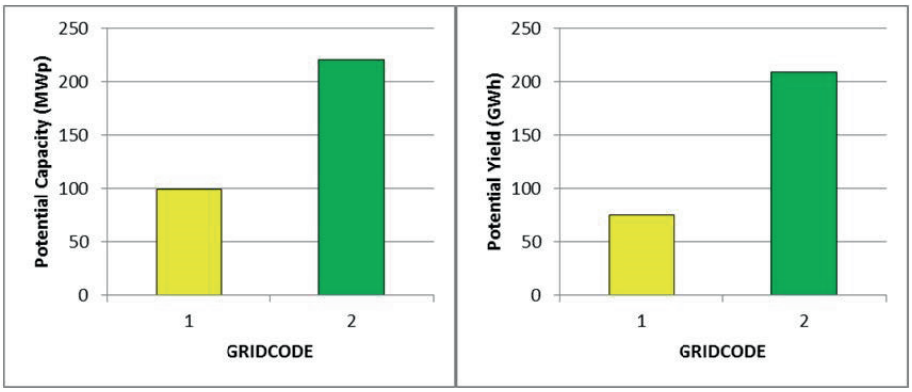

Figure 3-10:Potential capacity in MWp and expected yield in GWh of the optimally suitable area (Grid code 2) and partially suited areas (Grid code 1).

The application of this methodology to a city has shown that this method could be deployed in the whole country for accurate bottom-up determination of PV potential. This method could also be applied to the whole of the Netherlands, but proper extrapolation techniques have to be developed.

4.

PV Potential tool calibration

This chapter is based on the publication:

B. Kausika and W. van Sark, “Calibration and Validation of ArcGIS Solar Radiation Tool for Photovoltaic Potential Determination in the Netherlands,” Energies, vol. 14, no. 7, p. 1865, Mar. 2021, DOI: 10.3390/en14071865.

Abstract

Geographic information system (GIS) based tools have become popular for solar photovoltaic (PV) potential estimations, especially in urban areas. There are readily available tools for the mapping and estimation of solar irradiation that give results with the click of a button. Although these tools capture the complexities of the urban environment, they often miss the more important atmospheric parameters that determine the irradiation and potential estimations. Therefore, validation of these models is necessary for accurate potential energy yield and capacity estimations. This chapter demonstrates the calibration and validation of the solar radiation model developed by Fu and Rich, employed within ArcGIS, with a focus on the input atmospheric parameters, diffusivity and transmissivity for the Netherlands. In addition, factors affecting the model's performance with respect to the resolution of the input data were studied. Data were calibrated using ground measurements from Royal Netherlands Meteorological Institute (KNMI) stations in the Netherlands and validated with the station data from Cabauw. The results show that the default model values of diffusivity and transmissivity lead to substantial underestimation or overestimation of solar insolation. In addition, this chapter also shows that calibration can be performed at different time scales depending on the purpose and spatial resolution of the input data.

4.1. Introduction

Geographic Information System (GIS) based solar photovoltaic (PV) tools have been developed and used increasingly in the past decade, as they provide a remote assessment of PV siting, planning, integration and management [104]. These tools have been gaining popularity within the public sector (general public, governments, etc.) and also the private sector (PV installers, network operators, etc.). With increasing interest in sustainable solar energy generation, the mapping of solar PV potential has been explored by many at local [105,106], municipal [107,108] and regional scales [109]. At a local scale, it is easy and insightful to assess individual buildings. This information, once generated, can be used for answering several questions regarding the planning and siting of solar PV or solar thermal systems and even in urban planning and policy evaluations [110,111].

Early methods for PV potential calculations used computational solar radiation models which were either top-down or could not capture complex roof tops or probable shading due to the surroundings [112,113]. Then, a combination of computational models and GIS methods emerged for improving the solar irradiance calculations and for the estimation of technical [109,114–116] and socio-economic potential [117]. GIS based algorithms, on the other hand, help in capturing the spatio-temporal variation of solar irradiation and, consequently, PV yields [118]. A number of solar irradiation and PV mapping tools that are currently available and use different methodologies for rooftop PV potential analyses have been reviewed [31,119,120]. These algorithms are driven by geographic data and atmospheric parameters specific to the particular area. Most of the GIS based methods are based on some form of geographic data, such as satellite images, digital elevation models (DEM) [31,113,117] or LiDAR data [121–124]. These methods use different assumptions and, hence, differ in their accuracy and performance. Usually, the most common assumption is that every point on the rooftop receives an equal amount of solar radiation, irrespective of the slope, orientation and shading factors. Such assumptions often lead to inaccuracies [125]. When it comes to preparing maps or creating PV potential tools, it is necessary that the tool is customized to suit the

geographic area, as solar irradiation and its associated weather parameters change drastically depending on the location and time. Commonly used solar irradiance models have been reviewed and analysed [112,113,120]. Out of the few existing raster-based models, the GRASS r.sun model developed by Šúri and Hofierka [126] and ESRI's Solar Radiation used in ArcGIS [127], developed by Fu and Rich [128], allow for integration of attributes that vary spatially over large regions. In addition, these models also account for shadows from surrounding buildings and trees, while allowing modelling over inclined surfaces, which is of specific interest in the urban landscape.

For solar irradiance calculations, GRASS r.sun uses a Linke turbidity factor and beam and diffuse radiation coefficients, which are obtained from a data bank and calculated from decomposing global radiation measurements from a nearby weather station [129]. On the other hand, ArcGIS's Solar Radiation uses simplified models, in addition to an easily operable interface with high resolution geospatial graphics. In addition, in the Solar Radiation tool, sky transmissivity and diffusivity parameters for calculation of direct and diffuse insolation are values which can be changed via a time series; throughout the year, every month, or within a day. Diffusivity ranges from zero to one, with typical values of 0.2–0.3 for clear sky conditions. Transmissivity also ranges from zero to one, with 0.5–0.7 for clear skies. Note that transmissivity and diffusivity are inversely related [130]. The GRASS r.sun is an opensource software, while ESRI's Solar Radiation is a proprietary software.

The atmospheric parameters (Linke turbidity factor, clear-sky index, transmissivity, etc.) can have a significant impact on the calculated annual irradiation [124,131]. These atmospheric parameters are hard to model and customize for a particular location [126]. Using the tools without validating these variables can have a significant influence on the final results; therefore, using parameters closer to local insolation values reduces the variation in solar radiation estimation [122,132]. Especially, with the Solar Radiation, model validation is necessary since the actual values cannot be defined from atmospheric data prior to model implementation [113]. The Australian PV Institute's (APVI) Solar Potential Tool, developed by the University of New South Wales, uses the Solar Radiation model as the background

[133]. They used validation methods to estimate the accuracy of the APVI tool in comparison to measurements of the output AC power of PV systems and NREL's System Advisory Model (SAM [134]). The study also analysed the accuracy of ArcGIS's Solar Radiation tool with respect to insolation on shaded and unshaded surfaces [135]. Copper and Bruce [133] stated that a linear correction can be applied to ArcGIS's estimates of insolation in order to achieve better fits with the results from SAM. However, it was observed that studies do not validate these models before using them, despite the influence of this on the results.

This chapter, therefore, addresses the relevance and implementation of using calibrated values for diffusivity and transmissivity for estimation of global horizontal irradiation for varying spatial resolutions and geographic areas, using the Solar Radiation tool of ArcGIS, with particular focus on the Netherlands as a case study. We used the typical meteorological year data as well as the most recent 10 years irradiance data for calibration purposes.

This chapter is further organized as follows. In Section 4.2 the methods and data used are presented. Section 4.3 shows and discusses the results for the annual and monthly analysis of parameters with a validation case. Additionally, the model implemented for varying spatial resolutions is also presented. Section 4.4 concludes the chapter.

4.2. Materials and Methods

4.2.1. ArcGIS Solar Radiation Tool

It is evident that solar irradiation varies with time, during a day, in a month and throughout the year. It also varies with the climatic conditions and the position of the sun. Therefore, the challenge for the model is to predict the values as close as possible to reality. The tool is quite simple, requiring only a couple of atmospheric parameters. In the case of the Solar Radiation tool, it is hard to calibrate these atmospheric parameters of diffusivity and transmissivity before running the model.

The Solar Radiation tool of ArcGIS's Spatial Analyst Toolbox calculates the solar radiation over a geographic area or for specified point (latitude–longitude) locations, based on the hemispherical viewshed algorithm explained in [136–138]. This tool takes location, elevation, slope, orientation and atmospheric transmission as most the relevant inputs. The total amount of radiation calculated for a given location is given as global radiation in the (energy) units of Wh/m^2.

The variable parameters we discuss in this chapter are atmospheric diffusivity and transmissivity [130], which denote the proportion of global normal radiation flux that is diffuse and the fraction of radiation that passes through the atmosphere (averaged over all wavelengths), respectively. These values, thus, range from 0 to 1. All the calculations were performed under clear sky conditions.

The Solar Radiation tool uses a diffusivity value of 0.3 and transmissivity value of 0.5 as the default settings and this is referred to as the default model throughout this chapter. For calibration of the Solar Radiation tool, solar irradiation for all combinations of diffusivity (0.2–0.7) and transmissivity (0.3–0.7) parameters (modelled values) have been simulated. In the results, for the purpose of analysis, these values will be referred to as whole numbers preceded by D or T to denote diffusivity and transmissivity, respectively. For example, D3T5 refers to a diffusivity of 0.3 and transmissivity of 0.5.

4.2.2. Calibration Data

A major source of meteorological data in the Netherlands comes from the Royal Netherlands Meteorological Institute (KNMI) [139]. This institute provides a wide range of meteorological products and manages 50 automatic ground-based weather stations across the country, of which, 33 stations record the solar irradiance. Calibration of the atmospheric parameters was conducted using the measured values from the KNMI network. The KNMI station at De Bilt, in the Netherlands (52.10N, 5.18E) was chosen as a reference point for data calibration. Irradiation values obtained from the ground stations were mapped and interpolated to identify variations throughout the country for 10 years (2011–2020). The De Bilt station was

selected out of the 33 stations that provide irradiation data, as this station is located in the center of the Netherlands and is commonly used as a reference point by KNMI for describing and forecasting the weather in the whole of the Netherlands. In fact, the change in irradiation from coast to mainland is not very prominent (about 10%) [140] and, therefore, a single station (at the center) can well be used as a reference when performing nationwide calculations. The model will be implemented for the area of De Bilt and meteorological data from that station will be used for atmospheric data calibration. For calibration purposes, De Bilt values were chosen in order to see if it was performing adequately to be used for the whole country.

Out of the 33 stations which measure irradiance, 30 stations were selected due to interruptions in the data collection of 3 stations within the 10 years. The locations of these KNMI ground measurement stations and their classification as either coast or mainland used in this study are shown in Figure 4-1

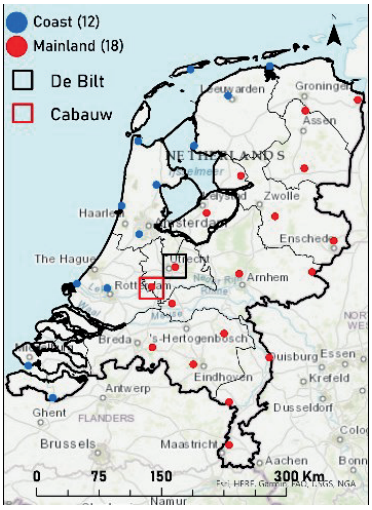

Figure 4-1:Royal Netherlands Meteorological Institute (KNMI) stations in the Netherlands. Stations are categorized as coast (blue dots) and mainland (red). The station in the center (black square) is the De Bilt KNMI Station, and the station in the red square is the Baseline Surface Radiation Network (BSRN) station Cabauw.

Daily sums of measured irradiance from the ground stations were gathered and aggregated per month and per year. In addition, irradiation maps for the country were created using a simple inverse distance weighted interpolation technique with irradiation data obtained from these 30 KNMI stations. This provides an insight into the variation in irradiance within the country over the years at low resolution, which is sufficient for checking for anomalies related to localized weather conditions or instrumentation errors [141].

In addition to the KNMI stations, there is a Baseline Surface Radiation Network (BSRN) station at Cabauw in the Netherlands. This is one of the stations that provides radiation measurements as part of a worldwide network [142,143]. There are about 40 stations in this global network in different climatic zones. These data are of primary importance for the validation and evaluation of various satellite and model estimates of radiation parameters. The Netherlands falls under the temperate maritime climate zone and Cabauw (51.97N, 4.93E) is a BSRN station in the Netherlands, which adheres to the highest achievable data measurement standards. Therefore, data from this station were used to validate the calibrated model [144]. This station is about 30 km southwest of De Bilt (see Figure 4-1).

4.2.3. Input Data for the Model

Since the Solar Radiation tool is GIS based, it requires inputs in terms of raster or vector data. In particular, the Area Solar Radiation tool requires a DEM as an input to model solar radiation over geographic areas. The DEM used as input in this study is of 50 cm resolution and was obtained from Actueel Hoogtebestand Nederlands (AHN) [145]. Additionally, a DEM of 5 m (AHN) and 30 m (Aster DEM) [146,147] were used for irradiance calculations to evaluate the effect of spatial resolution on the outputs generated. A vector dataset of the locations and attributes of the KNMI and BSRN stations was used to map the measured irradiance values. Spatial resolution is one of the key factors deciding the quality of the output, as can be observed from Figure 4-2. The higher the resolution, the greater the detail in the images. Therefore, this should be chosen depending on the purpose of use. Modelling irradiation on the rooftops can be performed with 50 cm data, as can be clearly seen

from Figure 4-2c. The slopes and orientations of the rooftops can also be calculated effectively at this resolution, which helps in potential estimations at the building level. With 5 m data, it is likely only possible to do this at the neighbourhood or block level. With 30 m data, regional or national level estimations are possible.

Figure 4-2:Example of varying spatial resolution of the digital elevation models; (a)30 m (b) 5 m and (c) 0.5 m. The white areas correspond to missing data.

4.2.4. Method

The Solar Radiation model was implemented for calibrating the model parameters T and D. The model has the capability to predict the irradiance values for varying temporal resolutions; daily, monthly, annual average and also within a specified time period. In this chapter, the values were calibrated for two cases of varying temporal resolutions; yearly (annual average) and monthly average since this gives better information for potential estimations. In addition to these two temporal scales, we evaluated the data at varying spatial resolutions. All the modelled values were validated against a reference set for the default case, modelled values calibrated per year and modelled values calibrated every month.

The Solar Radiation modelling tool is computationally intensive; the process can run from a few hours up to multiple days depending on the inputs provided. In this particular tool, the simulation time is exponentially proportional to the resolution of the sky size and the raster input [106]. This also means that the higher the resolution of the input image, the greater the detail in the results and longer processing time.

ArcGIS uses Python as a scripting module to perform geographic data analysis, data conversion, data management, and for map automation [148]. Therefore, a customized Python script to run all permutations of atmospheric parameters of the model was incorporated to automatically run and iterate all the combinations of D and T values without manual intervention. The computed values of different permutations and combinations were then calibrated using measured values from the KNMI ground station in De Bilt. The best fit parameters of diffusivity and transmissivity were estimated for each month and year separately. The percentage difference (PD) between measured and modelled values was used to find the best fit values per month and per year (Equation (4.1)) [149].

Data fitting is highly dependent on the purpose of use, and the spatial and temporal scales at which the result is needed. In this chapter, we chose to find the best fit values of global horizontal irradiation (GHI) for one location (De Bilt) over 10 years, assuming that the calibrated values from this location can be used for the whole country. The default model values, and the calibrated model values (GHI_{mod}) were then compared with the measurements from De Bilt (GHI_{meas}) using percent differences (PD) and mean bias error (MBE). MBE is the statistical model performance indicator, representing the systematic error of the prediction model to under or overestimate. The percentage difference PD and MBE are defined as:

$$\mathrm{PD} = |[(GHI_{meas} - GHI_{mod})/GHI_{meas}] \times 100 \tag{4.1}$$

$$\mathrm{MBE} = \frac{1}{N}\sum(GHI_{mod} - GHI_{meas}) \tag{4.2}$$

with N referring to the number of measurements and the subscripts “meas” and “mod” corresponding to the irradiation values measured at KNMI De Bilt and obtained from the Solar Radiation model for all settings of D and T, respectively. Modelled data are calibrated per month and once a year. Analysis at a local scale to depict buildings was also performed on an area close to the Cabauw station and this was chosen for validating the method.

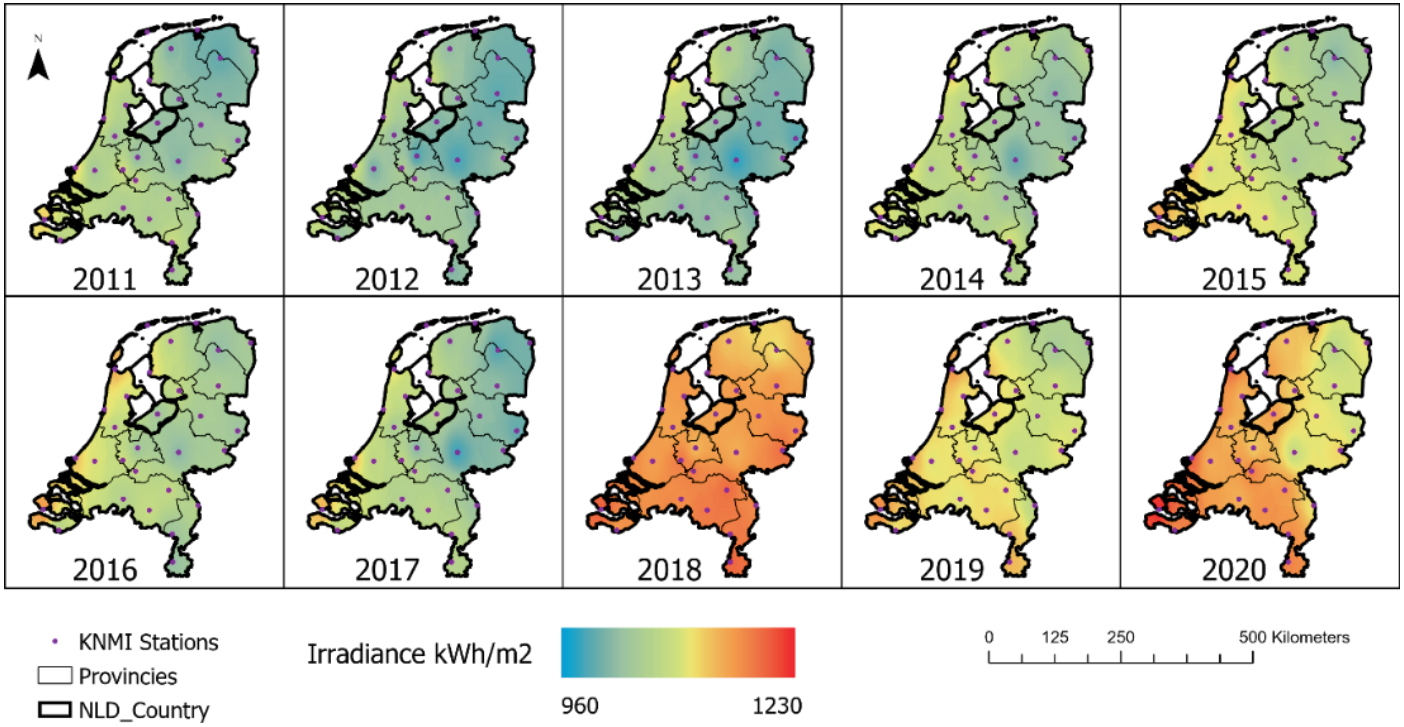

Figure 4-3:Annual global horizontal irradiation in kWh/m2 derived from KNMI stations across Netherlands for the years 2011–2020. Data have been interpolated to create a continuous irradiation map. The locations of the KNMI stations are also indicated as dots in the irradiation maps.

4.3. Results and Discussion

This section presents and discusses the results of the calibration and validation methods along with insights into the spatio-temporal variation of solar radiation within the Netherlands. In addition, the purpose of using a GIS based radiation model is presented.

4.3.1. Spatio-Temporal Variation of Solar Radiation in the Netherlands

Solar irradiation depends on the geographic position and local climatic variations. The spatial and temporal variations in the global solar irradiation in the Netherlands for the years ranging from 2011 till 2020 are shown in Figure 4-3. The coastal region generally has a higher level of irradiation compared to the mainland. De Bilt, which is in the center of the country, falls in the median zone. Irradiation values from this station can, therefore, be taken as the average for the whole country.

An overview of the ranges of values recorded at the 30 meteorological stations in the Netherlands is shown in Figure 4-4. The boxplots show the annual irradiation as recorded at the KNMI stations grouped as coast and mainland; 12 stations along the coast and 18 from the mainland (see Figure 4-1). It is clear that the coastal area has higher irradiation values compared to the mainland. It is worthy to mention that these values are larger than the 30-year average (983.41 kWh/m^2 measured between 1981–2010) used to characterize the Dutch climate [149]. Extremely high values have been recorded over the past three years.

From Figure 4-4, it is also evident that irradiation for location/locations is not the same every year. Even though the spatial variation of irradiation is prominent, even up to some 15% (Figure 4-3), we choose the De Bilt values for validation of the solar irradiance for the whole country, as this is the central location of the country.

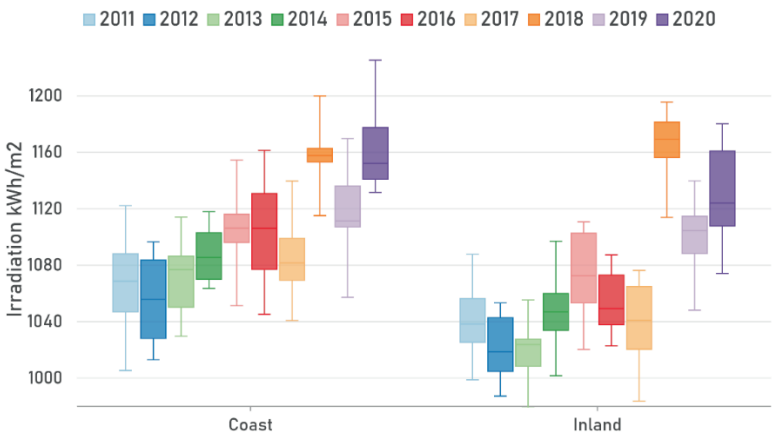

Figure 4-4: The range of irradiation values for all 30 stations categorized as coast (east) and inland (located west from the coast) for 10 years. Extremely high values were observed in the last 3 years, with record highs above 1200 kWh/m² for a few stations on the coast. The East to West variation of irradiation in the Netherlands can also be inferred from the graph.

4.3.2. Calibrated Values vs. Default Values

All combinations of D and T for the 10 years have been modelled for the location of De Bilt. Table 1 shows the GHI values measured at the De Bilt station per month for the year 2020 and modelled values from the same location with the default settings and calibrated values (best combinations of D and T) and their corresponding percentage difference (PD). Note, that the modelled values for different years are the same for every combination each month, except for leap years This is because solar irradiation modelling has been performed on a single location (De Bilt station) with a constant DEM for all the years, assuming that there are no height variations throughout the 10 years. The locations of the ground measurement systems are also usually unchanged and are placed in fields with no obstructions. This clearly indicates that the model is very sensitive to the provided height information, which in turn, can be used in a manner that is dependent on the purpose of the analysis.

From Table 4-1, it is clear that the default model substantially underestimates the GHI. On an annual basis, for the year 2020, the default model yields an annual sum of 891.12 kWh/m², which is about 21% less than the measured values at De Bilt. Only for two months (June and July) are the percentage differences below 6%, while in the winter months, the differences are much larger. If these values are not adjusted, they might lead to error propagation when these values used in further PV potential estimations. Therefore, it is necessary to find the right combination of D and T parameters in order to achieve better fits and, in turn, better accuracy. Choosing the correct temporal resolution for irradiance estimations is, therefore, important for the final results. For example, when trying to look at the production profile for a single household, hourly irradiance calculations can be very useful, in particular, for optimization of self-consumption. On the other hand, if the purpose is creating an irradiance map for the whole country, then it is more useful to select a seasonal or yearly variation.

Table 4-1: Global horizontal irradiation (GHI) from de Bilt from measured (GHI_{meas}), results from solar radiation default model D3T5 (GHI_{mod}) for the year 2020 and the corresponding percentage differences (PD).

Month	GHI_{meas} (kWh/m2)	GHI_{mod} (default)	PD (%)	GHI (calibrated)	PD (%)
Jan	16.58	6.94	58.17	17.73	6.93
Feb	31.76	20.33	35.99	30.18	4.98
Mar	93.94	58.73	37.48	100.25	6.73
Apr	155.53	103.23	33.62	151.32	2.70
May	194.33	148.42	23.62	194.94	0.32
Jun	163.95	160.52	2.09	160.52	2.09
Jul	149.01	156.99	5.36	148.31	0.46
Aug	142.56	121.23	14.97	145.79	2.26
Sep	98.51	71.92	26.99	98.96	0.45

Month	GHI_{meas} (kWh/m2)	GHI_{mod} (default)	PD (%)	GHI (calibrated)	PD (%)
Oct	39.66	29.71	25.09	40.66	2.52
Nov	25.90	9.05	65.08	25.96	0.23
Dec	13.53	4.05	70.07	12.53	7.39
Annual	1125.27	891.12	20.81	1090.25	3.11

The best combination of diffusivity D and transmissivity T values was studied for the Netherlands for every month and for a year as a whole at the De Bilt location. Best fit values for each month were determined by finding the lowest PD between GHI_{meas} and GHI_{mod} (Equation (1)). The results for the best combination of D and T and the corresponding error ranges for monthly fits are shown in Figure 4-5a,b and Figure 4-6a, respectively.

The difference in PD between the default and the calibrated model is huge (Figure 4-6a). The PD for the calibrated model is well below 7% for most of the fits. Here, the highest PD was also observed for the winter months, similar to the PD of the default model. Most repeating (four times in 10 years) D and T values are also from the winter months. The variation of best fit D and T values is shown separately for the 10 years in Figure 4-5a. Figure 4-6b shows the fits achieved by calibrating the model using the monthly and yearly fits, in comparison with the default model. It is evident as to how much error can be reduced by using calibrated values from Figure 4-6b. The MBE for the default model for 2020, as shown in Figure 4-6b, is negative, which means that the model is underestimating the value. Furthermore, analysing the MBE values for all the 10 years revealed that the default model is biased, which means that for all the 10 years under review, the default model has underestimated the GHI.

Calibrating the values using only one annual DT combination resulted in higher PD values than fitting the data using DT combinations optimized per month, as shown in Table 4-1. Modelled values, obtained by using one DT combination per year, underestimate the irradiance for winter months and overestimate the irradiance for summer months.

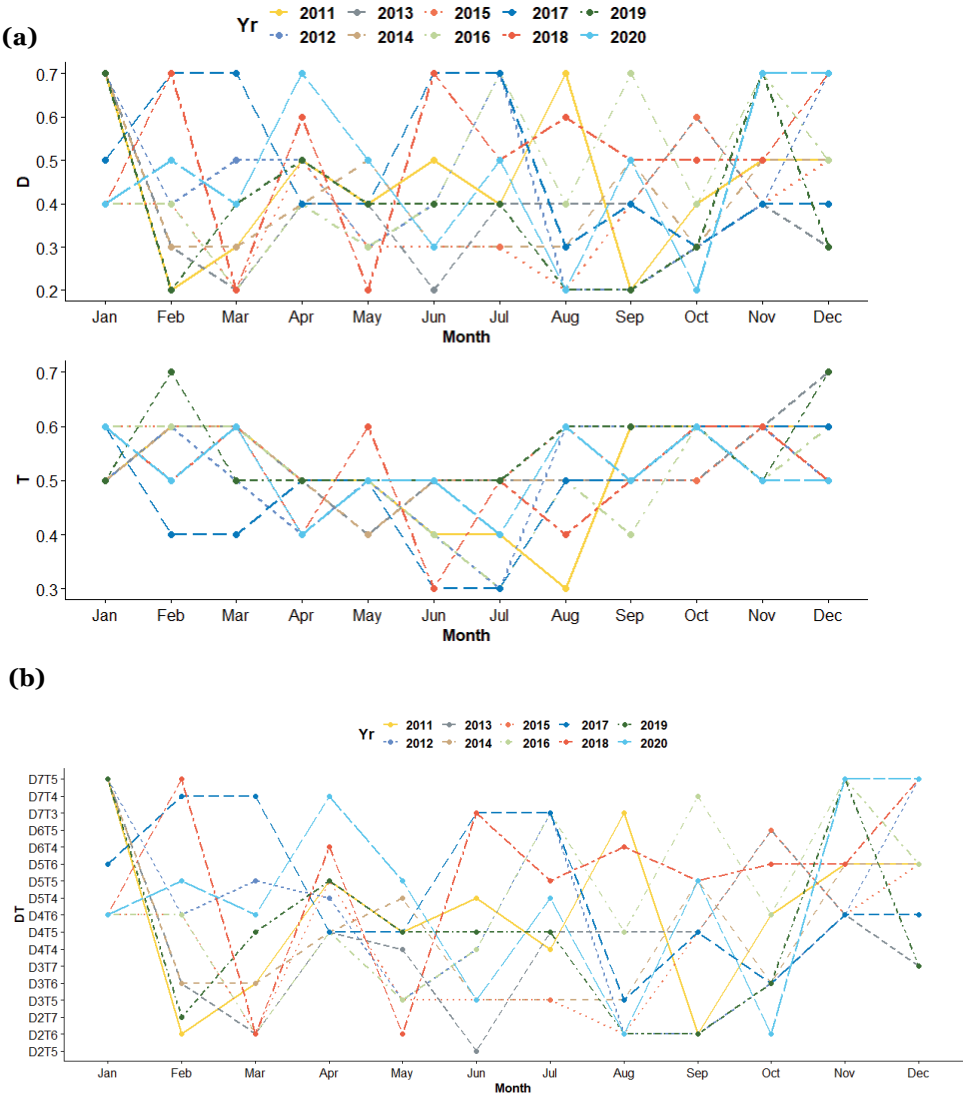

Figure 4-5: (a) Best fit D and T values for monthly calibrations over 10 years. The inverse relationship between D and T values is observed here, (b) Calibrated diffusivity (D) and transmissivity (T) combinations for 2011–2020. Although certain combinations are repeated, it is hard to find a pattern with these reoccurring combinations.

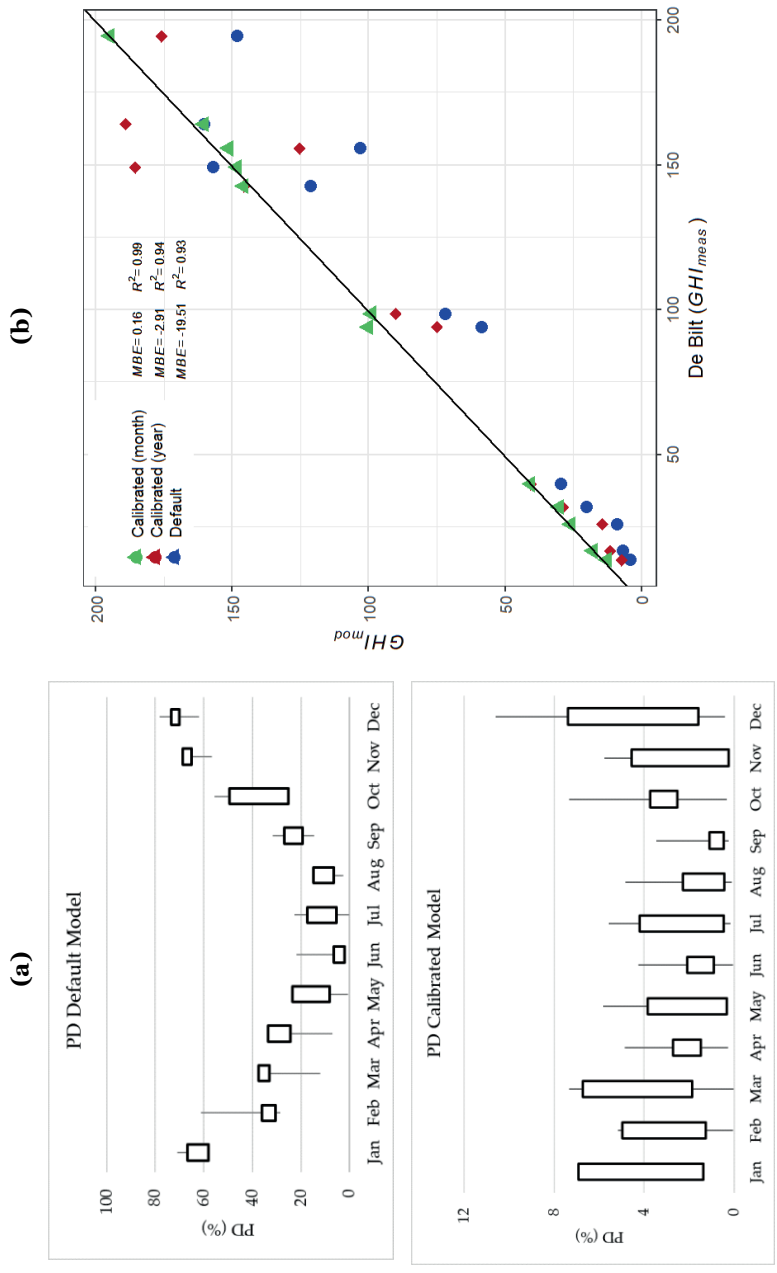

Figure 4-6:(a): Range of PD for the default model and the calibrated model for all the 10 years and (b) Scatterplot of default and best fit (calibrated values) per month and year vs. the measured values from de Bilt for 2020.

Therefore, over a year, the cumulative irradiation values are closer to the reference values. However, the monthly fits are much better when looking at higher temporal scales.On the other hand, if we are looking at lower spatial resolutions (district or country level), yearly fitting could suffice. This is because detailed information would be masked as the DEM input would be coarse (resolution of about 15 m–30 m or larger), which is not enough to distinguish between individual buildings.

To a large extent, yearly fits also reduce the error as compared to the default model, as shown in Table 4-2: Best fit DT values on an annual basis and the corresponding PD. The graph shown in Figure 4-7 plots the calibrated values of D and T when using one value for the whole year. It can be seen that certain years (2015, 2018–2020) with high levels of radiation have low diffusion and high transmission (D2T6), and low radiation years (2012 and 2013) have high diffusion and low transmission (D6T4), similar to what has been published recently [150]. The rest of the years have a median combination of diffusion and transmission (D4T5). Therefore, on the basis of the trend from these data, and the look up table (Table A2), it is feasible to predict the DT values for running the model, without the need to run simulations to recalibrate the model for annual estimations.

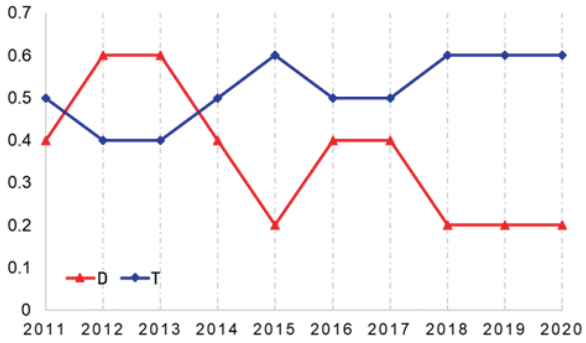

Figure 4-7: Graph with best fit D and T values plotted for the years 2011–2020.

Table 4-2: Best fit DT values on an annual basis and the corresponding PD

Year	DT Year	PD (%)	GHI_{meas}
2011	D4T5	0.78	1026.04
2012	D6T4	0.92	988.75
2013	D6T4	0.56	1003.51
2014	D4T5	2.18	1040.74
2015	D2T6	1.59	1073.18
2016	D4T5	2.07	1039.47
2017	D4T5	0.2	1020.04
2018	D2T6	4.13	1137.19
2019	D2T6	0.78	1098.79
2020	D2T6	3.11	1125.27

4.3.3. Validation of the Calibrated Values

The calibrated values for the year 2020 were used to model the irradiation for a built-up area close to Cabauw. The results of the default model and results with calibrated models are shown in Figure 4-8. Although, the underestimation in the default model is evident, it still captures the surroundings efficiently. The relationship of the default values to the calibrated year values is linear. For the case of the default model, building classification in terms of suitability and delineation of suitable areas on the rooftop can still be done on the basis of the regional min–max values of modelled solar irradiation. On the other hand, calibrated values provide more possibilities in terms of potential estimations. Therefore, potential area estimations can still be made when using the default model without calibration, as long as the irradiation values are not directly used to estimate the power production or capacity. This is especially valid for high resolution analyses. During the validation of images, high values were observed (see Figure 4-8), especially on south facing roofs, for the

calibrated models. This could be due to the fact that the model was calibrated using data from one point (the KNMI meteorological station at De Bilt).

The complexity involved in calibrating the ArcGIS model refers to the fact that one measured value is used for a whole geographic area, be it measurements from the closest ground station or a central location. In addition, the only atmospheric parameters which can be changed are the D and T. This means that for high resolution rooftop analyses, even the calibrated values may sometimes fall short. An example is shown in Figure 4-9, where the irradiation profiles from different roof types are presented. Figure 4-9a shows the DEM of a small selection from the area used for validation purposes along with the locations selected for creating the radiation profiles. Small areas on the rooftops with different orientations were selected, blue for north, red for south, pink for east, orange for west and green for flat. All these locations are highlighted in the figure.

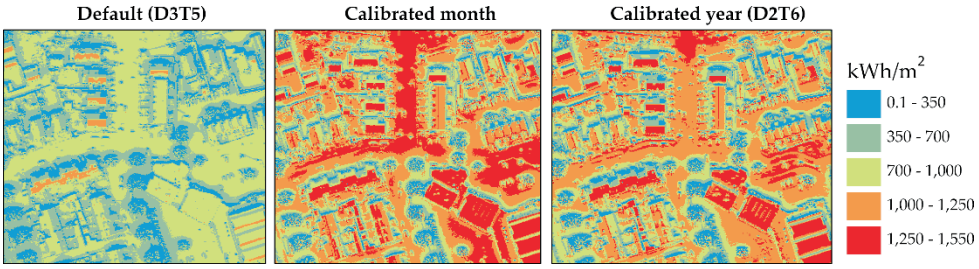

Figure 4-8: Modelled irradiation for a geographic area with default model (D3T5) and calibrated models.

Figure 4-9b shows the corresponding ranges of irradiation values for each image created by the default and calibrated models in boxplots and the mean values of the selected roof areas, plotted as lines. The measured value at Cabauw is depicted as a black line at 1155 kWh/m² (for 2020).This value is closer to the first quartile for the monthly calibrated model, median for the yearly calibrated model and third quartile

for the default model. In this scenario, using the calibrated model to model irradiation on the images or rather larger geographic areas instead of point locations, one DT fit per year can be seen to perform better.

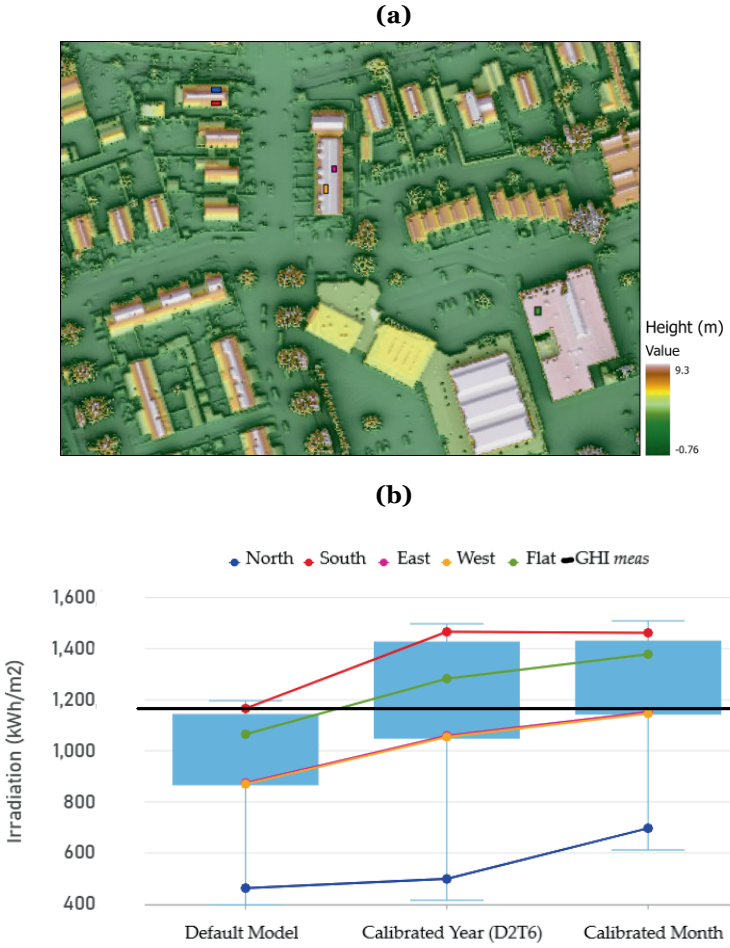

Figure 4-9: (a) Colorized digital elevation models (DEM) with selected areas on different roof orientations and slopes. (b) box plot of irradiation values in the images for the default and calibrated models for 2020 with mean lines from the selected areas of different roof types.

In all three cases east–west facing roofs have irradiation values closer to the first quartile. Flat roofs have a value that is larger than the median but only for the calibrated models, this is also larger than the measured irradiation. South and north facing roofs are closer to the maximum and the minimum values in the region and are significantly higher or lower than the measured values. The south facing and flat roof values from the default model are closer to the measured values, while the calibrated models overestimate the irradiation values. This suggests that the default model performs adequately when used for annual calculations and that it has a linear relation with the fitted models.

4.3.4. Irradiation Modelling with Varying Spatial Resolution

The purpose of using ArcGIS is to be able to analyse solar irradiation based on location. Locations can vary from a point (latitude–longitude), a particular building, a street, a neighbourhood or even a country. As mentioned earlier, the scale and purpose are important in selecting the required spatial resolution. Figure 4-10 shows the effect of spatial resolution in modelling solar radiation. It is evident as to which types of analysis are possible with the resulting images.

The very high resolution of 50 cm is quite good for bottom-up analyses in urban applications of suitability modelling or power production and capacity estimations. On the other hand, 5 m, for example, can be used for modelling parking areas or fields or even for providing a general suitability classification of neighbourhoods. Low resolution images can be useful at a regional or national level for very broad or generalized figures. It should also be noted that the processing time is also related to the input resolution. For this study area of about 1 km^2, the processing time recorded while running the default model was 01 m:12 s, 06 m:22 s, and 10 m:7 s, for 30 m, 5 m and 50 cm, respectively. It was executed on a Windows machine with an Intel i5 processor with four cores and eight GB RAM. This can become slightly complex, and the processing time increases when smaller time intervals, higher resolution and larger geographic areas are used.

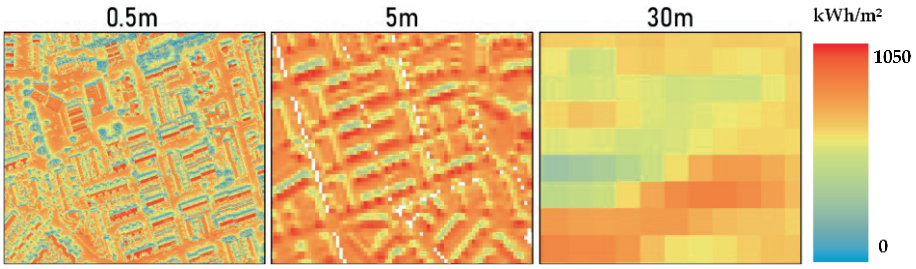

Figure 4-10: Solar Radiation with varying spatial resolution run with the default model in ArcGIS.

4.4. Conclusions

This chapter shows the importance of using validated values of transmissivity and diffusivity for performing irradiation analysis using the ArcGIS Solar Analyst Tool. The analysis shows that there is not one unique combination of D and T values that can be used as a constant for monthly fits; this also means that, for the prediction of solar irradiation for the future, other modelling methods, such as r.sun, are also preferable in terms of control of various atmospheric parameters. However, the Solar Radiation Tool is very simplistic (easy to execute with a minimum number of atmospheric parameters required) and at the same time, it can provide a detailed overview of shading or the effect of orientations and slopes when using high resolution data.

DT combinations are highly dependent on climatic conditions and calibrated values should be used depending on the purpose and scale. Calibrating this model is relatively easy when one has access to measured radiation values and can improve the potential calculations by at least 10–20%, depending on time scales used in the analysis. It was also observed that the monthly variation of the combinations leads to higher accuracy results, which is very useful when modelling energy profiles for households or even for generating accurate potential information which is closer to

reality. When looking at lower temporal scales (yearly) one DT combination will suffice.

When the model is used to predict the annual irradiation, a direct relation could be made with the measured values and, therefore, standardized values can be used, as demonstrated. However, it must be noted that we assume that one single location (De Bilt) is sufficient for calibrating the model. Hence, these values are reliable when using similar data and settings as those used in this study and, therefore, are reproducible and reusable. Better fits can be achieved when the model is calibrated using data from the closest ground measurement station, no matter which resolution or temporal scale is used.

Finally, the spatial and temporal resolution play an important role in this model, which are directly related to the accuracy of the model, level of detail and processing time. We demonstrated the use of ArcGIS in mapping the PV potential, with optimized and validated D and T values. While the method was applied to the Netherlands, it can successfully be applied to other regions. We finally recommend validating the ArcGIS model with local irradiation data before it is used for modelling/mapping purposes, if the values are to be used directly for potential estimations. This information can prove to be useful, especially in driving data dependent policies for PV penetration in order to encourage sustainable energy deployment.

5.

Visualization

This chapter is based on the publication:

B. Kausika, P. Moraitis, and W. van Sark, “Visualization of Operational Performance of Grid-Connected PV Systems in Selected European Countries,” *Energies*, vol. 11, no. 6, p. 1330, May 2018, DOI:10.3390/en11061330

Abstract

This chapter presents the results of the analyses of operational performance of small-sized residential PV systems, connected to the grid, in the Netherlands and some other European countries over three consecutive years. Web scraping techniques were employed to collect detailed yield data at high time resolution (5–15 min) from a large number (31,844) of systems with 741 MWp of total capacity, delivering data continuously for at least one year. Annual system yield data from small and medium-sized installations was compared. Cartography and spatial analysis techniques in a geographic information system (GIS) were used to visualize yield and performance ratio, which greatly facilitates the assessment of performance for geographically scattered systems. Variations in yield and performance ratios over the years were observed with higher values in 2015 due to higher irradiation values. The potential of specific yield and performance maps lies in the updating of monitoring databases, quality control of data, and availability of irradiation data. The automatic generation of performance maps could be a trend in future mapping.

5.1. Introduction

Recent years have seen a constant growth in solar photovoltaic technology (PV). Several countries have utilized this potential to create a competitive market in view of a green energy future, which led to an increase in small and medium-sized residential solar PV installations [151,152]. These small-sized installations (with capacities less than 10 kWp) are scattered and operate under diverse conditions without adequate monitoring equipment. Studies show that most of these systems perform adequately, but due to a lack of systematic data collection, performance validation was mainly focused on specific geographic areas with a limited amount of systems [153,154].

A "Photovoltaic Geographical Information System" (PVGIS) system was designed to provide performance assessments to an accuracy that is suitable for small installations and for estimating the potential solar energy over large regions at any location in Europe [155]. Although this large-scale GIS (Geographic Information System) database of solar radiation and ambient temperature has been created to estimate energy output from crystalline silicon PV systems and solar water heating systems, it does not provide continuous monitoring or performance evaluation for small-sized, grid-connected PV systems.

Currently available monitoring technology in the market is capable of providing owners with sophisticated web tools to monitor their production and system performance at any point during the day, besides measuring energy production. With the advent of such hardware and smart-metering technology, high-resolution monitoring data is publicly available, which is uploaded daily on web platforms, however, in some cases only owners can view this data.

With the huge amount of data that is available due to the monitoring equipment, abnormalities can be compared with additional data (remote sensing imagery) for identification of reasons for underperformance or fault detections [156]. Monitoring small grid-connected PV systems to minimize financial losses has also been explored [157] along with the need for long-term monitoring for reliability and increased PV

performance [154]. In [151,158], the authors show the importance of using a graphical supported analysis of monitoring and operation of PV installations for fault detections. In our earlier work [159,160], we show how technical aspects and geographical location of PV systems affect PV performance. In this chapter, geographic information systems (GIS) are employed to analyse, visualize, and map PV monitoring data from five countries, namely, the Netherlands, France, Germany, Belgium, and Italy. We also present and discuss methods for visualization and detection of underperforming or overperforming systems for further analysis, performance ratio analysis of systems, and spatio-temporal mapping of performance differences.

5.2. Method

Data used for the analyses was collected using online services provided by Solar Log [161] and SMA [162], which also ensured data legitimacy. Solar Log has users over a hundred countries and is one of the major key players in monitoring applications, though it has lost a lot of its clients after 2015. SMA is one of the specialists in photovoltaic inverter system technology. The code used in this research was developed to extract online data and was designed using Python programming [163]. The objective of the web scraping code was to mimic human navigation through web pages of SMA and Solar Log, and to locate and save information that was available to the user [159]. This means that the monitoring information pages of different PV systems was retrieved and saved accordingly. This information was later organized into datasheets. In this way, high temporal resolution yield data (5 min) and other system metadata like orientation, tilt, type of module, etc. were obtained. Recently, privacy constraints have been put on the data, and these data are not available publicly anymore. In total, data from about 31,844 systems were collected for the years 2012–2016 from 5 different countries in Europe, namely, the Netherlands, France, Germany, Belgium, and Italy.

In order to calculate the performance ratio (PR) of all the systems, system yield and reference yield are required. System yield is obtained from the data collected by web

scraping and reference yield is calculated using the Olmo model [164]. This model requires irradiation data [165]. Hourly global horizontal irradiation data obtained from the 31 ground-based stations of the Royal Netherlands Meteorological Institute (KNMI) were used to compute the reference yield for the Netherlands. These stations cover the entire country. For each installation in the database, irradiation data was collected by linking it to the closest ground station, in order to minimize the uncertainties in the irradiation data. Note that no system was further away than ~30 km from the nearest KNMI station. The tilt and orientation for every system has also been obtained from web-scraped data of PV systems. The Olmo model was then used to calculate the total irradiation in the plane of array on an hourly basis. This study does not take into account effects such as shading as the aim of the chapter is to visualize performance rather than detect reasons behind over- or underperformance [166].

The PR was calculated using equation.5.1, where Y_f is the final system yield and Y_r is the reference yield [165]. Since high-resolution, up-to-date annual irradiation data was not available for the rest of the countries, PR was calculated only for the Netherlands.

$$PR = \frac{Y_f}{Y_r} \tag{5.1}$$

Geographic Information System (GIS) is a "powerful set of tools for collecting, storing, retrieving at will, transforming, and displaying spatial data from the real world" [167]. Based on the principles of geography, cartography, etc., GIS is used for integration of different data types. It is a very powerful tool when it comes to analyses of spatial information, layering or organizing layers of information into visualizations using maps and 3D scenes[168]. There are several GIS software packages available in the market today, but ArcGIS [169] is a leading licensed tool for performing powerful geo-analyses, which will be used in this chapter as an example tool.

Visualizations of the performance ratio, the locations of the installations, and yield and performance maps were created using the ArcGIS platform. An inverse distance weighted (IDW) interpolation technique was used to create the performance ratio maps and specific yield maps for different years of data collection. Although data from around 31,800 systems was available (2012–2016), only those systems that recorded data continuously for three consecutive years (between 2014 and 2016) were used to compare the differences in yield generation. This provides an understanding of how system performance varies spatially (over geographic areas) and helps in identifying outliers in the data. In addition to being able to visualize the results, looking into the diffusion of distributed systems within a country or area allows for the computation of geo-statistics pertaining to the region which are useful for policy implementation.

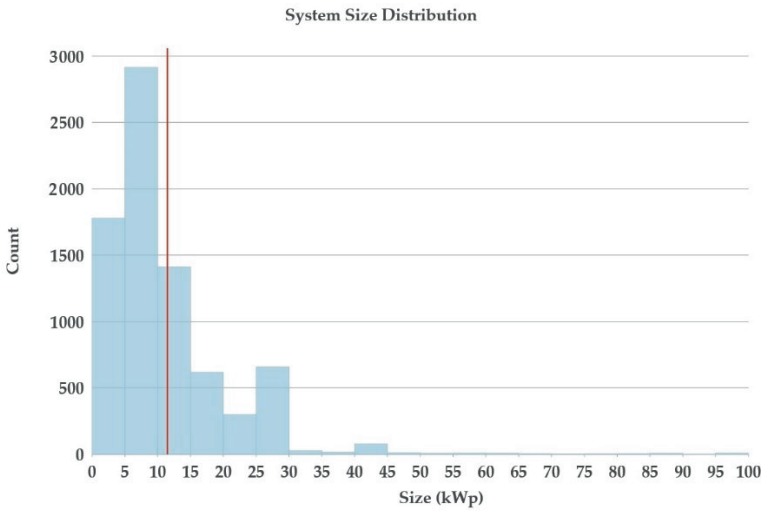

Figure 5-1:System size distribution of systems with capacity of less than 100 kWp for five countries. The red line illustrates the mean value of 12 kWp.

5.3. Results and Discussions

From 2011 to 2016, data from more than 31,800 systems was collected and analysed. However, only 7894 of them were consistently delivering valid data for more than 350 days per year for at least three consecutive years (2014–2016). The total capacity of these systems was about 102 MWp with 56% of them having a lower capacity than 10 kWp and only 1.1% being larger than 50 kWp (see Figure 5-1). The mean value was 12 kWp. The spatial distribution of all the installations with system size information is illustrated in Figure 5-2. The variation in average size and composition of the systems in each country is a direct reflection of the country's policies on PV subsidy schemes.

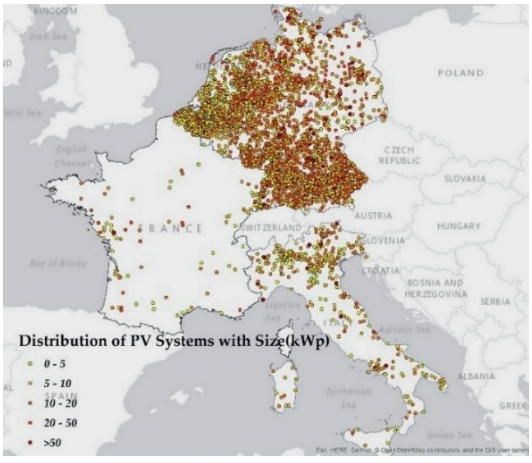

Figure 5-2: Spatial distribution of the data sample for the Netherlands, Belgium, France, Germany, and Italy.

A high concentration of small-scale domestic installations is observed in Germany, Belgium, and the Netherlands with 64% of the systems in Germany. The Netherlands and Belgium have most of the systems' total capacity under 5 kWp. While in Germany only 7.2% of the installations fall in this category, 45% of the PV of the systems installed are still below 10 kWp. Though the monitoring procedure might

have started at a later time, most of the systems from the sample were installed between 2008 and 2014.

Figure 5-2 shows the location of each PV system, categorized by system capacity. Data collected from the monitoring systems and organized in a database was imported into GIS to create this map. Clearly, large numbers of systems are concentrated in Germany, Belgium, and the Netherlands. Some of the systems had faulty location information and hence were not included in the map. From the collected data, density of the systems was higher in the North where irradiation is lower, rather than in the South where there is higher irradiation. The low concentration of systems could also be due to lack of data from the southern European countries.

5.3.1. Yield Analysis and Performance Ratio

The available data was found to be varying through different time periods as new installations were added every year. Also, not all the systems recorded data for all the years. Therefore, only those systems that had been consistently delivering data for the three consecutive years (2014–2016) have been considered for analysis. Furthermore, since the interest is in monitoring small-scale installations, annual yield analysis of systems below 20 kWp for the years 2014–2016 has been conducted for the Netherlands, France, Germany, Belgium, and Italy. These countries were found to have the highest amount of data records from the data collection.

The mean value and the standard deviation of the performance of systems of each sample is shown in Figure 5-3: here we show the annual specific yield, i.e., generated amount of energy divided by system capacity (kWh/kWp). These are known to be affected by a number of environmental and operational factors [170]. Moreover, a wider spread of yearly yield values can be expected from countries covering larger areas as a result of the variation of irradiation levels at different latitudes. The distribution of annual system yield for the Netherlands, Belgium, Germany, and Italy is shown in Figure 5-4. France has only 95 installations between 2014 and 2016 out of which 76 systems are below 20 kWp capacity, while Germany has nearly 3900

systems, and Belgium 1700. Therefore, France has higher mean yields and only four outliers due to sample size. Between 2014 and 2016, the annual yield increased in 2015. However, the decrease or increase in yields falls within standard deviations, but at the same time relates directly to the decrease or increase in solar irradiation on a country level.

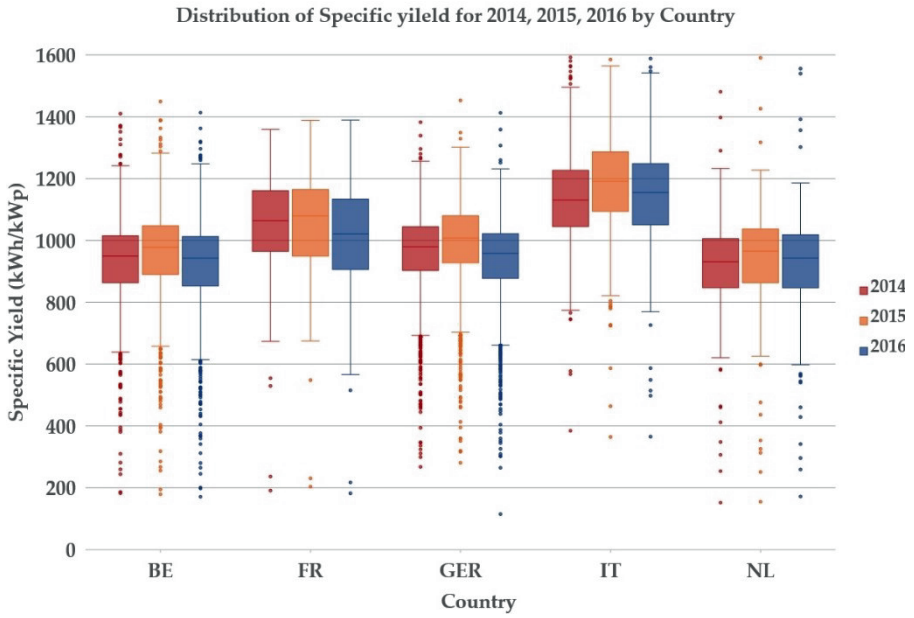

Figure 5-3: Distribution of specific yield by country from 2014 to 2016 for systems less than 20 kWp. Highest yields were recorded in 2015, with Italy (IT) having the highest mean, followed by France (FR), Germany (GER), Belgium (BE), and the Netherlands (NL), respectively.

Performance ratio (PR) analysis was conducted for the Netherlands which revealed a mean PR value of 79% for the year 2016 and 80% for 2014 and 2015. The PR values were calculated with an average daily PR value over a year. These values are close to the results of an earlier study performed in Germany [171]. The sample size for this estimation was about 600 installations. The number of PV installations in the Netherlands significantly increased from 2009, but their performance dropped in 2016 in comparison to 2014 (Figure 5-5). Systems installed in 2013 performed well in

2014 and 2015, while in 2016, a lot of outliers were observed. In some cases, the large variation in PR values could also be due to technical errors in data collection.

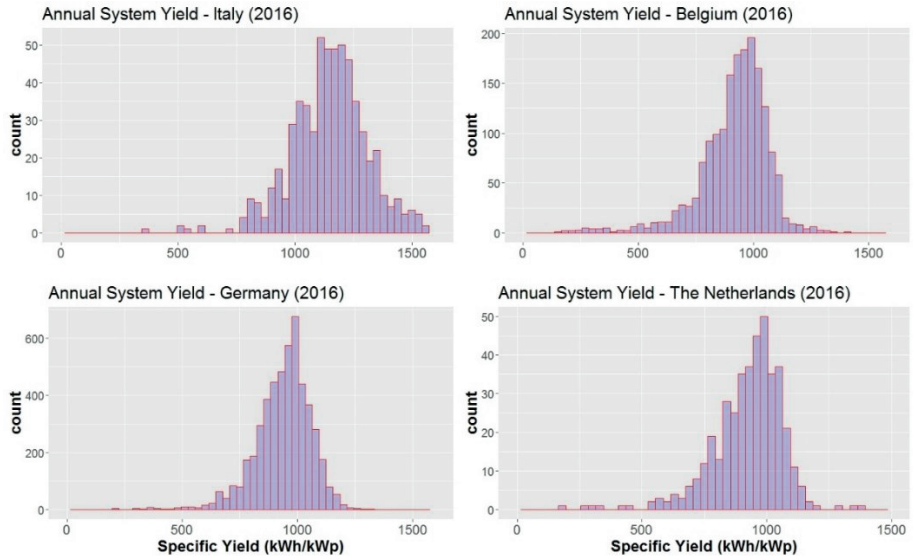

Figure 5-4: Distribution of specific yield for the year 2016 for Italy, Germany, Belgium, and the Netherlands.

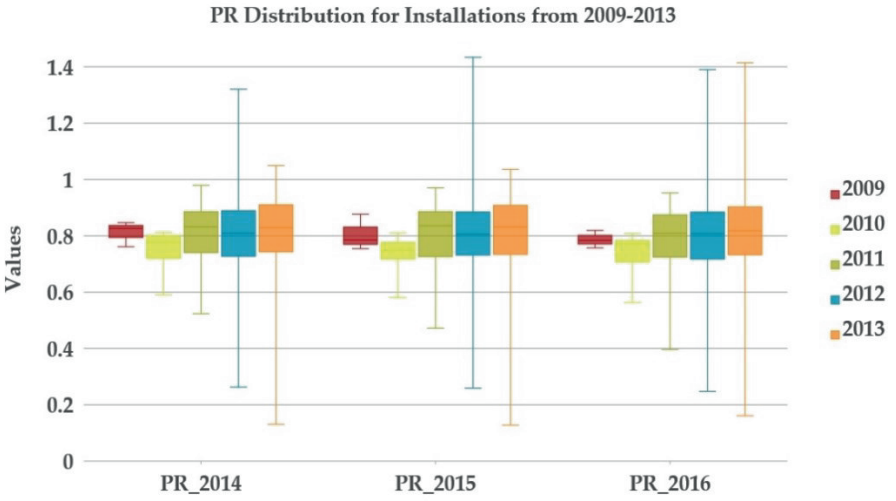

Figure 5-5:Distribution of performance ratio of the Netherlands between 2014 and 2016 for systems that have been installed from 2009 to 2013.

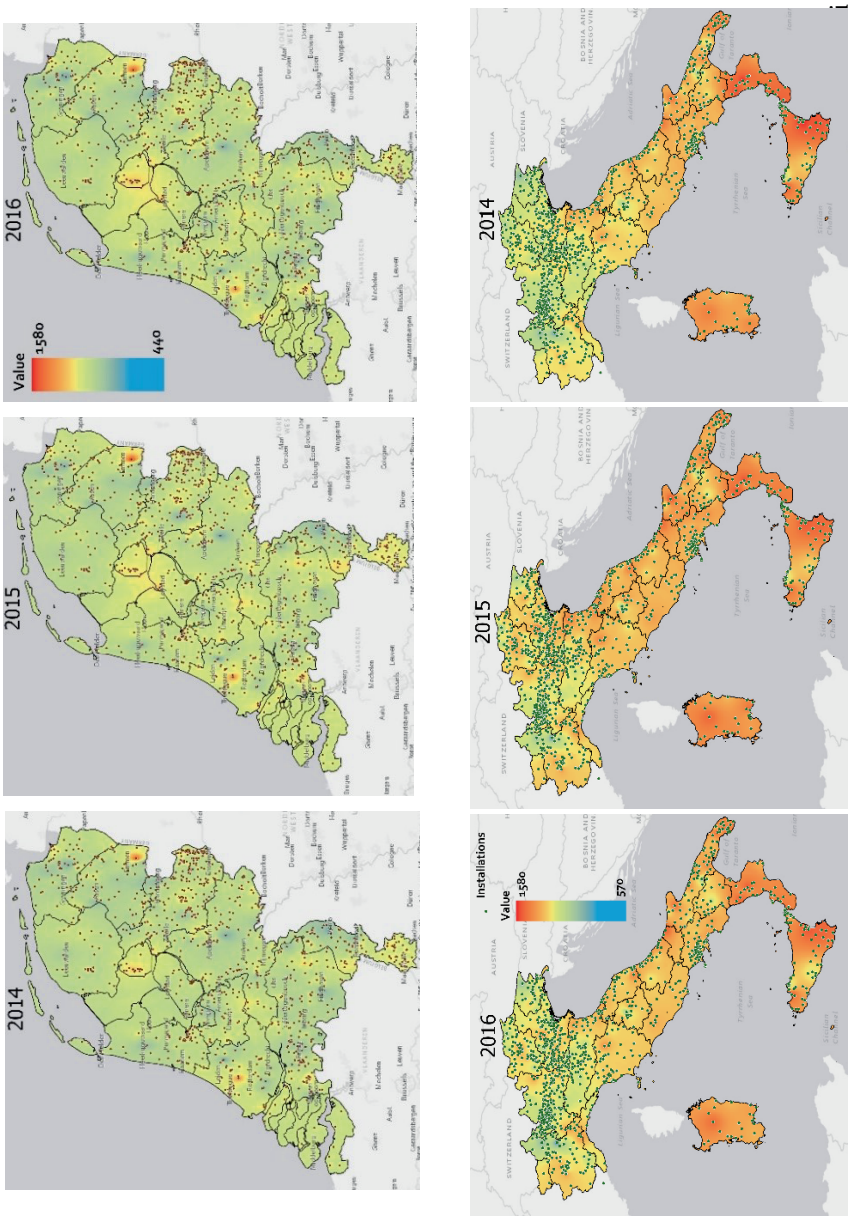

Figure 5-6: Annual specific yield variation from the installations (up to 20 kWp) in the Netherlands (**above**) and Italy (**below**) for the years 2014–2016, visualized using interpolation techniques

5.3.2. Geographical Variation of Specific Yield

Point data (vector information) collected from the web monitoring services has been converted to images (raster information) by using interpolation techniques. Interpolated data is visualized using colour scales stretched using specific bins of annual yield values. From these images/maps, outliers can be quickly discerned to locate PV systems with minimum or maximum yields, thus providing a starting point for further analyses into the reason behind the system's under- or overperformance. The maps can be compared to the country irradiance maps to check for irradiation trends in the particular year, as yield values are related to irradiation values. This provides a quick approximation of the variation of performance over the country. Figure 5-6 shows an interpolated map of annual yield of the Netherlands and Italy for three years with dots representing the location of the systems. Inverse Distance Weighted (IDW) interpolation technique was used to generate the maps. Higher yield values have warmer and darker shades (reds), and lower yield values have a blue shade. A variation in yield values is observed within the countries, while it should be noted that these variations can further be optimized using different colour scales and data stretching methods. A few examples of this are shown below.

Although variations over the years are not very prominent because of the type of stretch used for data visualization and the data sample (system size up to 20 kWp), it could still be distinguished that 2015 has higher annual yields. A min–max stretch was used to visualize data with the same scale of minimum and maximum values for the three years to maintain consistency.

When using a different data stretching method (see, for example, Figure 5-7a), extreme deviations in data (bright spots) can be identified around systems with extreme yield values. These extreme values carry a higher weight factor during interpolation causing the spot or bleeding effect. As mentioned earlier, these spots can be separated out as outliers or as inadequately performing systems. Moreover, if high resolution irradiation data is available, the database of collected information could be explored by irradiation zones in addition to spatial diffusion or technical criteria.

An example of different stretching techniques is shown in Figure 5-7, in which two types of data stretching were used over a colour scale. In Figure 5-7a, a percentage clip method was used, where the values displayed are cut-off percentages of highest and lowest values, while Figure 5-7b displays values between the actual or set minimum and maximum. A smoothing effect can also be seen in Figure 5-7b, while it is easier to pick out underperforming or overperforming systems to analyse them further from Figure 5-7a.

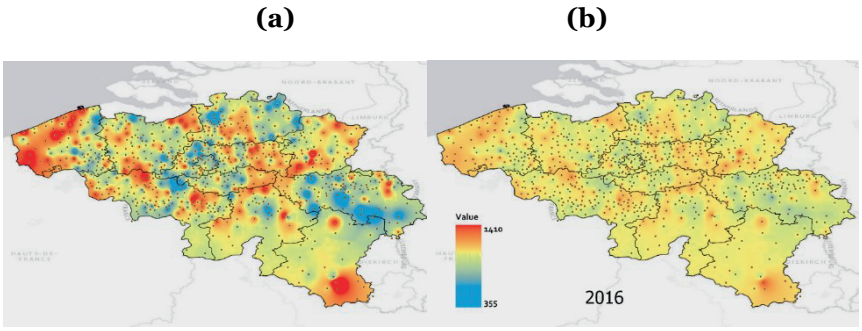

Figure 5-7:Annual specific yield variation from the installations (up to 20 kWp) for Belgium visualized using two different types of data stretching for 2016. Data stretching techniques (a) percent clip and (b) min-max used for data visualization.

Another example of the power of GIS in visualization is shown in Figure 5-8, where the mean specific yield for Germany using different thresholds of system sizes is presented. The variation in specific yield of systems up to 20 kWp is much smoother compared to when only systems up to 10 kWp are considered. For example, the systems in the highlighted area (red box in both images) shows underproduction when compared with larger systems (<20 kWp) while, on comparison with smaller systems (<10 kWp), they seem to be performing adequately. Also, it can be seen that a few systems seem to be less efficient in both categories, which means they could actually suffer from a malfunction.

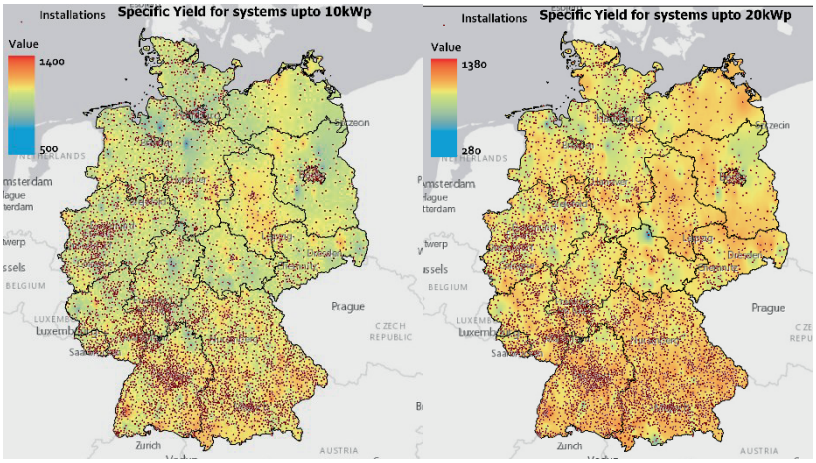

Figure 5-8: Specific yield variation from the installations in the Germany, for different system sizes.

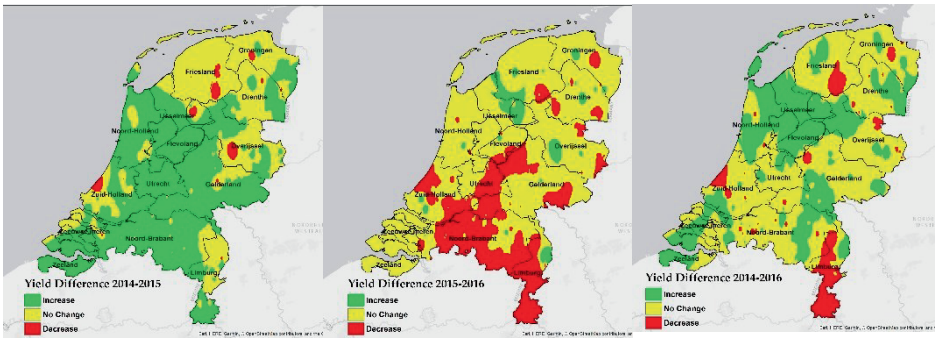

Figure 5-9: Specific yield difference maps for 2014–2016 for the Netherlands.

5.3.3. Mapping Performance Differences

Differences in specific yield for three years for the Netherlands are shown in Figure 5-9. This has been calculated based on the yield maps generated by interpolation. Areas in red show decrease in yield, while areas in green show increase in yield for different years. Yellow regions are regions of no change. The limits for no change were set at –20 to +20 kWh/kWp (~2% of annual specific yield) and anything higher or lower than these values was recorded as increase or decrease in yields. Increase in

yields were observed for most of the regions from 2014 to 2015, while from 2015 to 2016, the yields were either constant or decreased. When looking at differences from 2014 to 2016 compared to 2014–2015, lower yield values were observed in the south of the Netherlands. In general, these differences can also be visualized with scatter plots. The advantage of using mapping techniques to visualize difference data lies not only in knowing how large the change is, but also in being able to see where the change is taking place. Maps of yield differences should be used in conjunction with maps of irradiation differences to explain the yield differences, or one can map the performance ratio differences.

5.4. Conclusions

In this study, GIS has proven to be an excellent tool for visualization of yields and performance of scattered, small-sized, residential PV systems over wide-spread areas. We were able to successfully demonstrate this for the Netherlands and a few other countries like Italy, Germany, and Belgium. Additionally, geo-processing tools (hot-spot analyses, network analyses) could provide useful information to individuals or policymakers to make informed decisions. This could be done if information (system metadata) pertaining to all the installed PV systems is available.

This chapter further provides an update on performance of residential PV systems scattered in a few European countries. It was found that the year 2015 showed a higher specific yield in kWh/kWp compared to the years 2014–2016. Performance ratio for the Netherlands did not change with respect to earlier years, although there is an increase in extreme values with the increase in number of installations. Access to high-resolution irradiation data for all the countries is necessary to analyse temporal variations in performance ratios of PV systems. Recent reports suggest an increase in performance ratio values [171–173], however, long-term changes over expected lifetime of the systems should be analysed to show if performance ratio values still are increasing.

Building up and expanding the present PV performance databases to other countries will provide up-to-date performance maps of more countries. In addition, irradiation maps can be combined with yield maps in order to construct maps of performance to understand the relationship between climatic zones across the world and performance of PV systems.

6.

Policy Evaluation

This chapter is based on the publication:

B. B. Kausika, O. Dolla, and W. G. J. H. M. van Sark, “Assessment of policy based residential solar PV potential using GIS-based multicriteria decision analysis: A case study of Apeldoorn, The Netherlands,” Energy Procedia, vol. 134, pp. 110–120, Oct. 2017, DOI: 10.1016/j.egypro.2017.09.544.

Abstract

The Postal Code Rose policy is part of the 2013 Dutch Energy Agreement of the Social and Economic Council of the Netherlands, introduced to support sustainable energy growth. This chapter presents a case of the Dutch Postal code Rose policy by developing a method combining geographical information systems (GIS) and multicriteria decision analysis (MCDA), which allows determining the solar photovoltaic potential when fully applying this policy. As case study, the city of Apeldoorn in the Gelderland province of the Netherlands was selected. The research evaluates the technical potential of the city and then applies it to the Postal code Rose framework by using social criteria. The social criteria comprise of the most important factors that play a role in the adoption of solar PV. The results showed that by fully applying the Post Code Rose policy ~77% of the total electricity demand of Apeldoorn could be covered by solar PV.

6.1. Introduction

In recent years, the rapid depletion of fossil fuels and its association with climate change pushed the renewable energy technologies to the forefront. Diffusion of renewable technologies is of interest to policy makers and national agencies who wish to tackle global climate change. For example, the EU has defined its 20-20-20 goal: 20% reduction of greenhouse gas (GHG) emissions, 20% renewable energy and 20% reduction in energy use by 2020 [174]. In the Netherlands, a policy program called “Clean and Economical” (in Dutch: “Schoon en Zuinig”) from the Ministry of Housing, Spatial Planning and the Environment [175] has been introduced. This policy originally set a target of a 30% GHG emission reduction in 2020 compared to the levels of 1990 and 20% of the total energy demand covered by renewable energy sources. After a few years, these targets were reset to 20% reduction of the GHG emissions and 14% renewable energy production by 2020 [175].

Policies indirectly affect the reduction of GHG’s, by aiding the decision of adoption of renewable energy technologies. Policies can also induce change at the smallest scale: at household or an individual level. An example is the postal code rose (PCR) policy: a sustainable energy initiative, introduced by the Dutch government. It targets to increase energy generation using solar panels by local cooperatives. Investment in solar panels becomes attractive under such policies. In addition, the driving factors of solar photovoltaic (PV) adoption vary from financial, information regarding the technology and social learning. It is advantageous to look at the policy implications from a spatial perspective as it could provide insight as to which places have a high potential for the policy to succeed. This also provides information on the spatial patterns of PV diffusion which is of interest not only from a scholarly perspective, but also from a policy and marketing perspective [176].

As an attempt to quantify the potential for PV systems, that would be possible as part of the PCR policy, this chapter presents a method to estimate the PCR potential for a city (Apeldoorn) in the Netherlands. The method uses a combination of multi-criteria decision analysis (MCDA) and geographical information system (GIS) modelling. The MCDA method is suitable for comparing different factors that play

an important role in the adoption process of solar PV, and GIS helps with the spatial analysis of the criteria.

6.1.1. Postal Code Rose Policy

In 2008, the Dutch Ministry of Economic Affairs introduced a subsidy for power generation from solar panels, as part of the subsidy scheme renewable energy (SDE, "Stimulering Duurzame Energieproductie"). The subsidy was at € 0.33 /kWh with a payback period of 15 years (Renewable World Energy Press, 2008). After this, the development of solar energy was so fast that in 2012 the installed capacity from 146 MW rose to 371 MW. After the second half of 2012, PV became more attractive under the national investment subsidy of "energy and innovation" which provided a grant up to 15% of the investment cost for each system above 0.6 kWp and a maximum of € 650 per system. The budget was up to € 22 million and in 2013 it increased to an amount of 30 million. In terms of statistics, in February 2013 there were 52,221 solar system owners and in September 2013 this number increased to 106,998 and 665.47 MW of solar PV capacity installed [177,178]. By the end of 2015, about 400,000 system owners together have 1.5 GWp installed [179], see Figure 6-1.

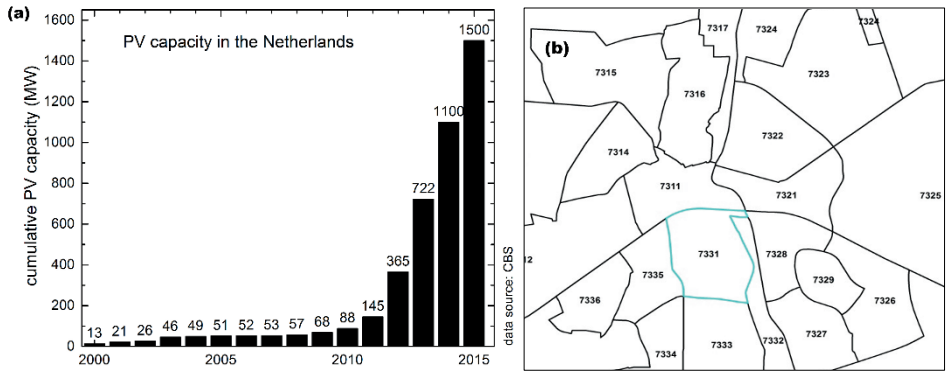

Figure 6-1:(a) Development of cumulative installed PV capacity in the Netherlands (data from CBS (2016)). (b) Postal Code Rose around a central postal code.

Recently, the Social and Economic Council of the Netherlands introduced the Energy Agreement in order to accelerate the pace of renewable energy technologies deployment mainly focusing on offshore wind. This agreement includes ten components that are linked to renewable energy, innovation and export, transmission network etc.

Without detailing the others, the third component of the Energy Agreement states that the main target is to decentralize the generation of renewable sources by people themselves and by cooperative initiatives [180]. Apart from the tax relief of € 0.075 per kWh (in 2013, changed to € 0.09 per kWh in January 2016), the policy focuses on the electricity generation by a cooperative or by an association of owners. This energy should be utilized by small-scale consumers and members that should be located within the postal code area surrounding the postal code in which an investor is registered [180]; this was termed as postal code rose (in Dutch "postcoderoos"), mimicking the rose flower with a central core and surrounding petals. To understand PCR (Figure 6-1b) suppose there is a sustainable energy initiative in the post code 7331, each participant in the zip codes 7333, 7334, 7335, 7311, 7321, 7328, 7332 and also 7331 itself can avail the so-called energy tax reduction on every kWh generated which is in proportion to the total yield of the overall project. The idea is that participation in the joint project will mean 50% return on the energy, along with returns from the project.

6.1.2. Factors Affecting Policy Diffusion

Studies have been performed in order to explore the characteristics of technology diffusion, such as the role of policies [181,182] and the social interactions towards a new product and economic factors [183,184]. When it comes to factors influencing the adoption of solar PV, there is little said and not all the factors have been addressed together. Studies show how consumer behaviour changes if a neighbour has PV or how income and knowledge affect financial incentives [176,185–193]. This chapter addresses socio-economic factors mainly due to data constraints. Since the focus is on policy at household level, we considered the following factors which were identified as quantifiable and relevant to the PCR policy.

- Economic factors like house value and average income
- Social factors/ peer effects
- Technical/knowledge factors

6.2. Data and Method

Data relating to socio-economic factors like household value, average income and electricity consumption were available at neighbourhood level. Since the PCR policy works at 4-digit postal code (PC4) level, all the data was aggregated to PC4 level. The procedure of building the database in GIS was made by ArcGIS 10.2. In order to implement the MCDA, the criteria that will be used for the evaluation must be expressed in quantitative values. Multicriteria evaluation of a problem is not easy, either economically or mathematically. Usually there is no optimal solution and hence the influence and the weighting of criteria should be adapted according to the problem. The methodology shown in Figure 6-2 consists of the following steps:

- Development of a digital GIS database that includes all spatial information.
- Determination of the evaluation criteria/sub criteria for the multiple criteria analysis.
- Implementation of the analytic hierarchy process method to calculate the criteria/sub criteria relative importance weights.
- Implementation of a MCDA to reveal the potential of PV capacity of the PCR policy.

When it comes to site selection problems or suitability models, the spatial MCDA (Weighted Overlay) is the most commonly used method [194]. Assigning weights to each criterion in a scientific way is necessary to ensure replicability and robustness of the model. Therefore, the Analytical Hierarchy Process (AHP) [195–197] was used to pairwise compare the criteria instead of assigning weights to each criterion directly. The steps of AHP which were implemented are as follows:

- Determine significant criteria.

- Set up criteria comparison matrix and grading.
- Normalize the comparison matrix.
- Check for consistency

After the grading, the influence or weights of each criterion is known. The influence is then used in the weighted overlay analysis in GIS. The flow diagram of the weighted analysis and the final determination of PCR potential per PC4 are shown in Figure 6-2 (A). All the criteria layers were divided into 3 subcategories and graded accordingly (1-3 in this case).

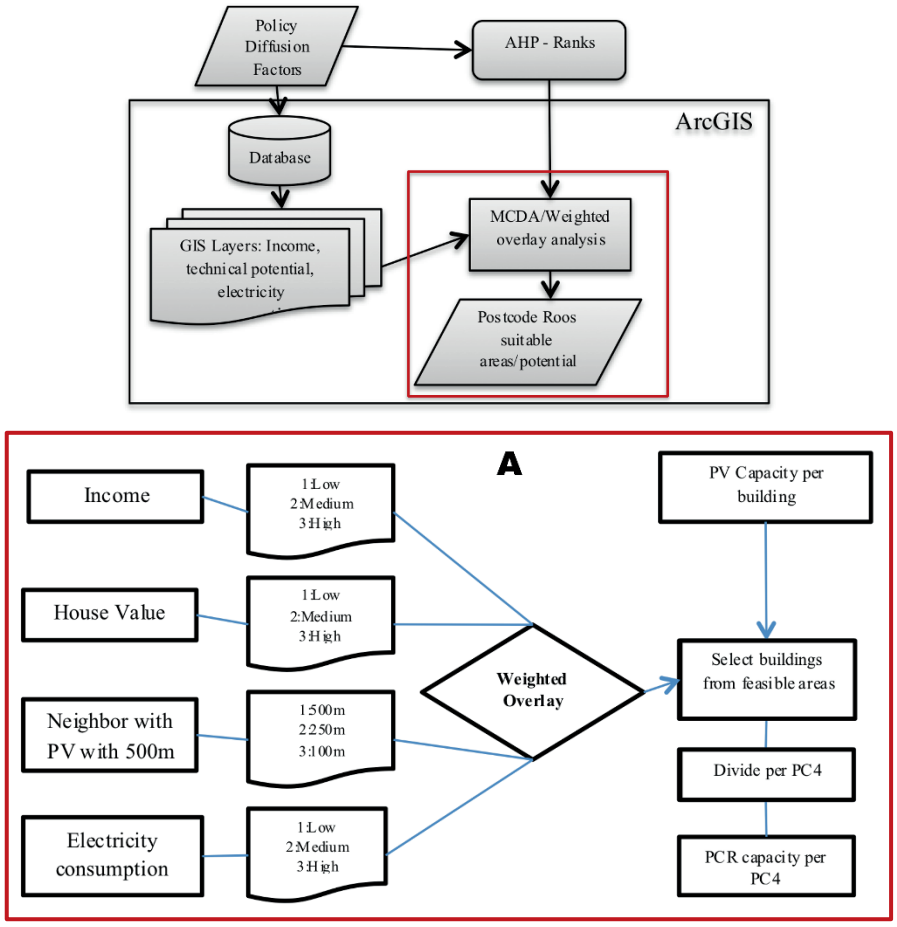

Figure 6-2: Methodology flowchart. (A) shows in detail the weighted analysis highlighted in the left image.

This means that if the income is high then the chance of PV adoption is higher, therefore, it is graded at 3. Similarly, for peer effects, the closer the neighbour with PV the greater the influence. In this case, buildings with existing PV panels have been mapped. For these buildings, a buffer up to 500 meters was calculated in 3 steps in order to see which buildings could be affected from the peer effect that increases the probability of solar PV adoption. The technical PV potential for the residential sector of the whole city was calculated using high resolution Lidar data. The PV capacity estimated per building was analysed by determining the rooftop suitability for PV siting and applicable calculations to estimate the capacity that can be installed [198]. This information was used after the weighted overlay, as a mask to single out buildings or suitable adopters.

6.3. Results

According to the data provided by the municipality of Apeldoorn, the income, house value and electricity consumption available at neighbourhood level was aggregated to post code level and mapped, see Figure 6-3. For neighbourhoods that have no data, average values were used, so that it would result in a better estimation. The low-income category is neighbourhoods with income up to € 30,000. The second category is between € 30,000 and € 40,000 in which most of the neighbourhoods are included. The last category is the optimal category for investing in Solar PV with more than € 40,000, as a significant amount of capital investment is needed. Similarly, house value and electricity consumption were divided in 3 categories as shown in Figure 6-3. It is evident from Figure 6-3 that the socio-economic demographics vary spatially. low-income groups are concentrated around the city centre, with low house values and high electricity consumption. As we move from the centre to the sub-urban parts of the city, the income is higher, and the house value also increases.

The technical PV potential was estimated at 275 MWp for the residential sector of Apeldoorn. According to the registry, about 2,279 panels with a capacity of 5.8 MWp has already been installed in Apeldoorn by 2015.

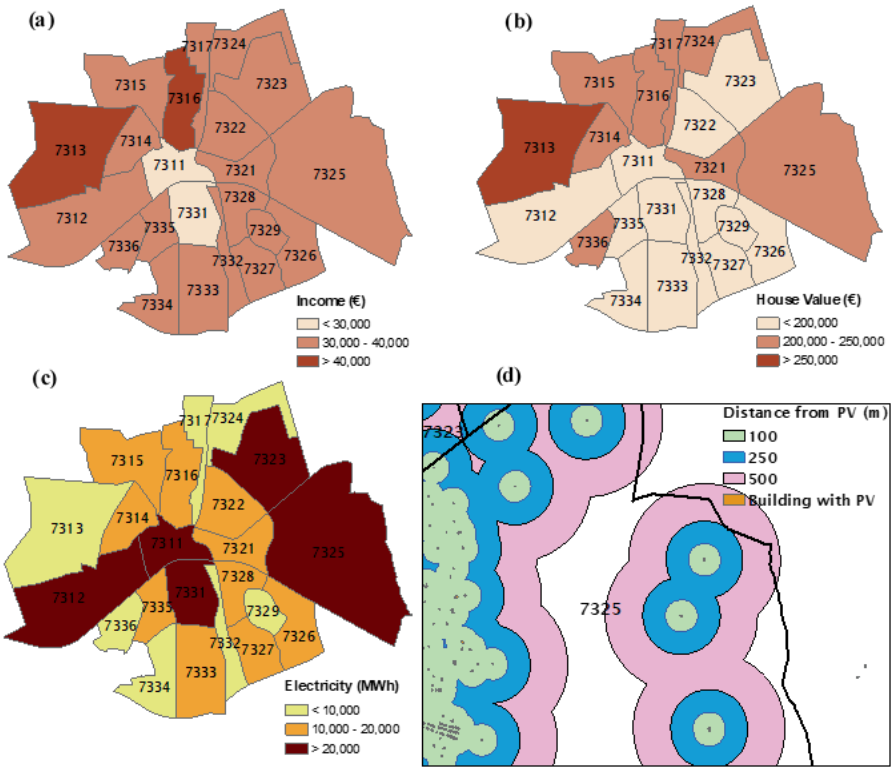

Figure 6-3: Map Layers after the categorization of criteria. (a) Income; (b) House Value; (c) Electricity consumption (d) Neighbor with PV within 500 m

In Table 6-1(A), the pairwise comparison of the four criteria is shown. AHP, i.e. the final grading after the normalisation of the pairwise comparison matrix and the ranking of the criteria (Table 6-2), was performed on data from Table 6-1. For example, the income of a household is considered more important than the house value (to be able to adopt PV), then a value3 is given which means that the income factor is moderately more important than the house value factor, see Table 6-1(B). Regarding the values that are less than 1, it means that the second factor compared is more important e.g., House value/Income =1/3 = 0.33.

Table 6-1: (A) Pairwise comparison matrix for selected criteria. (B) Grading of criteria based on relative comparison [23].

A

Criteria	Income	House value	Electricity consumption	Neighbor with PV
Income	1	3	4	3
House Value	0.33	1	3	1
Electricity consumption	0.25	0.33	1	0.33
Neighbor with PV	1	1	3	1
Total	1.91	5.33	11	5.33

B

Scale	Degree of preference
1	Equal importance
3	Moderate importance of one factor over
5	Strong or essential importance
7	Very strong importance
9	Extreme importance

Table 6-2: Final ranking of criteria and scoring.

Criteria	Influence	Rank
Income	50.7%	1
House Value	20.4%	2
Electricity consumption	20.4%	2
Neighbor with PV	8%	4

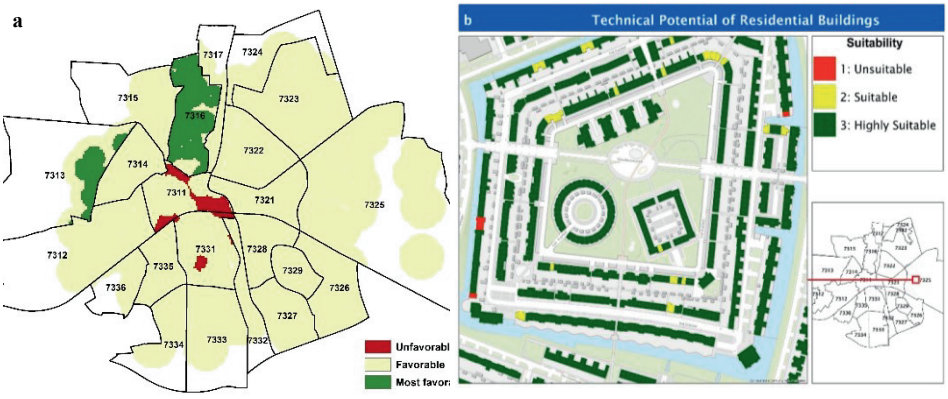

Figure 6-4: (a) PCR areas showing probability of solar PV adoption. Areas in green are likely to have the highest number of adopters, areas in red are least likely and areas in yellow could go either way. (b) Technical Potential map showing suitable and unsuitable rooftops (detail of postal code 7325).

The result of the combination of the four adoption criteria is the suitable areas that have higher probability of adoption. A weighted overlay analysis of all ranked criteria (based on Table 6-2) performed in GIS shows the most feasible adopters of solar PV. Furthermore, combining the suitable buildings with the suitable adopters with

design of PCR policy gives the PV potential of PCR policy per postal code. Figure 6-4(a) shows the favorable regions of for PV adoption. The green color shows the suitable areas and the red color the ones that are not likely to invest in solar PV.

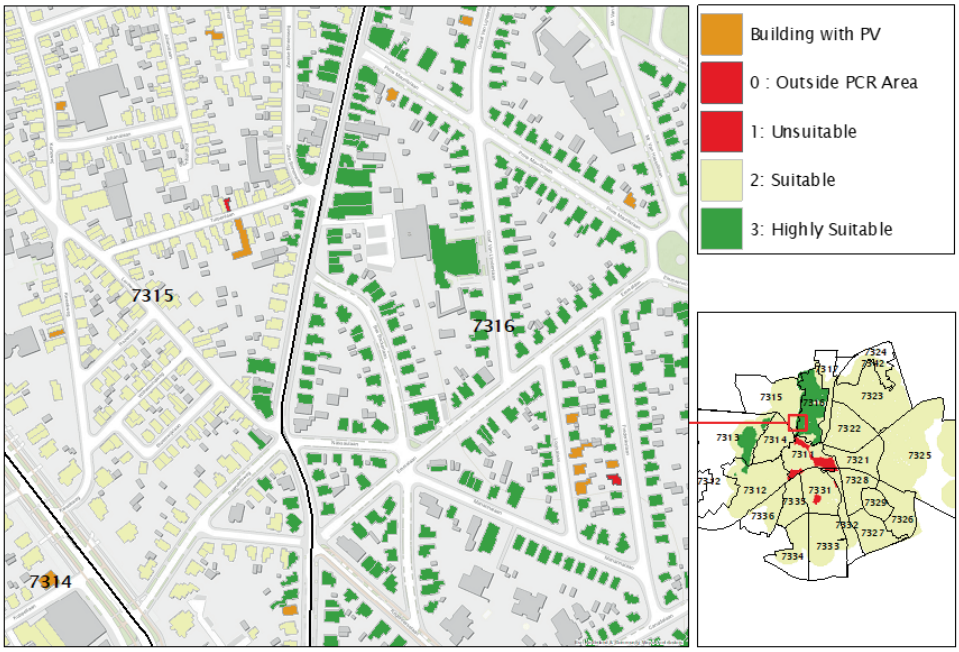

Figure 6-5: Residential buildings that could adopt solar PV due to PCR policy.

Combining the PCR areas with the buildings suitable for PV siting (Figure 6-4(b)) from the current status scenario, shows buildings that have a higher probability to adopt solar PV based on PCR policy. This final result is shown in Figure 6-5. Buildings that are within unfavorable areas (denoted in red) are excluded. Postal code 7316 and parts of 7313 were found to be the most suitable to adopt solar PV. Postal code 7311 has neighborhoods where solar PV adoption is not favored due to low income and low house values even though it is characterized by high electricity consumption. The peripheral postal codes, i.e., 7315, 7316, 7317 etc., would have influences from adjacent postal codes which are not considered in this case. This means that the PCR capacity from these postal codes could be underestimated or over estimated.

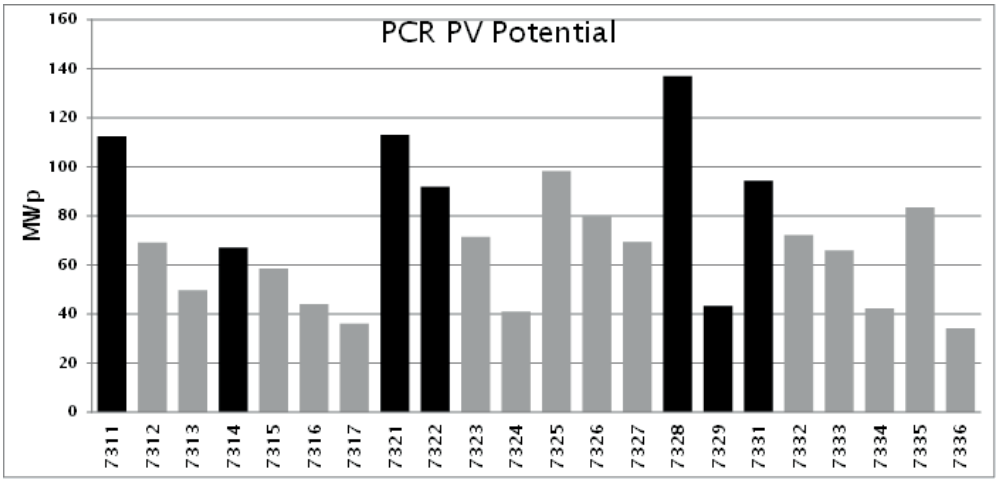

Figure 6-6: PCR capacity per postal code in MWp with the central postal codes in black.

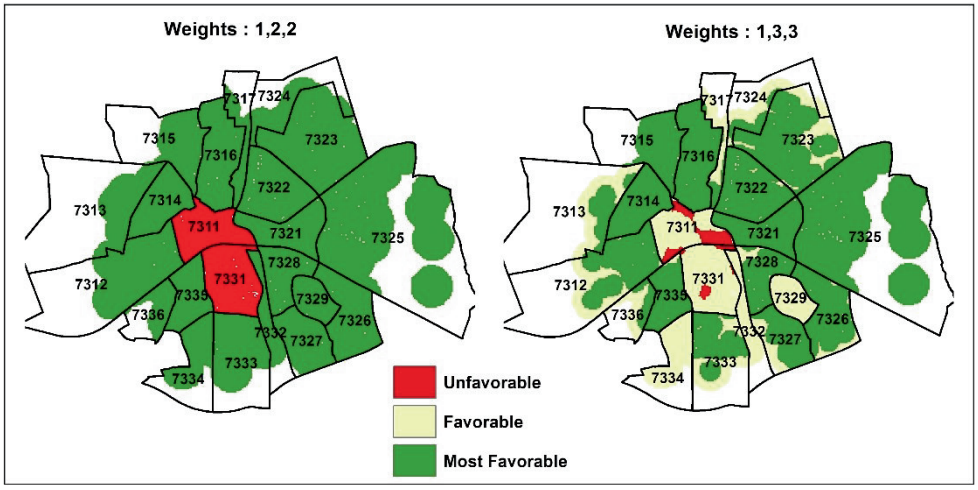

Figure 6-7: Sensitivity due to change in weighting.

For the central postal codes, i.e., 7311, 7314, 7321, 7322, 7328, 7329 and 7331, the PCR capacity can be estimated applying the full potential of the policy. They are perfect examples of the potential effect of PCR policy. These postal codes are also the ones with the highest potential as can be seen from Figure 6-6. The PV potential after applying the policy was found to be 260 MWp. The difference between the full technical potential and the potential after policy implementation is very little (3.5%).

6.4. Discussions

This chapter has shown that the combination of a multi-criteria analysis and GIS can make it easier to understand and analyse policy incentives for decision makers that target local PV adoption. By using illustrative maps, decision makers can solve accurately a lot of problems. This study has shown how a complex policy can be further decomposed to simple parts that can be communicated to and by anyone.

By applying certain necessity and sensitivity tests and analyses, policy makers can be aware of the factors that play a significant role in the decision-making problem. This will provide them with the knowledge of which factor they should be more aware of, and which factors need to be improved in quantitative terms. Hence, it can improve and optimize the criteria combination, change the analytical structure and reduce the sensitivity in criteria grading and make results qualitatively better, stronger and more convincing.

Regarding the limitations of the research the main issues come from the fact that social criteria were used in the research. This means that usually high uncertainties express this kind of data and grading of the criteria is highly dependent on the geographic conditions. In addition, the weighting analysis requires the grading/scaling of sub criteria. This means the weights should be assigned to the sub criteria as well and this has an impact on the final results. For example, in the analysis since all the factors were graded on a scale of 1-3, they have been weighed accordingly. If these weights were changed, for example all the factors (sub criteria) are now graded as 1, 2 and 2 i.e., the medium and high groups are given equal weights, the final result shows sharper boundaries as shown in Figure 6-7. Varying the weights of the sub criteria gives different outputs.

Data availability was one of the main limitations of this research, which was due to the fact of privacy restrictions regarding the residential sector. The methodology that was implemented might underestimate the PV potential and therefore the final probability of adoption, as the criteria for PV potential analysis were conservative,

i.e., the area should receive more than 50% of the average irradiation of the area and rooftop availability for PV siting was set at 40%.

In future research, the inclusion of essential sensitivity tests is expected to overcome the shortcomings of this research and many repeated operations of the MCDA and GIS models that were used in this study. More criteria such as environmental awareness of the adopter, and NIMBY effect etc., are expected to be used that could improve the model and more accurately forecast the adoption of solar PV systems. In addition, the inclusion of factors like age and knowledge could provide valuable insights. Furthermore, more detailed and better-quality data for the selected criteria could be used that would give more accurate results and finally a wider potential analysis that would not only be used for a specific area or city but for the whole country of the Netherlands could be developed.

6.5. Conclusion and policy implications

This chapter discussed the main drivers that could play an important role in the decision-making process of the residents regarding solar PV. GIS is very useful in exploring spatial relationships of complex problems like policy effects as shown and using these tools helped in the estimation of the maximum solar PV potential by applying four technical criteria: solar radiation, slope, elevation and orientation.

In order to apply the PCR policy to the maximum solar capacity four social criteria were applied which according to literature were the most important ones for the adoption of solar PV: income, house value, neighbors with PV and electricity consumption. The analysis of the policy was made on 4-digit postal code level that revealed that the potential after the application of the policy is 266 MWp for the case of Apeldoorn.

Using the established annual yield number that is used by the Dutch Statistics Bureau (CBS) of 875kWh/kWp [199], the amount of annual PV energy that could be generated is 222.75 GWh, which is ~77% of the average electricity demand of the city of Apeldoorn.

This methodology can be applied for any city or neighborhood that wants to apply the PCR policy. It showed that apart from the fact that there is a significant solar PV potential there are also factors that influence the solar PV diffusion such as social factors and are catalytic for the adoption of this technology. Furthermore, local and national authorities should take into account this kind of factors so that policies could capture the social effect of the adopters. If changes will be realized from the core level which is a small community this would facilitate the road to reach the ambitious national goals.

7.

Scenario Modelling

This chapter is based on the publication:

G.B.M.A. Litjens, B.B. Kausika, E. Worrell and W.G.J.H.M. van Sark. “A spatio-temporal city-scale assessment of residential photovoltaic power integration scenarios”. in: *Solar Energy* 174 (2018), pp. 1185-1197. DOI: 10.1016/j.solener.2018.09.055

Abstract

Cities have a significant potential to host residential photovoltaic systems (PV). The direct consumption of PV generated electricity reduces the need for electricity import, while excess PV electricity production can be stored for later usage or can be used directly to charge electric vehicles (EVs). In this way, more energy is locally consumed, greenhouse gas emissions are reduced, and self-sufficiency of cities can be increased. In this chapter, we present a spatio-temporal framework to evaluate the electricity demand that can be fulfilled by PV energy. We assess the impact of penetration of EVs and the influence of battery energy storage. We demonstrate the usefulness of this framework for 88 neighborhoods in the city of Utrecht, the Netherlands. Spatial mapping was used to identify areas with high potential for EVs and storage. Results shows that direct PV self-consumption ratios vary between 34% and 100%. When EVs charging is included in the neighborhoods, then self-consumption is increased on average by 12%. Battery energy storage increases self-consumption on average by 25%. The self-sufficiencies due to direct PV energy consumption are between 6% and 40% in the neighborhoods. These are decreased by EVs with an average of -0.6% and increased by battery energy storage with an average of 14%. Avoided life cycle greenhouse gas emissions over a 30-year period are on average 12 tCO_2-eq per address. The large variation in results between neighborhoods indicates that area dependent investments and supporting policies could improve the PV power integration in cities. Our developed framework can be easily adapted and used for other cities. Moreover, our results are useful for local governments to guide and design effective policies to accelerate the transition to more sustainable cities.

7.1. Introduction

Currently, cities host more than 50% of the global population and account for 70% of the global greenhouse gas (GHG) emissions [200]. One of the solutions to reduce CO2 emissions from cities is the deployment of residential solar photovoltaic (PV) systems. Yet, PV system installation may be limited due to lack of suitable space. An added difficulty is the daily power fluctuation of the solar resources. This results in export of surplus PV electricity during daytime from cities and requires import of electricity during night time. Shifting energy demand to daytime results in higher PV self-consumption within cities and reduces CO2 emissions from fossil-based backup power generation [201].

The use of battery energy storage systems (BESSs) allows storage of surplus PV electricity to be used at later moments. The cost of BESSs is rapidly decreasing due to their increasing deployment [202]. Currently, the number of electric vehicles (EVs) is rapidly increasing in the Netherlands, which increases the electricity demand within cities [19,203]. BESS and EVs are becoming more economically attractive, especially due to cost reduction of Li-ion storage technology [204]. Furthermore, EV costs are decreasing as a result of economic scaling effects. A shift from a gasoline-based car fleet to electric vehicles (EV) reduces emissions and air pollutants considerably, thereby contributing to improve air quality and quality of life in cities [205,206].

Due to increased deployment of PV, EVs and domestic electric heating, it is expected that more overloading will occur on the medium voltage grid than on the low voltage grid, [207]. Consuming more PV generated electricity in the city can lower medium voltage distribution grid losses and reduces investments in cables and transformers. Smart EV charging and battery energy storage help to increase urban PV self-consumption [208]. For all these benefits, enhancement of PV self-consumption is seen as an important accelerator to reach a higher share of domestic PV installations and at the same time contribute to a reduction in greenhouse emissions [209].

7.1.1. Literature Review

Commonly, spatio-temporal PV potential in urban areas is assessed using geographic information systems (GIS) combined with numerical solar irradiation algorithms [120,198]. PV integration studies focus mainly on using the generated PV electricity directly within the buildings or on community scale [210,211]. Some studies combined the PV integration assessment with local or regional energy demand. Most of these studies assessed the provision of the net electricity consumption on an annual basis. A study assessed the potential of PV systems on rooftops and facades of 27 European countries. They found that the produced PV energy could provide in 22% of the projected 2030 annual electricity demand for these countries [212].

A spatial model concluded that 2/3 of the current electricity demand could be covered by PV production for a small city in eastern Slovakia [213]. Of all the municipalities in Germany, 30% could be net self-sufficient when the full residential roof potential was used [214]. In another study involving 34 German municipalities, it was found that 77% of the net electricity consumption could be provided by PV [215]. Furthermore, rooftop PV systems could provide 25% of the total annual electricity demand in Switzerland [216]. A study including a municipality in Sweden found that 88% of the annual demand can be provided with PV. Yet over 3000 h a year have more PV production than demand [217]. A study of a city in Chile found that 24% of actual demand could be provided by PV, with the main limitation being the infrastructure of the grid [218].

Few studies included temporal (hourly, daily) factors to assess the spatial potential of PV systems. A real-time platform containing a PV simulator and a distribution network simulator was presented and tested for the city of Turin, Italy. It was found that the actual distribution grid was not adequate to accommodate all PV generated electricity, if the available rooftop surface would be fully used [219]. A PV penetration level of 40% was found for a German rural municipality to achieve a high PV self-consumption level [220]. Another spatio-temporal model analysed the impact of electric vehicles on the urban distribution network. This model provided insights in the critical local grid components that require upgrades for larger shares of electric

vehicles [221]. Only 27% of the electrical vehicles that are not in transit, are required to store excess PV produced power produced for the city of Yokohama, Japan [222].

7.1.2. Research aim

A limited number of studies are available that include both spatial and temporal effects of PV system integration. Furthermore, no research was found that assessed the spatial and temporal influence of electrical vehicles and storage on the PV self-consumption and PV self-sufficiency, except for a Dutch study with very coarse spatial resolution [19].

Therefore, this research aims to assess the role of EVs and BESSs for the PV self-consumption potential of a city. We developed a spatiotemporal framework that uses models to estimate the potential of PV yield, battery storage systems and electric vehicles. We demonstrate the framework using the city of Utrecht (the Netherlands) as a case study. The PV yield potential was assessed using the rooftop area of all residential buildings of this city. A time resolution of 5 min was used to assess the self-consumption and self-sufficiency potential at a neighbourhood level, over a 30-year lifetime. Neighbourhoods were identified that have surplus PV production to store in BESSs or charge EVs or have limited PV yield production due to roof space limitations. Furthermore, we estimate the avoided life cycle GHG emissions due to PV electricity from two perspectives.

This study also includes socio-economic factors, e.g., household statistics and current number of cars in a neighbourhood. Two EV charging algorithms were incorporated, i.e., normal (uncontrolled) charging and smart solar charging. The latter charging method aims to charge EVs at moments with surplus PV power enhancing PV self-consumption. The results on each neighbourhood give information on the potential usage of the transformers within these neighbourhoods. The area of buildings connected to the transformers usually does not cross the borders of the neighbourhood. As a consequence, obtained results are valuable for distribution system operators (DSOs) to plan grid extensions and EV charging infrastructure. Furthermore, the results help local governments to design realistic

and effective policies to develop carbon–neutral cities. The developed methodology can be modified and used for other cities and regions.

This study is arranged as follows. Section 7.2 explains the spatiotemporal framework and the used technical and environmental performance indicators. Section 7.3 presents the spatial results for the 88 neighbourhoods using maps of the city of Utrecht, the Netherlands. Section 7.4 assesses the sensitivity of the rooftop utilization rate, EV smart solar charging shares and battery storage capacities. Limitations concerning assumption, data availability and implementation challengers are discussed in Section 7.5 and the chapter finalises with key conclusion in Section 7.6.

7.2. Methods

7.2.1. Spatio-temporal framework

A spatio-temporal framework was developed to combine spatial and temporal parameters. An algorithm was developed that combines time and location of PV production with time and location of electricity demand in the city. The main inputs of this algorithm are two time series for each neighbourhood: PV yield and total electricity consumption. The latter time series consists of the electricity consumption profile of buildings, with and without the consumption profile of electric vehicles. Both PV production and consumption time series are used in algorithms that determined self-consumption ratios and self-sufficiency ratios over a lifetime of 30 years. An EV charging algorithm and BESS charging algorithm are used to assess the impact of EV and storage. An overview of the spatial level of the input data and model steps is shown in Figure 7-1. We used reference parameters to compare the spatial self-consumption and self-sufficiency influence of the neighbourhoods, see Table 7-1. Also, the avoided life cycle GHG emissions from the PV systems are determined.

The impact of the PV system potential on these parameters was assessed using four scenarios in the following sections:

- Neighbourhoods with PV systems only
- Neighbourhoods with PV systems and EVs
- Neighbourhoods with PV systems and BESS
- Neighbourhoods with PV systems, EVs and BESS

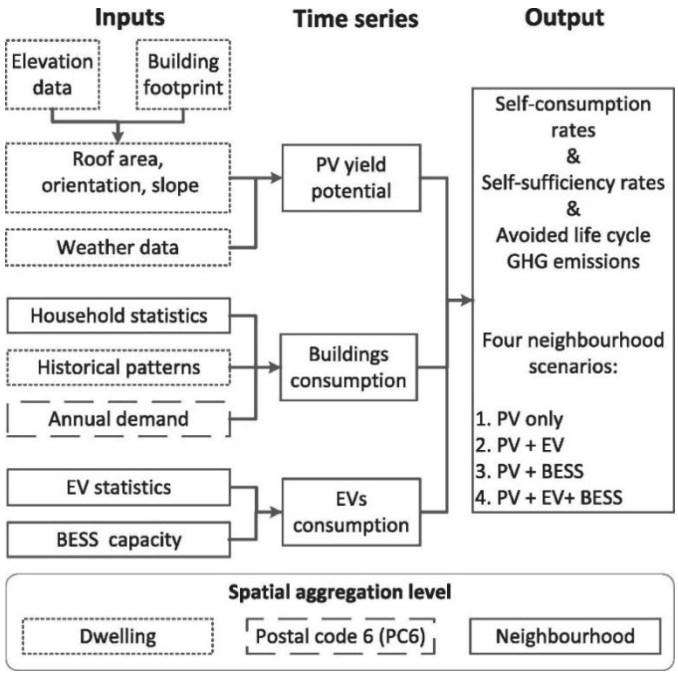

Figure 7-1: Overview of the input data and model steps with corresponding spatial level to model the self-consumption ratios, self-sufficiency ratios and avoided life cycle greenhouse gas emissions for four scenarios.

The framework was implemented using the city of Utrecht in the Netherlands. This city (latitude 52°05′38″ North, longitude 5°05′12″ East) is the fourth largest city in the Netherlands with 340,000 inhabitants. The city of Utrecht consists of 10 districts which make up 99 neighbourhoods. Neighbourhoods with 250 addresses or less were excluded from the analyses since these are mainly industrial or rural areas. As

a result, 9 districts and 88 neighbourhoods were selected for the study. Each neighbourhood is made up of smaller areas that are specified by a postal code 6 (PC6) level. A total of 63,494 buildings containing 132,671 residential addresses were used in the study. The distribution of buildings per PC6 area and within each neighbourhood is shown in Figure 7-2. The majority of PC6 areas consist of a single building. The number of buildings within each neighbourhood shows a large variation.

Table 7-1: Main reference model input parameters.

Reference parameter	**Value**	**Unit**
PV capacity	200	Wp/m^2
Rooftop utilization factor	50	%
EV constant charging share	75	%
EV smart solar charging share	25	%
Relative battery storage size	1	$kWh_{BESS}\ MWh_{demand}^{-1}$
Relative battery inverter rating	0.5	$kW/\ kWh_{BESS}\ MWh_{demand}^{-1}$

7.2.2. PV yield potential

Roof statistics

The first step to assess the PV potential is the calculation of the roof statistics for each of the 63,494 buildings. The rooftop statistics consist of the roof area, orientation (azimuth and tilt) and the incoming plane of array (POA) irradiance. The incoming POA irradiance was determined using the Area Solar Radiation Tool of the ArcGIS Spatial Analyst [223]. The Area Solar Radiation tools calculated the POA irradiation across areas based on the hemispherical viewshed algorithm. These tools were developed by Rich et al. [135] and further refined by Fu and Rich [137].

The Area Solar Radiation tools calculations require a building footprint layer and a digital elevation model (DEM). The building footprint layer for the city of Utrecht was obtained from the Basisregistratie Adressen en Gebouwen (BAG) which was provided by the Dutch Cadastre, Land Registry and Mapping Agency [74]. The DEM was derived from high resolution elevation data, which was obtained from the Actueel Hoogte Bestand (AHN) Nederland [100]. The DEM has a spatial resolution of 50 cm and was used as main input in the solar radiation tools. The roof area, slopes and azimuths for each roof top were calculated in GIS based on the DEM.

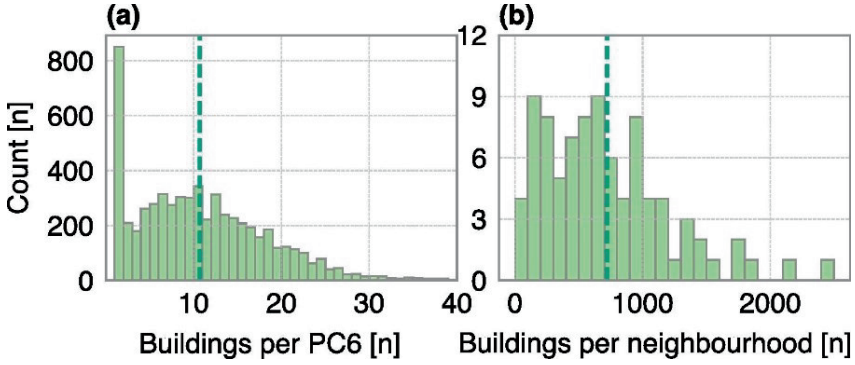

Figure 7-2: Distribution of buildings containing residential addresses within each postal code 6 areas (a) and distribution of these buildings within each neighbourhood (b), both shown using a histogram. Mean values of the distribution are indicated by the dashed lines. Histogram bins of 1 building per postal code 6 and 100 buildings per neighbourhood were used. Note that 50 postal code 6 areas have more than 40 buildings and are not shown in histogram (a).

The default settings of the Area Solar Radiation Tool model were used containing the following default settings [130]. The latitudes for the buildings were calculated automatically based on the DEM metadata. Sky size was set to 200 and proved to be sufficient for time interval of 14 days. Horizon angles (number of calculation angles) are set to 32 which is adequate for complex topography. Diffusivity was set at 0.3 and

transmissivity at 0.5 which is an indication of generally clear sky conditions. Using a fixed atmospheric value does impact the irradiation output on a smaller time scale (days or weeks). We observed that standard factors were sufficient to achieve a good fit with the measured values from the closest meteorological station (Royal Netherlands Meteorological Institute KNMI in De Bilt, The Netherlands).

The calculation took into account the effect of shadow due to nearby buildings, trees, and other roof obstacles like chimneys or gable style roofs. The digital surface model has been used as input for these calculations. The POA irradiation for each roof surface was calculated for the year 2015, with a 14 day interval. This time interval is used to calculate the sky sectors for the sun map (the sun's position in the sky across a period of time). These maps are used to calculate the total POA irradiance for a particular roof.

PV yield time series

The second step to determine the PV yield potential was to create a PV yield time series for each of the assessed rooftops. Buildings with addresses that have a residential function were selected from the building footprint layer. If a building contained only residential users than the full roof area was selected. However, some buildings have addresses with different functions, for example an office, shop or residence. For these buildings, the share of used surface for each function was obtained from the BAG dataset. The residential rooftop share was multiplied with the total roof area to define the roof area allocated for residential PV systems. We assumed that a maximum of 200 Wp/m^2 could be installed, based on a commercially available 320 Wp module with a dimension of 1.6 m by 1 m.

The PV yield timeseries was created using the open source Python package PVLIB [224]. The roof surface azimuth and tilt angles from the GIS model were binned to obtain 35 different combinations of roof slope and orientations. The roof surface azimuth angles were binned in steps of 45°, and roof slope angles in bins steps of 20°. A maximum tilt angle of 82.5° was selected. Facades were not included in our study. Furthermore, we assume that flat roofs will have a dual-tilt (or east–west) designed PV systems with a slope of 10°.

Radiation, wind speed, pressure and temperature data were obtained for 2015 from the Royal Netherlands Meteorological Institute KNMI in De Bilt, The Netherlands [139]. The measurement intervals of radiation were 10 min and one hour for remaining weather parameters. The weather data is linearly interpolated to 5 min interval and used as input for the PVLIB model. Furthermore, the module parameters of the Sanyo HIP-225HDE1 PV module are used to model the direct current (DC) PV yield time series [225]. This module has a relative low temperature coefficient temperature thus reducing the influence of temperature in the model. The DC time series were converted to alternating current (AC) time series using the efficiency parameters of the Enphase Energy M210 inverter [226]. The AC time series were linearly scaled to obtain a performance ratio of 85%, which is consistent with well performing PV systems in the Netherlands [141].

Also, the PVLIB model calculate the total POA irradiance from the solar radiation data (no shading conditions). This number is used to determine the shade loss factor for each rooftop. This is the POA irradiance with shading (determined by the Area Solar Radiation tools) divided by the POA irradiance on a surface with no shading (determined using PVLIB). An average shade loss factor of 83% was found for all residential buildings. The shade loss factor was multiplied with the AC PV yield time series to determine the PV yield under shaded conditions.

Finally, the PV yield time series were scaled using a rooftop utilization rate. Only a certain part of the roof area can be used for PV modules due to constraints from other roof structures (chimneys, ventilation systems or dormers). We used a 50% roof utilization factor for PV systems, based on a previous study [214]. The PV yield time series for each neighbourhood was created by aggregation of PV yield profiles for all buildings in that neighbourhood. The annual PV yield is reduced with 0.5% per year to account for PV system degradation [227].

7.2.3. Electricity consumption from buildings

Electricity consumption time series were created for each neighbourhood using three main data sources: household statistics, historical residential demand time series

and annual electricity consumption from residential grid connections. The household statistics from each neighbourhood in Utrecht are obtained from Statistics Netherlands (CBS) for 2015 [228]. This data contains statistics on family compositions: people living alone, people living as a couple and couples with children.

Electricity demand profiles for 30 different households were measured between 2012 and 2014, by a Dutch distribution system operator [229]. The time series were measured using a 15 min time step for one year. Three new time series were created for each family composition using the 30 measured demand profiles. These three time series were scaled with share of family composition of each neighbourhood and summed together to create one demand time series per neighbourhood. The annual electricity consumption for each residential grid connection per postal code 6 area is available as open data for 2015 [230]. We assumed that each residential address has one grid connection. The electricity consumption of all residential addresses within a neighbourhood was summed to determine the annual electricity consumption of a neighbourhood. This number was used to linearly scale the neighbourhood demand time series. Finally, the neighbourhood demand time series were linearly interpolated to a 5-min time interval. The demand time series of one year were repeated to obtain a 30-year period. The average electricity consumption of households was quite stable for the last 10 years [231]. Therefore, the annual demand is kept constant over the 30-year period.

7.2.4. Electric vehicle consumption

The number of registered cars per household in 2015 were obtained from CBS [228]. The average number of cars within a neighbourhood was 932, with a minimum of 105 and a maximum of 2690. This corresponds to an average of 0.61 cars per household, with a minimum of 0.10 and a maximum of 1.05 cars per household. This is lower than the average for the Netherlands, which is 0.93 cars per household [232]. Furthermore, it is expected that electric vehicles will have a market share of 100% around 2040 [19]. Therefore, we assumed that all current light duty gasoline vehicles will be replaced with electric vehicles. The daily power consumption of an

EV depends on the average driving consumption multiplied by a seasonal factor. This factor accounts for the seasonal variability of the EV consumption mainly due to the cabin climate control and the battery efficiency. A seasonal factor of 0.8 was used for summer period and 1.2 for the winter period [233]. The summer period consists of the months June until August and the winter period December until February. Furthermore, we assumed an average driving power consumption of 7.24 kWh per day of which 50% will be charged within the neighbourhood [232]. In addition, a EV charging and discharging efficiency of 90% was assumed [203]. This results in a daily EV demand of 4.01 kWh and an annual demand of 1463 kWh.

The moments at which cars are connected to the charging stations are highly uncertain and are not well studied. Therefore, we developed an algorithm to assess the impact of two different charging strategies on the EV integration potential. In the first strategy, the daily EV charging demand within a neighbourhood is gradually spread over the day. In this case, we assume that the summation of charging demands of each individual EV results in a flattened EV charging profile of a neighbourhood. Hence a constant EV consumption over the day was assumed. In the second option, the EV is directly charged with the produced PV energy. We call this option smart solar charging [234]. In this case, the EV is charged with the excess PV production in the neighbourhood. A maximum charging capacity of 11 kW per EV was assumed, to reduce the impact on the electricity grid. If adequate PV production is not available during the day, then the remaining charging demand is fulfilled when the solar elevation angle is < 0. Thus, the EV demand is charged using the electricity grid. The charging profiles of both strategies were added to the neighbourhood electricity consumption profile. In the reference case, we assume that 75% of cars are charged using the first strategy and 25% of cars using the second strategy.

The distribution of residential neighbourhood annual electricity consumption including EV charging and the EV share are shown in Figure 7-3. The total annual electricity consumption per neighbourhood ranges between 1 GWh and 16.3 GWh, with an average of 6.7 GWh. The share of EV consumption varies between 1.8% and 30.1%, with an average of 20.6%. These numbers show that there is a larger diversity of electricity consumption within each neighbourhood, mainly related to the number

of inhabitants. Also, the EV charging demand within the neighbourhood is assumed to be constant over the 30-year assessment period. The total electricity demand of the 88 neighbourhoods is 466 GWh excluding EV charging and 587 GWh including EV charging.

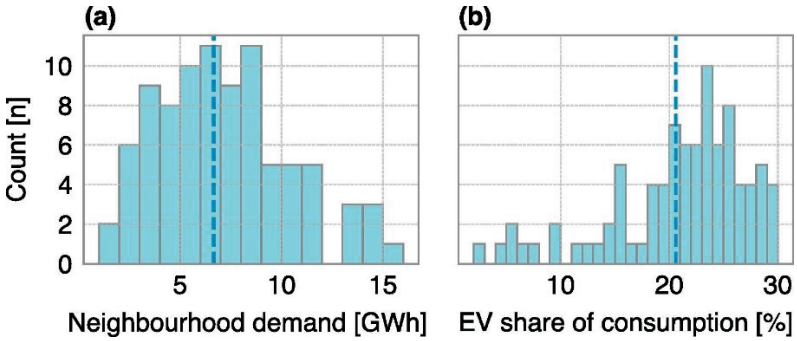

Figure 7-3: Distribution of residential neighbourhood annual electricity consumption with EVs (a) and share of electricity consumption by EV charging (b) shown using a histogram. Mean values of the distribution are indicated by the dashed lines. Histogram bins of 2.5 GWh for neighbourhood energy demand and 1% for EV share were used.

7.2.5. BESS charging algorithm

Battery charging and discharging was simulated with a simple control strategy, obtained from previous research and written in Python (v3.5) [235]. If more PV electricity is generated than consumed by the neighbourhood, then the battery was charged. If more electricity was consumed than generated, then the battery was discharged. The battery was discharged to fulfil electricity demand of the building. If the battery inverter and battery storage capacity was available, then the battery was also used to charge the electric vehicle.

An AC-coupled PV-battery system was assumed. This means that the PV array is connected via an inverter to the electricity grid and the battery storage pack with a battery inverter to the electricity grid. This is a commonly installed system type and

is very suitable for retrofitting or installing community energy storage systems [236]. A battery storage capacity of 1 kWh battery storage capacity per MWh of annual electricity consumption per neighbourhood is used in the reference case [236]. Note that if EVs were included in the modelling, then the annual consumption in neighbourhoods is higher and thus larger battery sizes are used.

The battery inverter capacity is set to a C-rate of 0.5, meaning that it would require 2 h to fully charge the battery. Battery state of charge (SOC) is set to a minimum of 0% and a maximum of 100%. In this way, we assess the maximum storage potential to enhance self-consumption. Battery inverter efficiencies were obtained from the inverter efficiency curve of a SMA Sunny Boy Storage inverter, using a step size of 0.01% [237]. A constant battery roundtrip efficiency of 92% was used, close to the round trip efficiency of a Tesla Powerwall [238]. Furthermore, a calendric lifetime of 15 years and a battery cycle lifetime of 5000 full equivalent cycles is used to model the battery capacity degradation [239]. The amount of diminished storage capacity is determined annually and subtracted from the previous year. The battery degradation model is explained in detail in a previous study [240]. We assume that the battery storage is replaced after 15 years, thus the storage capacity is set similar to the original storage capacity for year 16.

7.2.6. Calculation of PV integration indicators

Two temporal PV integration indicators were assessed: self-consumption ratio (SCR) and self-sufficiency ratio (SSR). Self-consumption ratio is used to quantify the share of electricity that is self-consumed from the total annual produced PV energy. Self-sufficiency ratio is the share of electricity consumption that is fulfilled by PV electricity. The self-consumed power consists of the total direct consumed power by the neighbourhood (P_{directSC}) and the total power that is used for charging the battery (P_{Bcharge}). The direct consumed power is the PV power (P_{PV}) that is directly consumed as a result of the electricity demand of a building. (P_{demand}). The self-consumed energy is aggregated over the year from timestep (t=1) till the last time step (t_{end}), see Eq. (7.1).

Self-sufficiency ratio is an indicator for the share of electricity consumption that is fulfilled by using PV electricity. This is the share of electricity demand that is fulfilled by the direct consumed PV power and the discharged power that is discharged from the battery ($PB_{\text{discharge}}$), see Eq. (7.2).

$$P_{\text{direct SC}} = \begin{cases} P_{PV} & \text{if } P_{PV} < P_{\text{demand}} \\ P_{\text{demand}} & \text{if } P_{PV} \geq P_{\text{demand}} \end{cases} \tag{7.1a}$$

$$\text{SCR} = \frac{\sum_{t=1}^{t_{end}} \left(P_{\text{direct-consumed,t}} + P_{\text{B charge,t}}\right) . \Delta t}{\sum_{t=1}^{t_{end}} \left(P_{\text{PV,t}}\right) . \Delta t} \tag{7.1b}$$

$$\text{SCR} = \frac{\sum_{t=1}^{t_{end}} \left(P_{\text{direct-consumed,t}} + P_{\text{B discharge,t}}\right) . \Delta t}{\sum_{t=1}^{t_{end}} \left(P_{\text{demand,t}}\right) . \Delta t} \tag{7.2}$$

7.2.7. Calculation of avoided life cycle GHG emissions

A rough indication of the avoided life cycle GHG emissions by the PV systems and battery energy storage systems was provided. Emissions due to manufacturing of the PV systems and BESS (GHG_{mfg}), and the avoided emissions by the PV electricity production are determined. The emissions of manufacturing the PV system depends on the production location [201]. We assume that PV systems are made in China as this country produces the majority of the PV cells and PV modules globally [241]. Emissions from producing PV systems in this country are assumed to be 1590 gCO_2-eq for each Wp [242]. The production of Li-Ion battery energy storage systems uses 110 gCO2-eq for each Wh [243]. We assumed that emissions from manufacturing a battery inverter are comparable to the emissions from manufacturing a PV inverter and assumed 124 gCO_2-eq per W. de Wild-Scholten [242]. The PV and battery inverter, and the battery storage are replaced after 15 years. Emissions from manufacturing are expected to be 25% lower when these components are replaced.

The avoided emissions by PV electricity production depend on the emission factor of electricity (EFE) from the grid. We assume that these emissions will reduce linearly from current emissions (2016) to zero emissions in 2050, based on the Dutch energy agreement for sustainable growth [244]. Thus, the carbon intensity will decrease linearly from 490 gCO2-eq per kWh in year 1 to 60 gCO_2-eq per kWh in year 30 [245].

The avoided emissions are determined for two system perspectives, i.e., from an electricity system perspective (GHG_{system}) and from a neighbourhood perspective ($GHG_{\text{neighb.}}$). In the electricity system perspective, all PV electricity that was used is allocated as replacing electricity from the grid. The PV power that was used from a system perspective ($P_{\text{PV system}}$), is the PV produced power minus the battery energy storage losses. In the neighbourhood perspective, all PV power used within the neighbourhood is allocated as replacing electricity from the grid. Hence, avoided emissions from electricity exported to the grid are not included in this perspective. The PV power used ($P_{\text{PV neighb.}}$), is the sum of the direct consumed PV and the electricity discharged from storage. The used PV electricity of both perspectives was multiplied with the carbon intensity of the electricity grid for each year. Then, the emissions from manufacturing were subtracted from the total emissions over 30 years to determine the avoided life cycle GHG emissions. The avoided emissions are normalized with the number of addresses within a neighbourhood (N_{address}), see Eq. (7.3).

$$P_{\text{PV system}} = P_{\text{PV,t}} - P_{\text{B charge}} - P_{\text{B discharge}} \tag{7.3a}$$

$$P_{\text{PV neighb.}} = P_{\text{direct-consumed}} + P_{\text{B discharge,t}} \tag{7.3b}$$

$$GHG_{\text{system}} = \frac{\sum_{t=1}^{t_{end}} \left(\text{EFE}, t \,.\, P_{\text{PV system, t}}\right) - GHG_{mfg}}{N_{\text{address}}} \tag{7.3c}$$

$$GHG_{\text{neighb.}} = \frac{\sum_{t=1}^{t_{end}} \left(\text{EFE}, t \,.\, P_{\text{PV neighb., t}}\right) - GHG_{mfg}}{N_{\text{address}}} \tag{7.3d}$$

7.3. Results

7.3.1. PV yield potential

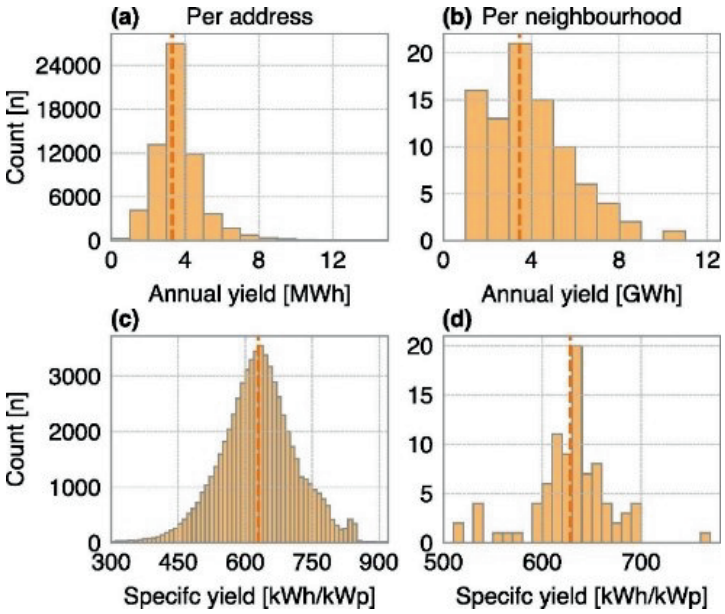

Figure 7-4: Distribution of average annual PV yield for each address (a), average annual PV yield for each neighbourhood (b), average annual specific yield for each address (c) and average annual specific yield for each neighbourhood (d). Mean values of the distributions are indicated by the dashed lines. Annual yield is shown using bins of 1 MWh for each address and 1 GWh of each neighbourhood. Specific yield is shown using bins of 10 kWh/kWp. Note that 198 addresses have an annual yield higher than 15 MWh and are not shown on the histogram (a). Also 138 addresses with a specific yield of lower than 300 kWh/ kWp are not shown on the histogram (c)

The PV yield potential for each of the 88 neighbourhoods was analysed over a period of 30 years using the reference parameters given in Table 7-1. The distributions of average annual PV yield for each address and the average annual PV yield for each neighbourhood are shown in Figure 7-4. Also, the average annual specific yield for each address and each neighbourhood is presented. Average annual PV yield is 3.3

MWh per address and for the neighbourhoods 3.5 GWh. The specific yields show a larger distribution range for the addresses, with an average of 629 kWh per kWp. Specific yield for neighbourhoods is between 513 and 773 kWh/kWp, with an annual average of 628 kWh per kWp. The average specific yield decrease from 677 kWh/kWp in the first year to 579 kWh/kWp in year 30 due to PV system degradation. This specific yield is significantly lower than the current average specific yield for the Netherlands [141]. This is mainly due to the inclusion of all orientations and the reduced incoming irradiance due to shading. The total PV capacity from all neighbourhoods is 488 MWp and the average annual production 306 GWh.

The ratio between the total PV production and the total electricity consumption for a period of 30 years provided an indication on the contribution of PV to fulfil the electricity demand. This ratio is shown for each of the 88 neighbourhoods of the city of Utrecht in Figure 7-5. The ratio is shown for two scenarios, only PV systems and PV systems with EVs. A ratio higher than 100% shows that there is more PV production than electricity consumption. This is the case for 5 neighbourhoods in the PV only scenarios. Neighbourhoods with PV systems only show an average of 68% and neighbourhoods with PV systems and EVs 53%.

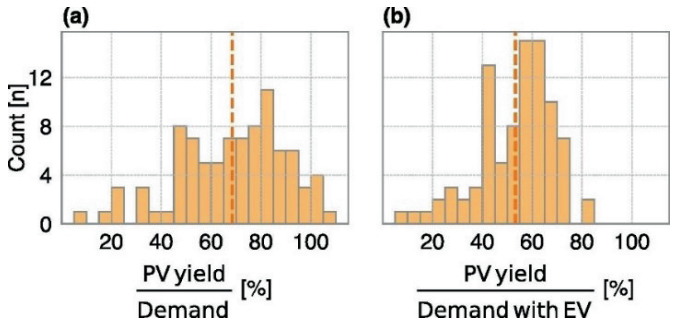

Figure 7-5: Distribution of ratio between the total PV production and the total consumption of neighbourhoods with PV systems only (a) and neighbourhoods with PV and EVs (b) Mean values of the distribution are indicated by the dashed lines, and bins of 5% were used.

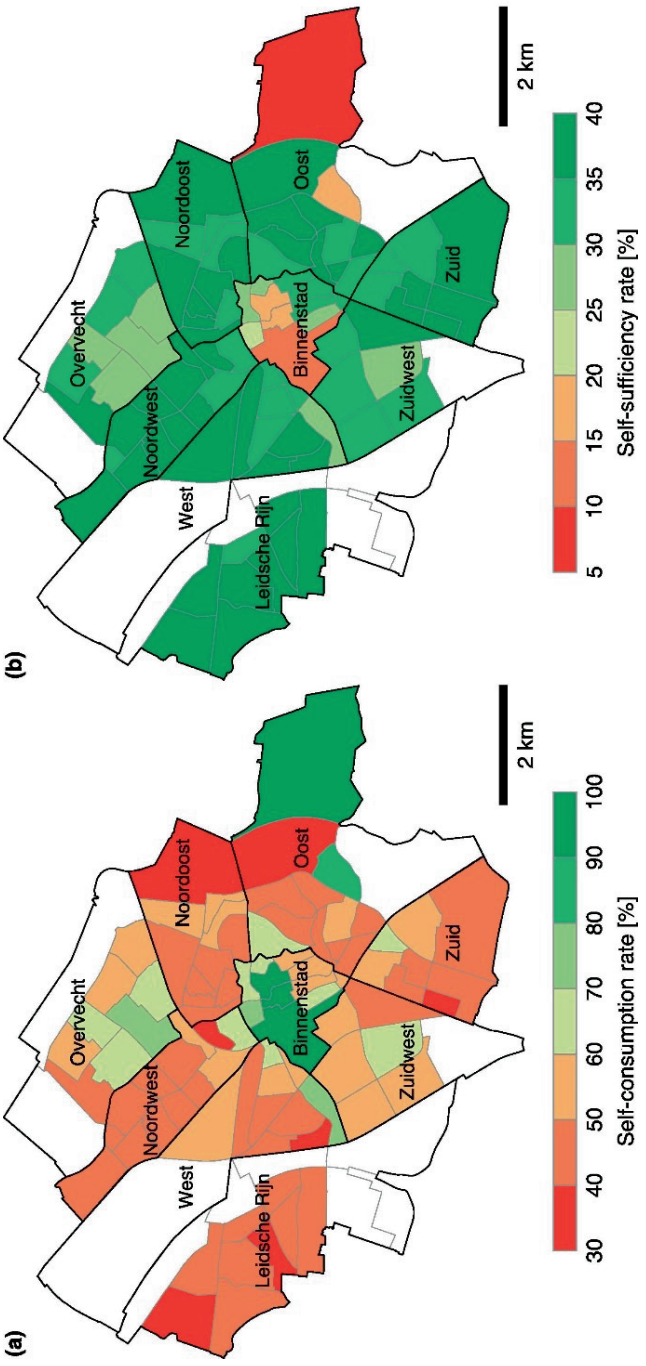

Figure 7-6: . Potential PV self-consumption ratio (a) and self-sufficiency ratio (b) for 88 neighbourhoods with only PV systems, for the city of Utrecht

7.3.2. Impact of PV systems only

The spatial impact of PV systems on the self-consumption ratio and self-sufficiency ratio for each neighbourhood is visualized using on a color-coded map in Figure 7-6. Results are shown for 88 neighbourhoods which are separated by grey borders. The 9 districts are separated with solid black lines and the district names are indicated. The areas in white are neighbourhoods that were excluded from the study. For example, the left most neighbourhood in district West is a commercial area with a limited number of residential dwellings. The average SCR of the neighbourhoods is 53%, which demonstrates that the PV produced in a neighbourhood can be used most within the same neighbourhood. Low SCR is seen for the suburb of Leidsche Rijn, and in the Noordwest (North-West) district, indicating a large surplus of produced PV energy. These areas contain mainly terraced houses with sufficient roof space available for PV systems.

High SCR was observed in the historical Binnenstad (Inner-city), Oost (East) and Overvecht districts. The inner-city area has a limited PV potential due to high concentration of historical buildings with relatively small roof areas and a high variation in roof shape and height. These roofs induce shading which reduces the plane-of-array irradiance and as a consequence the PV electricity generation. In addition, population density in the inner city is higher compared to other districts due to the smaller dwellings and apartments. This results in relatively high electricity consumption per unit area and thus a higher SCR. The district of Overvecht contains tall (mostly 10-storey) residential apartment buildings that limit the PV production potential per resident. Also, the district to the extreme East, in which the university campus is located, shows a high SCR. In this area, tall apartment buildings, which serve as student housing are located. Therefore, the roof area available per address is small.

An average SSR of 33% was determined for the neighbourhoods, ranging from 6% to 40%. Low SSRs are observed for the inner-city area, indicating that PV potential is not sufficient to fulfil the electricity demand. Higher self-sufficiency is observed for the suburb Leidsche Rijn, and in the Zuid (South) district. Areas with high SCR and

low SSR have limited area to install PV systems and therefore limited PV yield. Areas with relatively lower SCR and higher SSR have more moments in which surplus of PV energy production occurs. The limited SSR indicates that the PV yield potential is not sufficient and electricity import to the city is a requirement.

7.3.3. Impact of EV's or BESS

The influence of two scenarios, PV systems with EVs and PV systems with BESSs, on the self-consumption enhancement is presented in Figure 7-7. Deployment of BESSs shows a larger impact on the SCR than the deployment of EVs. The replacement of gasoline-based cars by EVs results in an average increase in SCR of 12% points in the neighbourhoods. The SCR increase varies between 0% and 17% , showing a distinct impact of electric vehicles. The effect of EVs on SCR in neighbourhoods with already high self-consumption due to the electricity consumption of the residential buildings is limited. The average self-sufficiency of neighbourhoods with introduction of EVs has barely changed. Observed differences in SSR are between −2.0% and 0.1% with an average of −0.7%. Only for two neighbourhoods EVs have a positive impact on SSR, namely Rijnsweerd and Hoge Weide. These neighbourhoods are in the Oost (East) and the Leidsche Rijn districts, respectively. The Rijnsweerd neighbourhood also has the lowest SCR without EVs. This shows that for almost all neighbourhoods the additional EV demand increases the need for imported electricity.

An average SCR increase of 25% can be achieved with a battery capacity of 1 kWh for each MWh of electricity consumption. The SCR enhancement varies between 0% and 30%. Neighbourhoods with a low self-consumption of PV systems only (Leidsche Rijn) have a SCR impact of 20% from battery storage. In this case, the influence is limited by the battery storage capacity. The neighbourhoods with a high initial SCR (Binnenstad) have a limited BESS impact since most of the electricity is directly consumed and the storage capacity is not utilized. Neighbourhoods with an initial self-consumption of around 60%(Overvecht) show the largest self-consumption impact. These neighbourhoods can store most surplus PV production and utilize the storage capacity. In addition, the SSR impact by storage varies between 0% and 18%

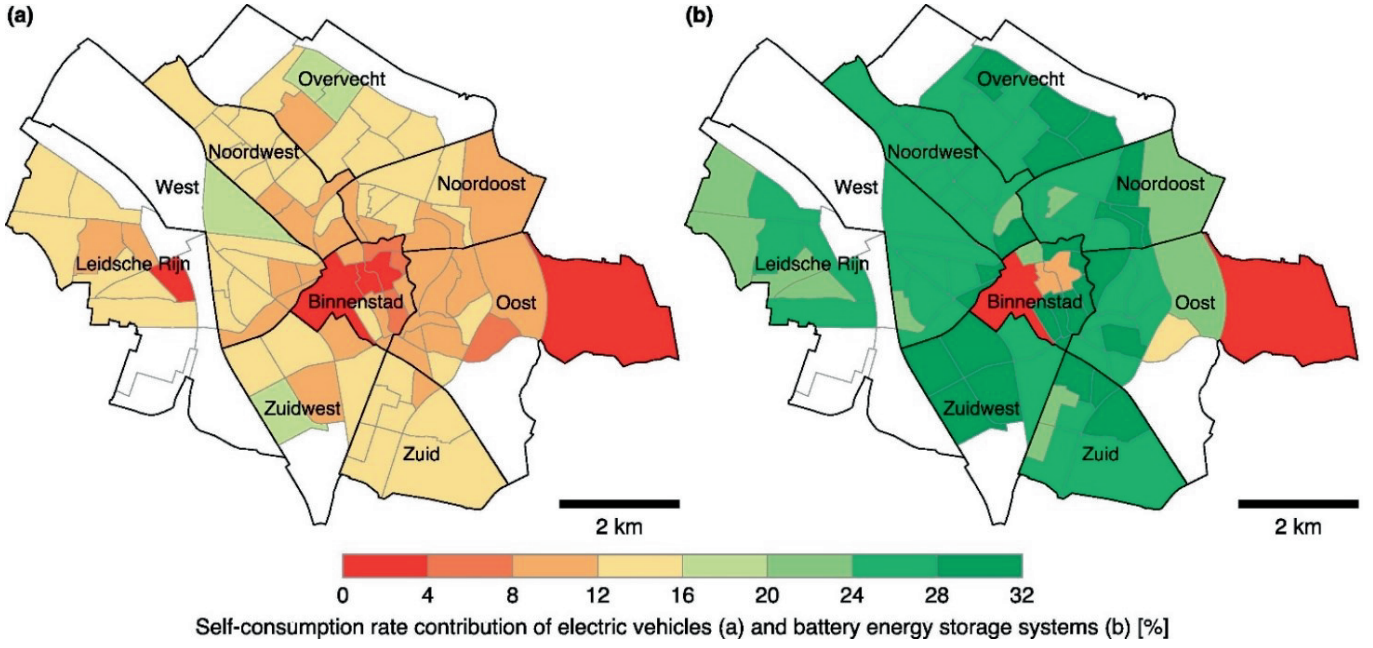

Figure 7-7: . Potential contribution of electric vehicles to the PV self-consumption ratio (a) and potential contribution of battery energy storage systems to the PV self-consumption ratio (b) for 88 neighbourhoods.

with an average of 14%. As a result, 42 neighbourhoods obtain a self-sufficiency ratio > 50%.

For a dwelling owner with a PV system, it could be advantageous to use storage under certain economic conditions [246]. However, if this dwelling is located within a neighbourhood with low impact of storage on self-consumption, then this electricity could better be used by dwellings with insufficient roof space for a PV system. As a result, more electricity is directly used, and less electricity is lost by energy storage conversions. Moreover, some neighbourhoods are surrounded by neighbourhoods with a high initial SCR. For, example the North-West district has a relatively low SCR, but is surrounded by districts with higher SCR. Hence, it could be more beneficial to export surplus PV to these areas, instead of increasing storage capacities. On the other hand, the historical inner-city is enclosed by neighbourhoods with lower SCR. These neighbourhoods could provide the inner-city with electricity instead of storing surplus PV electricity in batteries.

7.3.4. Combined impact of EV's and BESS

The impact of the PV systems with electric vehicles and battery storage on SCR and SSR are presented in

Figure 7-8. A total of 10 neighbourhoods have a self-consumption ratio of almost 100%, indicated by the blue dots. For the majority of these neighbourhoods a SCR impact of around < 15% is seen. Overall, an average SCR enhancement of 35% can be achieved when EV and storage are added to the neighbourhoods. This results in a high average SCR of 88% within the neighbourhoods, with a range from 67% till 100%. The self-sufficiency ratios show an average increase of 10% due to EVs and storage, ranging between −0.6% and 16%. The SSR impacts show negative values in two neighbourhoods. These neighbourhoods have a larger additional electricity demand by EVs, than the demand that can be shifted by battery energy storage. Overall, the average SSR increases to 43%, ranging between 6 % and 54%. Also, 17 neighbourhoods have a SSR > 50% with EV and storage.

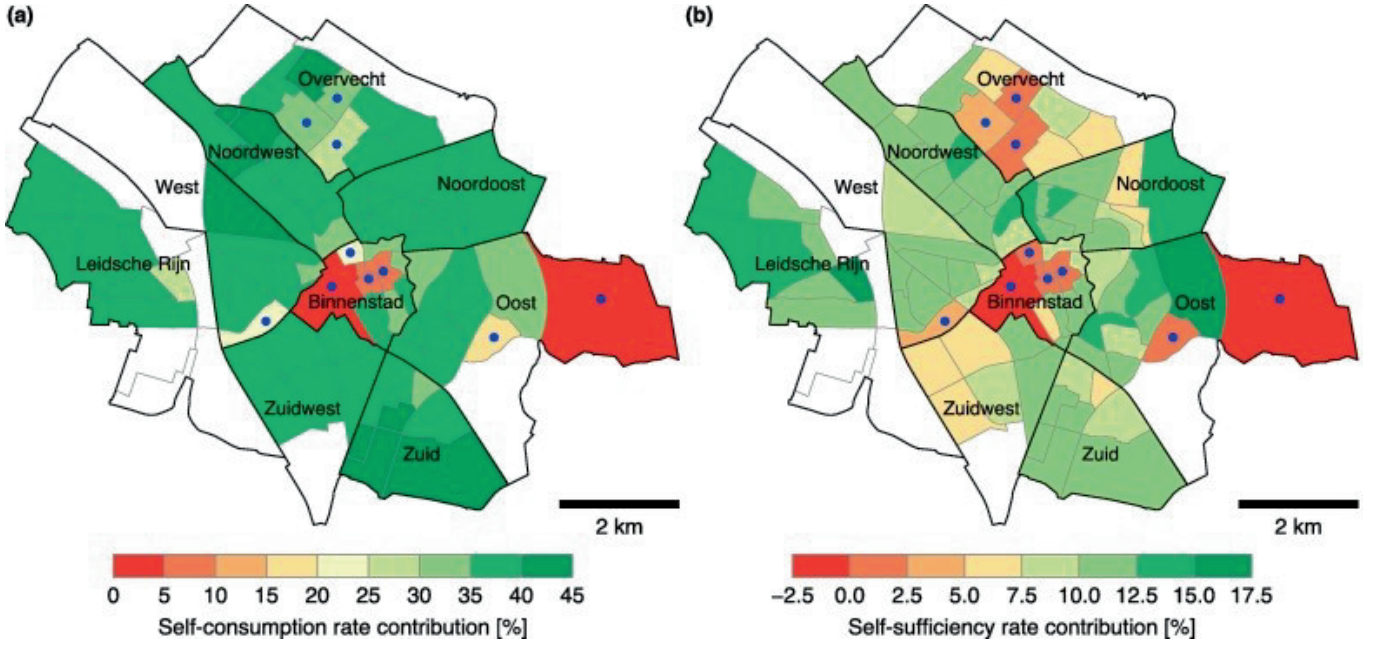

Figure 7-8: . Potential contribution of electric vehicles with battery energy storage system to the PV self-consumption ratio (a) and contribution to the self-sufficiency ratio (b) for 88 neighbourhoods. Areas with a self-consumption ratio of > 99% are indicated by the blue dot.

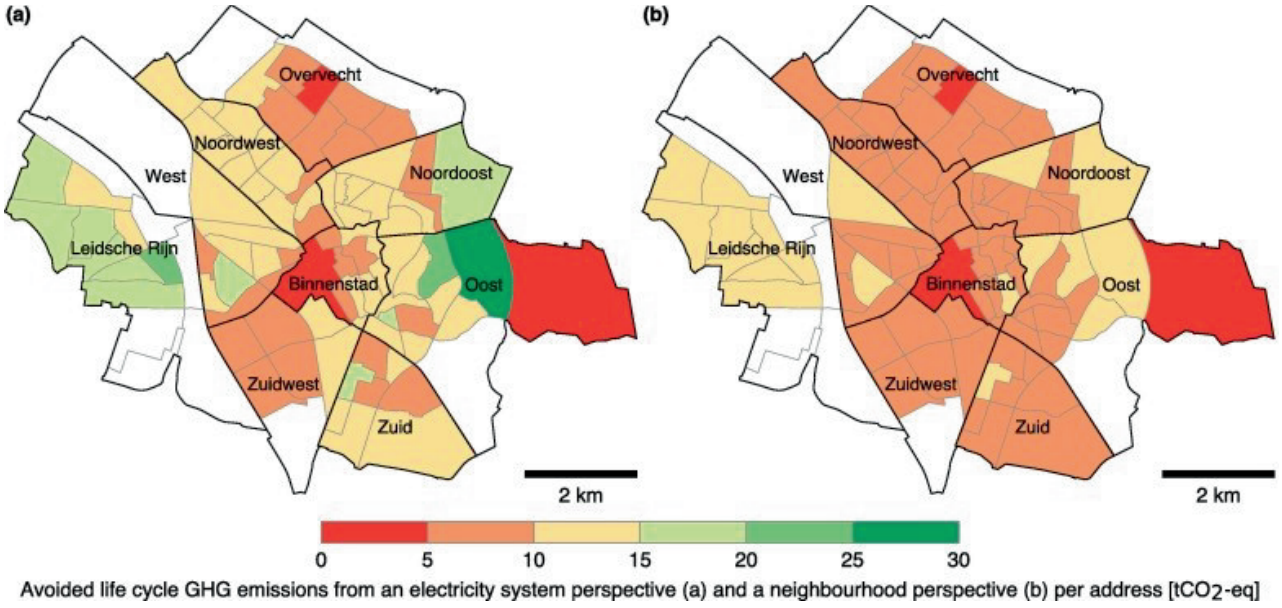

Figure 7-9: Potential of avoided life cycle GHG emissions per address from an electricity system perspective (a) and from a neighbourhood perspective (b). The avoided emissions are presented for the reference scenario including electric vehicles and battery storage. Note that the avoided emissions are normalized with the number of addresses within each neighbourhood.

7.3.5. Avoided life cycle emissions

The avoided life cycle GHG emissions from an electricity system and neighbourhood perspective were assessed with the reference parameters including electric vehicles and battery energy storage system, see Figure 7-9. The avoided GHG emissions are given for the 30-year period per residential address. The emissions show large differences between the neighbourhoods. Avoided GHG emissions from an electricity system perspective are on average 11.5 tCO_2-eq, ranging between 0.3 to 28.1 tCO_2-eq per address. Average avoided GHG emissions from a neighbourhood perspective are 8.6 tCO_2-eq per address, which is around 0.3 tCO_2-eq for each year.

Neighbourhoods with 100% self-consumption ratios have almost similar emissions from an electricity system perspective as from a neighbourhood perspective, since all PV electricity is directly used. These neighbourhoods are located in the centre of the city. The suburb Leidsche Rijn shows high avoided emissions from a neighbourhood perspective, due to high PV potential and the large SCR impact by storage and electric vehicles. The North-West district has similar SCR as the Leidsche Rijn suburb, yet lower avoided emissions are seen here. This is due to the lower electricity demand and the lower PV yield potential for each address in North-West district. The neighbourhood with the lowest self-consumption ratio (Rijnsweerd in the East district) shows the largest emission reductions from system perspective.

PV modules made in Europe are produced with lower greenhouse gas emissions compared to PV made in China, due to the lower carbon intensity of the electricity generation mix in Europe. We compared the impact of PV made in China with PV made in the EU on the avoided emissions. 824 gCO_2-eq for each Wp were assumed as emissions from PV produced in Europe [242].The avoided GHG emissions of China and Europe, and the relative change between these areas are shown from an electricity system perspective and neighbourhood perspective in Figure 7-10. No change in emissions from manufacturing battery storage was assumed. When using PV modules manufactured in the EU, the avoided emissions are increasing to averages of 14.4 tCO_2-eq from an electricity system perspective and to 11.5 tCO_2-eq

from a neighbourhood perspective. The relative change in avoided emissions between China and Europe are significantly higher from a neighbourhood perspective than from an electricity system perspective. An average of 28% is shown for the system perspective and 36% from a neighbourhood perspective. Neighbourhoods with high PV system potential have larger emissions from manufacturing and therefore relatively lower avoided emissions from a neighbourhood perspective. Consequently, the distribution in relative change of avoided emissions from a neighbourhood perspective is larger compared to the avoided emissions from a system perspective.

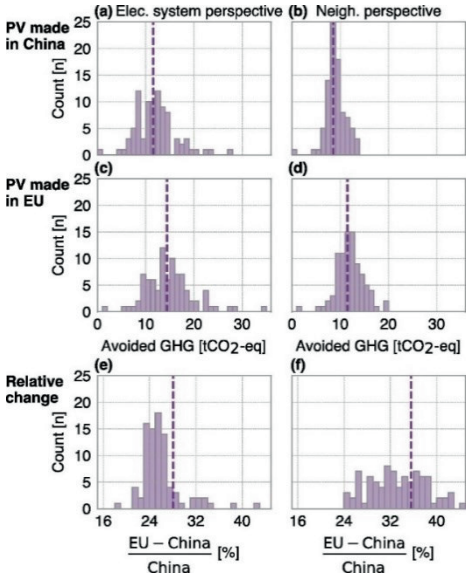

Figure 7-10: Distribution of avoided life cycle GHG emissions per address with PV made in China (a & b), PV made in Europe (c & d) and the relative change in avoided emissions between these areas (e & f), The left column shows the avoided emissions from an electricity system perspective and the right columns shows the avoided emissions from a neighbourhood perspective. Mean values of the distribution are indicated by the dashed lines. Histogram bins of 1 tCO2-eq were used for the avoided emissions and bins of 1% for the relative change. Note that a relative change larger than 45% is observed for one neighbourhood from an electricity system perspective, and two neighbourhoods from a neighbourhood perspective. These are not shown in histogram (e) and (f).

7.4. Sensitivity Analysis

A sensitivity analysis was conducted for four different rooftop utilization rates. These utilization rates were combined with a larger share of EV solar charging or with smaller or larger battery storage capacities. Other input parameters, see Table 7-1, were kept constant. Three parameters were assessed; SCR, SSR and avoided life cycle GHG emissions per address from a neighborhood perspective. The avoided emissions from a system perspective were not shown, since these are less dependent on the PV self-consumption. Some of the scenarios assessed here are not realistic but purely theoretical. A 100% rooftop utilization rate is currently not practical to implement. Moreover, a high smart solar charging share, of 75% or even 100%, requires major investments in charging infrastructures. Furthermore, EVs should be available for charging within the neighborhood.

7.4.1. EV smart solar charging share

The influence of five smart solar charging shares of four rooftop utilization rates is presented in Figure 7-11. The 25% rooftop utilization scenario shows an average SCR of 85% when no EV is smart charged. This is increased by 11%, if all EVs would apply smart solar charging. In this rooftop utilization scenario, a > 99% SCR is reached for 20 neighbourhoods. This limits the average increase of the SCR. Battery energy storage shows an average SCR close to 100%, for all EV smart charging shares. Thus, energy storage reduces the impact of smart solar charging to almost nothing. Therefore, it is not recommended to invest in smart charging infrastructure with storage under the 25% rooftop utilization rates.

Under the 50% rooftop utilization, a shift from 0% solar charging share to a 100% solar charging share increases the average SCR by 12% points. This is a slightly larger increase than shown for the 25% rooftop utilization rate. Fewer neighbourhoods reach the maximum SCR, thus the average increase in SCR is larger. However, under the 75% rooftop utilization, the increase in SCR due to higher smart charging shares is reduced to 9.6%, which is 2% lower than under the 50% rooftop utilization rate.

Higher rooftop utilization rates have significantly more surplus PV available. Therefore, the impact of smart charging share on the SCR is reduced.

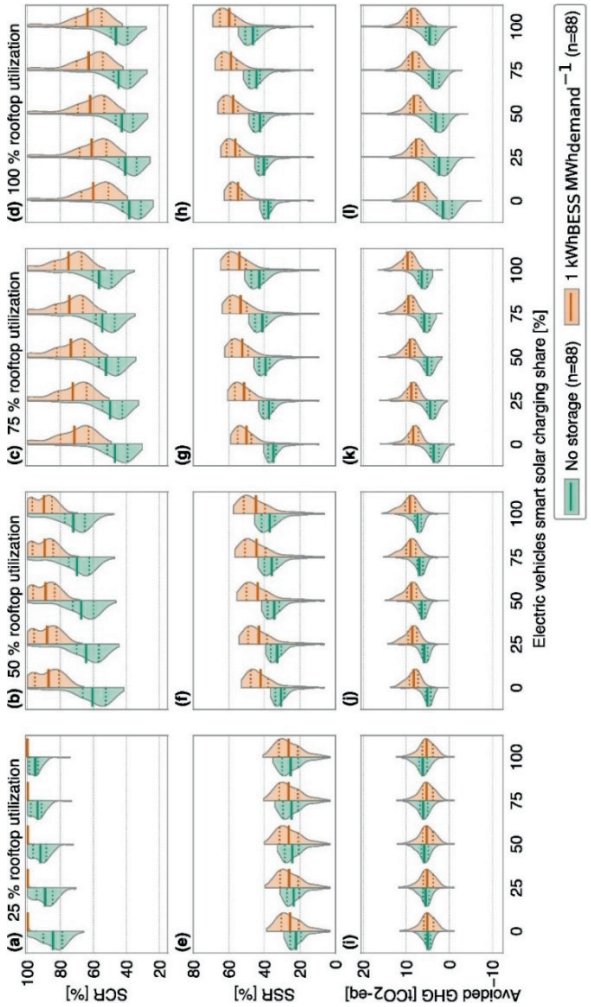

Figure 7-11: . Influence of the rooftop utilization factor on the self-consumption ratio (a to d), self-sufficiency ratio (e to h) and avoided life cycle emissions per address from a neighbourhood perspective (i to l). The distributions are shown for the 88 neighbourhoods and five electric vehicle charging scenarios using violin plots. The left side of the violin plot shows the distributions without battery storage and the right side of the violin plot shows the distributions with a 1 kWh storage capacity for each MWh of annual electricity consumption. Mean values are indicated by the solid lines and 25% and 75% percentiles are indicated by dotted lines.

Neighbourhoods with storage have a larger PV self-consumption. Consequently, the SCR increase due to a larger solar charging share is reduced to 2.8% points under the 50% rooftop utilization scenario. This number is increased to 3.6% under the 100% rooftop utilization rate, since more surplus PV energy is available for storage. Also, the widest distribution between neighbourhoods is seen with a 100% rooftop utilization rate. A larger smart solar charging share reduces the surplus PV that can be stored in batteries. Subsequently, the SCR impact of storage is reduced with higher EV smart solar charging shares. Still, these high smart solar charging shares are not realistic, thus investing in battery energy storage could be worthwhile.

Self-sufficiencies increase slightly for the 25% rooftop utilization rate, with averages from 22% with no smart solar charging to 25% for a 100% solar charging share. SSR are limited when storage is added, with an average of around 26%. Yet, the impact of storage is significantly higher with a 50% utilization rate, and largest for a 100% rooftop utilization rate. Furthermore, the increase in EV smart solar charges share shows a significantly larger impact on the SSR. For a 50% utilization rate and no storage, a shift from 0% to 100% solar charging share results in a SSR increase of 6.5% points. This difference increased by 8.7% points under a

100% rooftop utilization rate. When storage is added to the neighbourhoods, then this increase is 4.8% points. An increase in rooftop utilization rates causes an expansion of the first 25% percentile for both neighbourhoods with and without storage. Neighbourhoods with a low SSR have a far higher electricity demand. Hence, the absolute increase in SSR due to higher PV capacity is smaller for neighbourhoods that already show high SSR.

Avoided life cycle GHG emissions, from a neighbourhood perspective and per addresses, were found to be increasing from a 25% to a 75% rooftop utilization rate. However, the avoided emissions have decreased for a 100% rooftop utilization compared to a 75% rooftop utilization. Some neighbourhoods even showed negative values. This means that the emissions due to manufacturing of PV and storage systems are larger than the avoided emissions due to the direct consumption at the neighbourhood level. Furthermore, under the 25% rooftop utilization rate, avoided emissions are lower for neighbourhoods with storage than without storage.

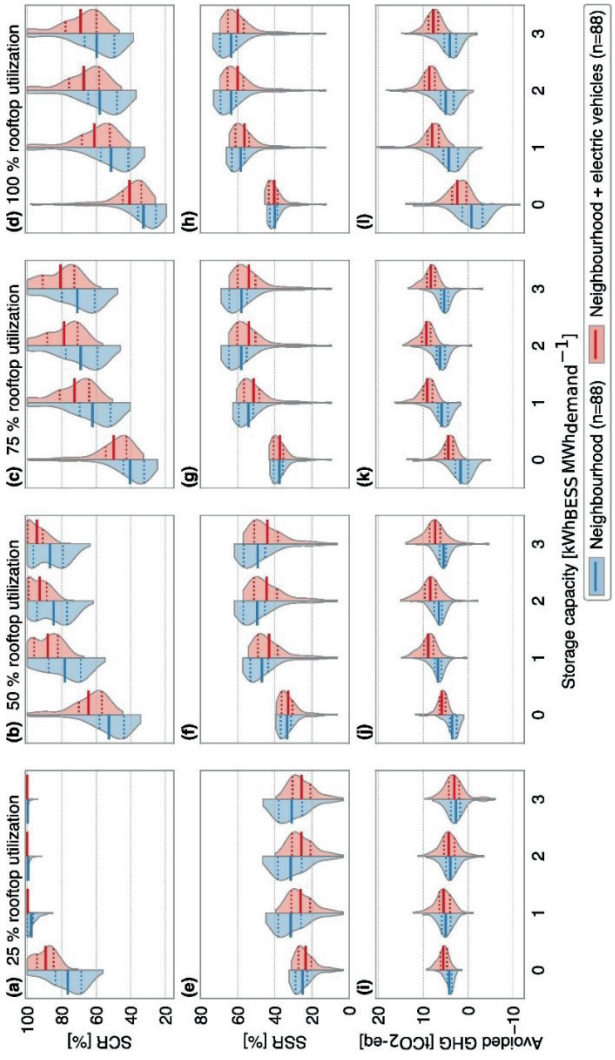

Figure 7-12: . Influence of the rooftop utilization factor on the self-consumption ratio (a to d), self-sufficiency ratio (e to h) and avoided life cycle emissions per address from a neighbourhood perspective (i to l). The distributions are shown for the 88 neighbourhoods and four battery storage capacities using violin plots. The left side of the violin plot shows the distributions with electricity consumption of the neighbourhood only and the right side of the violin plot shows the distributions of the neighbourhood with electric vehicles. The electric vehicles have a 25% solar charging share. Mean values are indicated by the solid lines and 25% and 75% percentiles are indicated by dotted lines.

Yet, from an electricity system perspective, the average avoided emissions increased by rooftop utilization rates. Neighbourhoods without storage and a 25% solar smart share showed averages of 7, 14, 21 and 27 tCO_2-eq of avoided emissions for 25, 50, 75 and 100% rooftop utilization rates respectively. Neighbourhoods with storage and a 25% solar smart share showed lower avoided emissions of 5, 12, 18 and 25 tCO_2-eq of for 25, 50, 75 and 100% rooftop utilization rates respectively.

7.4.2. Battery storage capacity

The influence of increasing battery storage capacities under four rooftop utilization rates is presented in Figure 7-12. SCR increased under all scenarios with larger storage capacities and when EVs are included. With 25% of rooftop utilization, the SCR is maximized with the use of energy storage and electric vehicles. With 50% rooftop utilization, we found that a 2 kWh storage system per MWh demand does not impact the upper 25% percentile of the neighbourhoods. Hence, a quarter of the neighbourhoods can consume all locally produced PV electricity under these conditions. A 75% and 100% rooftop utilization rate results in a higher impact of larger battery storage capacities. The addition of electric vehicles to the neighbourhoods results in higher SCR values. For these high rooftop utilization rates, the average SCR impact from energy storage is quite similar for neighbourhoods with and without EVs. Also in this case, surplus PV electricity is not fully utilized by EVs charging and therefore storage can have a similar impact. Furthermore, additional demand is added with EVs, which results in relatively larger storage capacities and thus higher SCR.

Self-sufficiency ratios gradually increase with higher rooftop utilization rates. With 25% rooftop utilization, the highest SSR were observed for a battery size of 1 kWh per MWh demand. Larger storage capacities resulted in more electricity losses caused by charging and discharging of the batteries. Consequently, self-sufficiency is reduced within the neighbourhood. Neighbourhoods with EVs have a higher direct PV self-consumption, thus less surplus PV electricity can be shifted by storage. As a result, the influence of storage is smaller for neighbourhoods with EVs than for neighbourhoods without EVs. Under the no storage scenarios, similar SSR

distributions were observed for neighbourhoods with EVs and without EVs. This indicates that power consumption time series of the EVs is comparable to the electricity consumption time series of the neighbourhoods.

Avoided emissions per address are largely dependent on rooftop utilization rate and installed storage capacities. Under the 25% rooftop utilization scenario, the increase in storage capacity shows a significant reduction in avoided emissions. For higher rooftop utilization rates, an increase in avoided emissions can be seen when shifting from no storage to 1 kWh per MWh capacity. However, larger storage capacities show a reduction of avoided emissions. For these larger capacities, the emissions due to manufacturing are higher than the avoided emissions due to the self-consumption. Moreover, EVs add demand to the neighbourhood and therefore avoided life-cycle emissions increase.

7.5. Discussion

This research showed that PV self-consumption and self-sufficiency potential varies significantly between neighbourhoods. These variations are primarily related to limited residential roof area for PV siting, higher electricity demand, or higher expected electric vehicle penetration rates. A number of limitations concerning assumptions and data availability were made in this research that could impact the outcome substantially.

7.5.1. Data limitations

The PV potential of facades from residential buildings was not included in the study. Especially, facades from tall residential buildings can significantly increase the PV potential in neighbourhoods [210]. For example, the district of Overvecht contains numerous tall residential buildings, consequently limiting the self-sufficiency ratio. Also, including facades would substantially increase the self-sufficiency ratio of these types of buildings. Furthermore, by using east and west oriented facades, the PV yield over the day is extended beyond the noon peak to early morning and late

afternoon. This will provide a higher direct PV self-consumption and decrease the need for storage [247]. However, assessment of PV potential of facades is computation-intensive, since another dimension is added to the radiation model [248]. Furthermore, information about the share of windows and other building facade components makes the model complex. In addition, this information is not easily available.

The annual incoming POA irradiance on each rooftop was assessed using the ArcGIS tools. This number was used to linearly scale down PV yield time series obtained from the PVLIB model. Consequently, we assumed that the shade was homogenous homogeneously spread over the PV yield time series. However, the impact of shade on the PV yield depends on the position of the sun in the sky and the location of the obstructions which block the direct sunlight. We aggregated the individual PV time series of each roof to a time series for a neighbourhood. Also, we assumed the shades on each PV system in the neighbourhood do not occur simultaneously. Subsequently, the influence of shade on individual PV system decreases. Determining incoming POA irradiance for each roof for a smaller time step is recommended for further research. However, this requires significant more computation time or different calculation tools. Furthermore, we assumed that all incoming irradiance on the PV module would be converted to electricity. This conversion could be decreased due to partial shading of the module. The impact of partial shading on the PV yield depends on the installed system architecture and the module design [249].

We used one year of data (2015) to assess the rooftop PV potential and corresponding PV integration parameters, due to data availability and computation time. The year 2015 had a relative high annual irradiance compared to pre 2015 years [247]. Consequently, the PV yield production is overestimated with a few percent. Subsequently a higher self-consumption is expected but also a lower self-sufficiency. Furthermore, we assumed that excess PV power is distributed to other residential buildings within the neighbourhood using the low voltage grid. Power and voltage constraints within the low voltage grid were not considered. A detailed map of the low voltage grid should be included for future research for assessment of these potential limitations.

We assumed a constant emission factor for electricity over the year. Consequently, results showed that storage does not contribute to emission reductions from an electricity system perspective. However, with a larger share of renewables, a higher variability of emission factors from power generation can be expected. Consequently, the avoided emissions from storage could increase. If batteries would discharge at moments with a large share of fossil fuel fired power plants in the power generation mix, then this would avoid more emissions. Battery control strategies that include the marginal emissions factor should be developed.

7.5.2. Implementation considerations

Currently, over 90% of residential buildings are heated using natural gas-based systems [231]. The Dutch government has set goals to replace these with other technologies, e.g., heat pumps. This could increase the electricity demand of cities in the Netherlands. But the expected electricity demand of heat pumps in cities is hard to predict. Firstly, the residential buildings should be selected in which heat pumps are the most economically viable option to replace natural gas boilers. For example, district heating systems can also be used to replace natural gas heating systems, especially in densely populated cities [250]. Secondly, the electricity demand of heat pumps mainly depends on the heat source (air or ground) and the characteristics of the buildings. Especially old buildings should be insulated before installation of any heat pump system. The assessment of future electricity demand from residential buildings due to electric heating is highly recommended in future research.

The electricity demand for electric vehicles could be underestimated if more people will charge their EV within the city than was assumed. This could potentially occur when fast charging stations are introduced within the city, yet this would also require additional grid expansion measures. On the other hand, this demand could be overestimated due to reduced policy support for charging stations within cities. Furthermore, car sharing could result in less need for privately owned cars, and therefore reduce the demand. Moreover, a lack of parking spots or improved public transport can reduce the number of electric vehicles.

The technical PV potential in our study was assessed using 50% of the roof area. However, the estimated economic potential is lower due to the following reasons. First, the net-metering policy is established in the Netherlands. Consequently, dwelling owners with a relatively large roof area will probably only install a PV capacity sufficient to provide in their annual electricity consumption. Second, PV systems with a relatively low specific PV yield will not be installed due to a significantly larger payback period.

PV power density of 200 Wp/m^2 are assumed but are expected to increase in the future due to higher module efficiencies. This would increase the PV yield potential and decrease the self-consumption but increase the self-sufficiency. Also, we expect that future cost of PV systems will decrease based on the historical learning rates of around 20% [201]. Consequently, the economic profitability of PV systems for orientations with lower incoming irradiance will increase.

7.6. Conclusion

This study developed a spatio-temporal model that aimed to assess residential PV electricity integration options. The impact of electricity consumptions from buildings, electric vehicles and battery energy storage system was investigated for each neighbourhood in the city of Utrecht, the Netherlands. A large variety in PV yield potential, self-consumption ratio and self-sufficiency ratio was found between the neighbourhoods. Self-consumption ratios are between 34% and 100% for the neighbourhoods. This could be increased on average by 12% by electric vehicles and 25% with battery storage. Avoided life cycle emissions are between 0 and 28 tCO_2-eq, with an average of 12 tCO_2-eq per address.

The spatial analysis identified neighbourhoods with potential surplus PV electricity that could be used to provide electricity to surrounding neighbourhoods with lower PV potential. We recommend using battery storage capacities only in areas in which storage has a high impact on self-consumption enhancement. Also, supporting policies for smart solar charging of electric vehicles should focus on neighbourhoods

with large PV potential and relatively low electricity consumption. Especially for neighbourhoods where the low voltage grids require considerable expansion to host the potential PV capacity. Moreover, PV supporting policies should focus on neighbourhoods with a higher potential of avoided life cycle GHG emissions. The dissimilarity of results between the neighbourhoods indicates that area dependent investments and supporting policies could improve the PV power integration in cities. Therefore, we recommend the use of our spatio-temporal model for other cities to assist local governments and district system operators in the transition towards sustainable cities.

8.

Synthesis and Conclusions

8.1. Research context

International efforts for tackling climate change acknowledge the need for a total transformation of energy systems [6]. Advancements in technology and access to large amounts of data, may be the solution to catch up on our understanding of the current situation and reveal new insights and perspectives on how to proceed further with the energy transition [7]. On the path to create a sustainable energy future and climate resilient urban sprawls, technology used to understand, evaluate, and visualize various scenarios related to this complex phenomenon plays an important role. Adding a spatial perspective to this dynamic interconnected energy eco-system could help understand and provide necessary information on renewable energy strategies that are required to mitigate climate change.

Mapping and visualizing how energy is being used, locating potential sites for deployment of renewable energy, analyzing scenarios for development of visualization of policy implications are a few of the many possibilities of using geospatial analysis in support of applying solar PV. These are also the aspects that were addressed in this thesis. This chapter will synthesize the results and answer the research questions relating to the impact of GIS for solar PV.

8.2. Answers to research questions

The goal of this research is to assess the impact of geospatial technologies for application in renewable solar energy evaluation. In this context, four key areas have been identified which can have an impact on the evaluation in the usefulness of GIS, namely, the present status, potential, visualization, and policy evaluation. The sub-questions defined in Chapter 1 are addressed first followed by the main question.

Q1. How can data regarding current PV installations and solar potential be enriched using geospatial techniques?

Chapter 2 and 3 addressed the use of geospatial data and techniques for detection of PV installations and estimation of solar potential on rooftop level. The advantages of these bottom-up approaches over top-down studies zero down to the level of detail, and accuracies that can be achieved. In Chapter 2 the power of AI was harnessed in combination with spatial analysis to detect locations of existing PV installations on buildings using high-resolution aerial imagery. This information can be enriched with estimates of generating capacity in relation to panel area and buildings related information. Statistics departments which heavily rely on registers and people to update data can make use of these techniques to improve their existing database. A recent study deployed similar techniques to create a worldwide data set of large PV installations and related it to land-use studies providing valuable information on how different countries have different strategies when deploying large PV plants [251]. We showed how GeoAI techniques could be the way to detect connected or off-grid small-scale PV installations. This technique could be employed in countries where PV installation registration is not mandatory or where unregistered systems tapping into the grid could cause problems.

When it comes to PV potential studies, it has been established that remotely sensed data can provide detailed information on suitability of rooftops for siting PV depending on the resolution of the input data. One such method has been described in Chapter 3, where a very high-resolution height model has been used to model irradiation on rooftops and categorize them as suitable or not suitable based on

estimated production output. We show that geo-based irradiation models can replicate reality and incorporate layers of relevant data especially in suitability analysis. It was shown how slope, orientation, and irradiation layers along with building footprint data was combined to create a PV suitability map. The output reflects where shadows are most prominent and which parts of the roof are most suitable. In addition, calculation of important parameters like slope and orientation of the roofs which is usually modelled or assumed in most studies related to potential estimations is possible and relatively easy when using geospatial data.

The effect of scale, resolution, time, and validation of geo-based irradiation models was addressed in Chapter 4. With higher temporal frequencies incorporated within the model one could easily model the effect of shadows throughout the day or over months. It should be noted that higher level of detail entails higher processing times and eventually higher costs. Chapter 4 also presented the effect of resolution, particularly the advantages of high-resolution irradiation analysis in estimating energy production on varying rooftop conditions (see Figure 4-9). We have demonstrated how geospatial techniques can be used for scaling and aggregating data to create relevant information for different stakeholders in Chapters 2, 3 and 6.

Furthermore, combining different data layers (PV installations and PV potential), one could also estimate the left-over potential as shown in Figure 8-1. To conclude, Chapter 2, 3 and 6 provide methods that could improve information on solar installations and PV potential when geospatial techniques are used. As more and more earth observation data with high spatial and temporal resolution becomes available, use of AI and geospatial techniques could be integral in providing fast, accurate and detailed results which can be used for monitoring, planning of PV installations pertaining to rooftops and building façades [252].

(a)

(b)

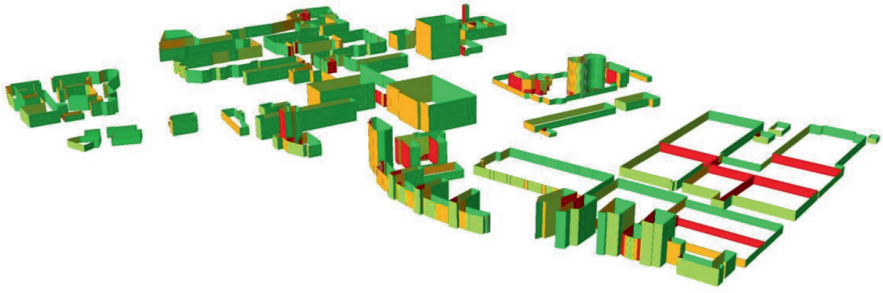

Figure 8-1:(a) Left-over potential (hatched lines) after combining PV potential and PV installation layers, (b) solar potential calculations on building facades for the area of Jaarbeurs in Utrecht. Red wall surfaces are unsuitable surfaces, and the green surfaces are most suitable. Source [252].

In relation to mapping and visualization which is fundamental to GIS, the ability to understand and present information incorporating space, time and scale was investigated. The research question addressed in this perspective is:

Q2. How can GIS mapping and visualization techniques be harnessed for monitoring and identifying trends in PV diffusion and performance?

With the ability to overlay data and display layers of information be it images, vector data or a combination of both, GIS can present the user with an interactive interface and mapping capabilities that are easy to comprehend as demonstrated in Chapter 5. We have mapped locations and performance data pertaining to PV installations from five different countries derived from web scraping techniques. It has been shown how by simply interpolating this data, one could create maps that illustrate the performance of PV systems and quickly identify the underperforming and overperforming systems and the underlying cause for a large geographic area. However, data stretching techniques used for visualization purposes must be addressed carefully depending on the subject matter that is being mapped. Mapping and visualization are highly dependent on cartographic principles like scale, resolution, data stretching, content and contrast. The effect of these factors has been addressed in Chapters 4 and 5. These make all the difference in understanding the content that is being presented. If the same data is drawn using different color schemes or data stretching techniques, one could even arrive at different conclusions (Figure 5.7).

Mapping helps put data into context. It does not only identify sites but also can effectively accredit the underlying factors that influence the data being mapped. In the case of locating or mapping PV installations as shown in Chapter 2, the first impression is the spread and density of these installations across the region under evaluation. However, one could also investigate the driving factors behind the density of the installations, why certain neighbourhoods have more PV installations than the others and if it relates directly to the socio-economic status of these

neighborhoods and so on. With multicriteria mapping one can visualize the effect of many data layers at once instead of looking at them individually, this is especially useful when looking at large datasets as shown in Chapter 6. Finally, visualization capturing dynamic changes within neighborhoods as described in Chapter 7 aids in creating policies targeted at specific neighborhoods or regions which could be effective in the future.

Advancements in computer vision and data science have had a positive effect on visualization and capability to model and visualize time-series data in GIS environment. Availability of detailed 3D models, high resolution aerial or drone imagery over the years or even real-time data, has made mapping, manipulating, and visualizing this data relatively easy with proper infrastructure. Nevertheless, one should still evaluate whether the use of such data and techniques is well suited for the designated purpose as that could potentially save time and costs.

Q3. How can spatial or spatio-temporal analysis be used in evaluating policy effectiveness or for modelling future scenarios for energy transition?

Policy making and planning go hand in hand, and this cannot be truer in the case of the energy transition. Up until now energy policies have been largely generalized. With new insights from spatial planning, it is evident that the geographical location plays a far more greater role in shaping policy [253]. For the Dutch scenario of localized strategies to effectively tackle energy transition issues, regional and local analytics play an important role. In this context, using GIS as a decision support tool in energy modelling [254–256] and policy development [253,257,258] has already shown tremendous added value.

In addition to the demonstrated use case of locating potential sites for solar energy deployment with the help of GIS techniques, we have demonstrated how GIS can be used to check the implications of a policy in Chapter 6. Potential solar diffusion was evaluated by assigning weights to socio-economic factors affecting solar PV adoption and processing them using an analytical hierarchical process within a GIS system.

We used the Postal Code Rose policy (in force until April 2021) which focused on encouraging citizens to invest in solar PV in a neighboring postal code if their rooftop was not suitable.

We identified income, house value, electricity consumption and peer effect as significant factors for PV adoption and modelled this data to create a corresponding weights and scale layer which was then used in the geographic overlay analysis (see Figure 6-3 and Table 6-1). Finally, it was shown that after applying the policy, the city of Apeldoorn could produce ~77% of its electricity demand through PV. The study considered social factors which are dynamic and complex to model especially on postal code level and the data is privacy sensitive and hard to access. Therefore, sensitivity tests were performed to see how much the results deviate if the weights for the factors changed. This gives a level of flexibility to the policy makers if they were to adopt a similar process to evaluate policies. Overall, the presented method shows potential of applying geo-spatial analysis for policy evaluation in terms of PV diffusion.

Spatio-temporal analysis is also very helpful in scenario studies as demonstrated in Chapter 7. The capability to model data from different locations over various time periods makes GIS a versatile tool. The extent to which PV can be integrated within cities was evaluated considering various parameters and scenarios. The spatio-temporal dynamics within the neighborhoods changed when different integration factors were considered, and effect of choices made was be analyzed and visualized. Once established such model frameworks are easy to scale in a GIS environment. The greatest flexibility is the ability to change the physical or political boundaries of analysis. Instead of neighborhoods, we could investigate the dynamics within cities or even conduct the analysis at municipality level.

Main research question

To what extent is GIS instrumental in the field of Solar PV?

In this thesis the technological impact of using GIS techniques and the influence of spatial thinking in the field of solar PV was evaluated. The synthesized results are based on four aspects; evaluation of the present status, potential estimation, monitoring through visualization and finally effect of policies.

Present PV status

GeoAI has brought about a paradigm shift in geo-data analysis. Locating PV installations from remotely sensed data be it satellite images, aerial photographs or even data gathered from drones can be accomplished in a relatively short time with good accuracies. GeoAI techniques are particularly useful for counting off-grid systems or scaling up processes that usually take lifetimes when done manually. With recent escalation in publicly available AI algorithms, workflows, training data, and knowledge, GeoAI methods are easy to scale and reuse. However, since GeoAI is largely dependent on remote sensing imagery, lack of very high-resolution imagery could be a bottleneck to adopt this method for detecting rooftop installations in many countries. At the same time there is discussion around the safety, ethics, and inexplicability of the algorithm's behavior (black-box nature) when using AI, which makes it a contentious choice.

Potential estimation

From rooftop solar potential calculations to comprehensive nation-wide mapping of solar potential is a viable option when GIS techniques are incorporated with remote sensing data. Digital elevation models (DEM) along with atmospheric parameters form the basis of this analysis. The raster image resolution can be selected depending on the goal of the project and scaling up is relatively easy once a baseline is established. Site suitability studies have been an integral part of GIS systems from a long time. With insights from spatial planning, urban planners, network operators can combine PV potential data to design cities or plan infrastructure in a GIS environment. The resolution of the DEM's currently available as open data is

sufficient to provide necessary information for most European countries. Potential estimations at rooftop level when combined with building characteristics and functional attributes lead to actual potential that is realizable.

Visualization and monitoring

GIS system can present spatial and non-spatial data to analyze or interpret. Spatial relationships between objects within a layer or different layers can be explored. Geo-spatial analytics have the capability to combine or summarize data with diverse scales or varying borders with a user-friendly system that is easy to navigate. The visual flexibility provided by a GIS system allows for quick monitoring of objects under scrutiny with layers of information that can interact with each other. However, adhering to cartographic principles such as the use of color, symbol, scale and choosing the right theme based on data type is of utmost importance to make a compelling visualization that is practical, readable, and useful. Time series data is easily incorporated, and growth of PV installations or lack thereof can be either controlled visually or via spatial analysis.

Policy evaluation

The ability to create and explore spatially explicit models involving dynamic processes which are non-stationary in space makes GIS very useful in policy development and evaluation. When the above-mentioned analysis and data regarding PV installations, solar potential, demographic, social and economic attributes is combined, it could eventually lead to information useful for formulation of new policy. On the other hand, GIS as a tool is also useful in evaluating the effect of policy on adoption of renewable technologies. Moreover, scenario modelling with space and time as parameters provide the necessary information that is required to take decisions or make policies, which is useful in assessing spatial implications of future energy transition road maps.

8.3. Perspectives on GIS4PV and recommendations

We have demonstrated and established that GIS can provide a holistic approach that has the capability to incorporate and model space, time, and scale as driving factors to understand and solve complex problems related to the energy transition. However, the integration or acceptance of GIS is neither simple nor without hurdles. Moreover, this thesis presented case studies that can be improved, especially given that there have been technological developments that make many recommendations suggested in the chapters possible. To utilize the benefits of such distinct technology for societal applications, identifying current problems and sectors where GIS could help speed up the sustainable transition process is vital. Thus, this section focuses on current bottlenecks and perspective solutions for GIS integration.

8.3.1. Bridging the gap between policy and research

The brightest minds of our century are working harder than ever to solve the climate crisis, and there are two sides to it. On the one hand it is innovation, technology, or research and on the other economy, society, and politics, which lead to policy.

Policies are heavily reliant on data, statistics and citizen interaction and are "evidence based". The evidence which is a result of research or innovation is not as plain or simple as it seems. It is a product of models that have assumptions, data that is diverse and liable to quality issues and finally the way the results are interpreted. It is therefore imperative that policy makers are aware of these assumptions or at least their implications. On the other hand, the researchers' approach to create evidence or data required for policy is often tunneled, with little awareness on governance and what goes into policy making. This leads to disparity in ideas and understanding especially when looking at data or results but interpreting it in different ways or unable to comprehend the effect of assumptions. The results in chapter 7 are a consequence of many assumptions. For example, we considered only buildings with residential function in the analysis, however the technical constraints of the roof itself for PV siting was not considered. Basing the analysis purely on

available roof top area means either over estimation or underestimation of available area in certain neighborhoods, which has a huge impact on the final results. In addition, the solar irradiation model used in the study also has certain assumptions. In scenario studies like these it might be possible to mention all the assumptions although it is hard to quantify them and their effect. Therefore, it is of utmost importance to ask questions and build up dialog to bridge this gap so that relevant policies that are in line with climate goals can be made and implemented.

In this context, it is useful to exploit the advantages of GIS to present compelling information with an impact on the specified audience. **Dashboards and story maps** could be the bridge between researchers and policy makers. Dashboards allow for interactive visualization and analysis of data which could allow policy makers to associate with the information being presented including the consequences of the choices made. This was witnessed during the pandemic with the corona dashboard where one could keep track of the spread of infections in real-time and world health organization was able to make decisions and suggestions accordingly [259]. Dashboards could also be the way to engage with the citizens, consider their opinions to include them in the dialog. This provides a setting where individuals can visualize changes based on choices and the impact it has on their environment.

8.3.2. Emerging technologies

Technology is evolving at an unprecedented pace and to keep up with it without losing insight of its basic purpose of simplifying things is an irony. GIS has evolved from being desktop-based systems to web and server-based enterprise systems and now it is even being deployed on the cloud as Software as a Service (SaaS) which offers users to make choices based on their needs. The average user is presented with choices that not only vary in price to performance-ratio (in the case of GIS open-source vs proprietary) but also the ease of use, personal preference for using a graphical user interface (GUI) vs command line interface (CLI) and the technical support and the level of flexibility it provides. Nowadays, upgrading and maintaining desktop systems to keep at par with technological developments is turning out to be more expensive compared to exchanging the systems for cloud technology. Cloud

storage and computation technologies are providing the necessary possibilities to experiment and innovate with data without limitations on data size and storage. A glimpse of the interaction between the emerging technologies discussed below and GIS to provide a holistic approach to deal with energy management is presented in Figure 8-2.

Internet of Things (IoT) is an emerging technology that collects and shares data from sensors from all around the world, be it real-time or static [260]. The connection with GIS is then the location of the sensor itself that provides the necessary geographic context for processing the data and taking necessary action, something that is typical in case of smart cities. Data from the sensors are separate entities interacting on the server. The added value is real-time spatial analytics with observed or measured data. If a weather condition (overcast sky) affects the PV energy production in a neighborhood, data from smart meters, pyranometers, and weather forecasting can be used to predict the future of this weather pattern to alert the network operators to take necessary action to account for the sudden dip in electricity production (ramp down) in the concerned neighborhoods. Conversely, this can also be used for ramping up of energy production. Data thus collected over long periods of time when connected with a GIS system could be used for analyzing spatio-temporal patterns and for generating visualizations or animations on the fly. In addition, integrating GIS with building information models can provide detailed information on the indoor built environment useful in energy studies.

Digital twin (DT) is another concept that is gaining popularity rapidly. A digital twin encompasses a virtual representation of real-world object/process that can be used to simulate strategies to evaluate the success or performance before implementing it in the real world. City information models are being built to serve as a Geodata hubs [261]. However, to build these digital twins, the above-mentioned tools and technologies are essential.

8.3.3. Data

The purpose of a GIS system is to model real world data to understand and analyse the effect of physical and human process that occur on earth. Thus, data has a significant role and is central for effective functioning of a GIS system. The effect of technology is also evident from the availability of different data modalities and formats. Future GIS systems should be able to evolve accordingly to accommodate various data types and modalities as shown in Figure 8-2.

The problem however is associated with data availability and formats. Not every country has resources to spend on high resolution data and in some countries optical imagery is not sufficiently detailed. Developing countries which do not have access to high resolution data have to work with medium resolution data that might not be sufficient for solar potential studies mentioned in this thesis. In addition, the density of cities and building characteristics in developing countries vary to a degree that it is challenging to capture data with one single sensor. Although drones are a good alternative in providing high precision data, they have limited range mapping capabilities.

If data availability and access is one side of the problem, dealing with numerous data formats and interoperability between systems and software is another. Different data modalities and processes lead to different data formats and software required to process the data. Although, national and global bodies that support spatial data infrastructures are doing their best to create an ecosystem to facilitate geospatial data collection, storage, access and sharing, issues with interoperability still exist [262]. Strict adherence to Open Geospatial Consortium **(OGC) standards** [263] can help overcome this issue.

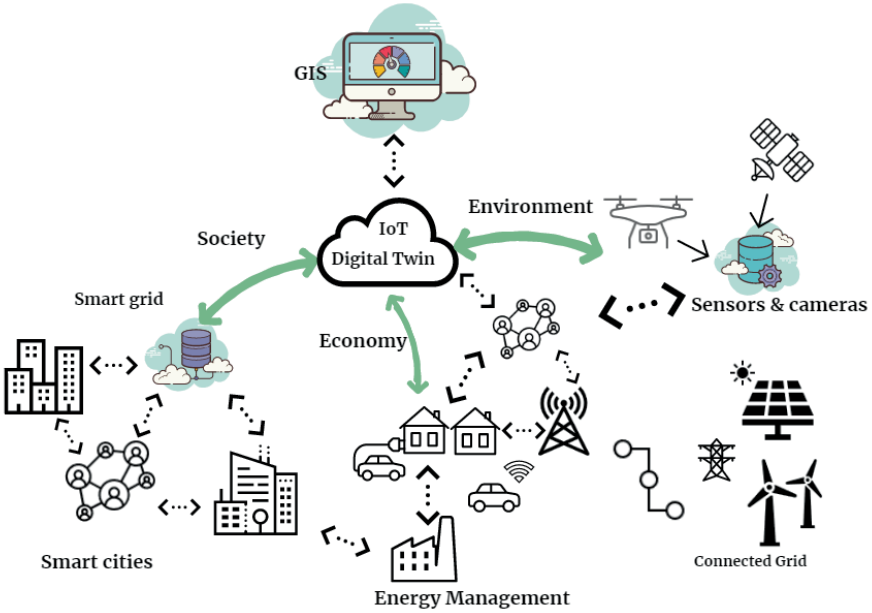

Figure 8-2: An example of how future technological systems may interact and how geospatial technologies could be deployed for providing a comprehensive overview leading to sustainable energy management. A part of this workflow is already in place where cloud-based computing is replacing desktop and traditional storage systems.

Figure 8-3: explanation of 3D models available at different level of detail. Source: [264]

Yet another data aspect that creates discrepancies is scale. It is imperative that appropriate data with respect to resolution is chosen based on the purpose or goal of the analysis. Although, data aggregation techniques and low-medium resolution datasets suffice while creating nation-wide datasets, it is worthwhile investigating

automatic data scaling techniques. This could provide homogenous and reliable information without having to worry about scaling issues.

Solar potential analysis must be extended to include building façades as solar siting on rooftops alone may not be sufficient to fulfil the energy needs. Analysis based on 3D models instead of 2.5D elevation rasters can be used to calculate the **solar irradiation on building façades**. With 3D models available at level of detail (**LOD)** 3 (see Figure 8-3), or higher, solar potential analysis can provide accurate details on available surface area and potential production factors. Moreover, with Building Integration Models **(BIM)** building energy efficiency studies can be conducted.

When it comes to monitoring and mapping PV performance presented in Chapter 6, efficient data storage and analysis can help in identifying trends and changes. In addition, inclusion of the **environmental impact to quantify emissions** that can be avoided from transportation in addition to tracking the life cycle of a PV panel from production to installation can be studied. The environmental impact of utilizing locally produced vs imported PV is thus brought into focus, where consumers can make a conscious choice.

8.4. Epilogue

Energy transition is a huge part of climate crisis, which needs appropriate attention. The global energy system is dynamic and in order to understand this complex process that is affected by earth's physical processes to human interaction; data processing and visualization techniques are of utmost importance. Remote sensing and earth observation are providing the necessary data and with geo-spatial analysis one could provide the context essential for management of the energy systems. This thesis is an endeavor to present the implications of geo-spatial science for energy studies, with a focus on solar PV. We hope to have inspired and contributed in part to the collective effort towards realizing a sustainable energy future.

References

1. International Energy Agency Global Energy Review 2021. Assessing the Effects of Economic Recoveries on Global Energy Demand and CO2 Emissions in 2021. **2021**, 36.
2. *The Limits to Growth: A Report for the Club of Rome's Project on the Predicament of Mankind*; Meadows, D.H., Club of Rome, Eds.; Universe Books: New York, 1972; ISBN 978-0-87663-165-2.
3. European Union Communication from the Commission to the European Parliament, the Council, the European Economic and Social Committee and the Committee of the Regions. *Energy 2020. A strategy for competitive, sustainable and secure energy* **2010**.
4. International Energy Agency *World Energy Outlook Executive Summary 2018*; 2018;
5. European Union Communication from the Commission to the European Parliament, the Council, the European Economic and Social Committee and the Committee of the Regions. *Forging a climate-resilient Europe - the new EU Strategy on Adaptation to Climate Change* **2021**.
6. International Energy Agency *World Energy Outlook 2020*; Paris, 2020;
7. International Energy Agency *Net Zero by 2050 - A Roadmap for the Global Energy Sector*; p. 224;.
8. Gholami, H.; Røstvik, H.N. Economic Analysis of BIPV Systems as a Building Envelope Material for Building Skins in Europe. *Energy* **2020**, *204*, 117931, doi:10.1016/j.energy.2020.117931.
9. Kamlesh, V.H.; Patel, A.S. Building Integrated Photovoltaics: Replacing with the Conventional Building Materials and Studying Its Cost Effectiveness. **2020**, *07*, 5.
10. Verberne, G.; Bonomo, P.; Frontini, F.; Van Den Donker, M.N.; Chatzipanagi, A.; Sinapis, K.; Folkerts, W. BIPV Products for Facades and Roofs: A Market Analysis. In Proceedings of the 29th European Photovoltaic Solar Energy Conference and Exhibition; 2014; pp. 3630–3636.
11. Martín-Chivelet, N.; Gutiérrez, J.; Alonso-Abella, M.; Chenlo, F.; Cuenca, J. Building Retrofit with Photovoltaics: Construction and Performance of a BIPV Ventilated Façade. *Energies* **2018**, *11*, 1719, doi:10.3390/en11071719.
12. van Sark, W.; Bontekoe, E. Towards a Near-Zero Energy Landmark Building Using Building Integrated Photovoltaics: The Case of the Van Unnik Building at Utrecht Science Park. In *Sustainability in Energy and Buildings*; Littlewood, J., Howlett, R.J., Capozzoli, A., Jain, L.C., Eds.; Smart Innovation, Systems and Technologies; Springer Singapore: Singapore, 2020; Vol. 163, pp. 339–348 ISBN 978-981-329-867-5.

13. BP Statistical Review of World Energy | Energy Economics | Home Available online: https://www.bp.com/en/global/corporate/energy-economics/statistical-review-of-world-energy.html (accessed on 28 May 2021).

14. International Energy Agency *Snapshot of Global PV Markets - 2020*; International Energy Agency, 2020; p. 20;.

15. DNE Research *Dutch Solar Trend Report 2021*; 2021; p. 76;.

16. Snow, J. 1813-1858.; Frost, W.H. 1880-1938.; Richardson, B.W. 1828-1896. *Snow on Cholera : Being a Reprint of Two Papers*; Hafner Pub. Co.: New York, 1965;

17. Sunak, Y.; Höfer, T.; Siddique, H.; Madlener, R. *E.ON Energy Research Center Series*.

18. Awange, J.; Kiema, J. Fundamentals of GIS. In *Environmental Geoinformatics: Extreme Hydro-Climatic and Food Security Challenges: Exploiting the Big Data*; Awange, J., Kiema, J., Eds.; Springer International Publishing: Cham, 2019; pp. 203–212 ISBN 978-3-030-03017-9.

19. van der Kam, M.J.; Meelen, A.A.H.; van Sark, W.G.J.H.M.; Alkemade, F. Diffusion of Solar Photovoltaic Systems and Electric Vehicles among Dutch Consumers: Implications for the Energy Transition. *Energy Research & Social Science* **2018**, *46*, 68–85, doi:10.1016/j.erss.2018.06.003.

20. Louwen, A.; Schropp, R.E.I.; van Sark, W.G.J.H.M.; Faaij, A.P.C. Geospatial Analysis of the Energy Yield and Environmental Footprint of Different Photovoltaic Module Technologies. *Solar Energy* **2017**, *155*, 1339–1353, doi:10.1016/j.solener.2017.07.056.

21. Moraitis, P.; Kausika, B.; Nortier, N.; van Sark, W. Urban Environment and Solar PV Performance: The Case of the Netherlands. *Energies* **2018**, *11*, 1333, doi:10.3390/en11061333.

22. Botzenhart, F.; Blaschke, T.; Hamacher, T.; Biberacher, M.; Schardinger, I. Integrating Spatial Models into Regional Energy System Optimisation: Focusing on Biomass. *Int J of Energy Sector Man* **2012**, *6*, 5–32, doi:10.1108/17506221211216517.

23. Blaschke, T.; Biberacher, M.; Gadocha, S.; Schardinger, I. 'Energy Landscapes': Meeting Energy Demands and Human Aspirations. *Biomass and Bioenergy* **2013**, *55*, 3–16, doi:10.1016/j.biombioe.2012.11.022.

24. Resch, B.; Sagl, G.; Törnros, T.; Bachmaier, A.; Eggers, J.-B.; Herkel, S.; Narmsara, S.; Gündra, H. GIS-Based Planning and Modeling for Renewable Energy: Challenges and Future Research Avenues. *ISPRS International Journal of Geo-Information* **2014**, *3*, 662–692, doi:10.3390/ijgi3020662.

25. Ministry of Economic Affairs *Energy Report. Transition to Sustainable Energy*; Ministry of Economic Affairs, 2016;

26. VIVET Available online: https://www.regionale-energiestrategie.nl/vivet_info/default.aspx (accessed on 23 February 2021).

27. Curier, R.L.; De Jong, T.; Strauch, K.; Cramer, K.; Rosenski, N.; Schartner, C.; Debusschere, M.; Ziemons, H.; Iren, D.; Bromuri, S. *Monitoring Spatial Sustainable*

Development: Semi-Automated Analysis of Satellite and Aerial Images for Energy Transition and Sustainability Indicators.; 2018; p. 24;.

28. TKI Urban Energy; Generation Energy *Ruimtelijk potentieel van zonnestroom in Nederland*; 2021; p. 100;.

29. Suri, M.; Hofierka, J. A New GIS-Based Solar Radiation Model and Its Application to Photovoltaic Assessments. *Transactions in GIS* **2004**, *8*, 175–190, doi:10.1111/j.1467-9671.2004.00174.x.

30. Gassar, A.A.A.; Cha, S.H. Review of Geographic Information Systems-Based Rooftop Solar Photovoltaic Potential Estimation Approaches at Urban Scales. *Applied Energy* **2021**, *291*, 116817, doi:10.1016/j.apenergy.2021.116817.

31. Bódis, K.; Kougias, I.; Jäger-Waldau, A.; Taylor, N.; Szabó, S. A High-Resolution Geospatial Assessment of the Rooftop Solar Photovoltaic Potential in the European Union. *Renewable and Sustainable Energy Reviews* **2019**, *114*, 109309, doi:10.1016/j.rser.2019.109309.

32. Choi, Y.; Suh, J.; Kim, S.-M. GIS-Based Solar Radiation Mapping, Site Evaluation, and Potential Assessment: A Review. *Applied Sciences* **2019**, *9*, 1960, doi:10.3390/app9091960.

33. Borfecchia, F.; Caiaffa, E.; Pollino, M.; De Cecco, L.; Martini, S.; La Porta, L.; Marucci, A. Remote Sensing and GIS in Planning Photovoltaic Potential of Urban Areas. *European Journal of Remote Sensing* **2014**, *47*, 195–216, doi:10.5721/EuJRS20144713.

34. Romero Rodríguez, L.; Duminil, E.; Sánchez Ramos, J.; Eicker, U. Assessment of the Photovoltaic Potential at Urban Level Based on 3D City Models: A Case Study and New Methodological Approach. *Solar Energy* **2017**, *146*, 264–275, doi:10.1016/j.solener.2017.02.043.

35. Brito, M.C.; Freitas, S.; Guimarães, S.; Catita, C.; Redweik, P. The Importance of Facades for the Solar PV Potential of a Mediterranean City Using LiDAR Data. *Renewable Energy* **2017**, *111*, 85–94, doi:10.1016/j.renene.2017.03.085.

36. Bremer, M.; Mayr, A.; Wichmann, V.; Schmidtner, K.; Rutzinger, M. A New Multi-Scale 3D-GIS-Approach for the Assessment and Dissemination of Solar Income of Digital City Models. *Computers, Environment and Urban Systems* **2016**, *57*, 144–154, doi:10.1016/j.compenvurbsys.2016.02.007.

37. Centraal Bureau voor de Statistiek CBS Open Data StatLine Available online: https://opendata.cbs.nl/portal.html?_la=nl&_catalog=CBS&tableId=84783NED&_theme=280 (accessed on 28 May 2021).

38. *Climate Change 2021: The Physical Science Basis. Contribution of Working Group I to the Sixth Assessment Report of the Intergovernmental Panel on Climate Change*; Masson-Delmotte, V., Zhai, P., Pirani, A., Connors, S.L., Péan, C., Berger, S., Caud, N., Chen, Y., Goldfarb, L., Gomis, M.I., Huang, M., Leitzell, K., Lonnoy, E., Matthews, J.B.R., Maycock, T.K., Waterfield, T., Yelekçi, Ö., Yu, R., Zhou, B., Eds.; Cambridge University Press, 2021;

39. Oudes, D.; Stremke, S. Spatial Transition Analysis: Spatially Explicit and Evidence-Based Targets for Sustainable Energy Transition at the Local and Regional Scale.

Landscape and Urban Planning **2018**, *169*, 1–11, doi:10.1016/j.landurbplan.2017.07.018.

40. Macharis, C.; Pekin, E. Assessing Policy Measures for the Stimulation of Intermodal Transport: A GIS-Based Policy Analysis. *Journal of Transport Geography* **2009**, *17*, 500–508, doi:10.1016/j.jtrangeo.2008.10.004.

41. Asdrubali, F.; Presciutti, A.; Scrucca, F. Development of a Greenhouse Gas Accounting GIS-Based Tool to Support Local Policy Making—Application to an Italian Municipality. *Energy Policy* **2013**, *61*, 587–594, doi:10.1016/j.enpol.2013.05.116.

42. Mrówczyńska, M.; Skiba, M.; Sztubecka, M.; Bazan-Krzywoszańska, A.; Kazak, J.K.; Gajownik, P. Scenarios as a Tool Supporting Decisions in Urban Energy Policy: The Analysis Using Fuzzy Logic, Multi-Criteria Analysis and GIS Tools. *Renewable and Sustainable Energy Reviews* **2021**, *137*, 110598, doi:10.1016/j.rser.2020.110598.

43. Gao, S. Geospatial Artificial Intelligence (GeoAI). In *Geography*; Oxford University Press, 2021 ISBN 978-0-19-987400-2.

44. Ferreira, M.P.; Almeida, D.R.A. de; Papa, D. de A.; Minervino, J.B.S.; Veras, H.F.P.; Formighieri, A.; Santos, C.A.N.; Ferreira, M.A.D.; Figueiredo, E.O.; Ferreira, E.J.L. Individual Tree Detection and Species Classification of Amazonian Palms Using UAV Images and Deep Learning. *Forest Ecology and Management* **2020**, *475*, 118397, doi:10.1016/j.foreco.2020.118397.

45. Guo, Z.; Feng, C.-C. Using Multi-Scale and Hierarchical Deep Convolutional Features for 3D Semantic Classification of TLS Point Clouds. *International Journal of Geographical Information Science* **2020**, *34*, 661–680, doi:10.1080/13658816.2018.1552790.

46. LeCun, Y.; Bengio, Y.; Hinton, G. Deep Learning. *Nature* **2015**, *521*, 436–444, doi:10.1038/nature14539.

47. Bejiga, M.; Zeggada, A.; Nouffidj, A.; Melgani, F. A Convolutional Neural Network Approach for Assisting Avalanche Search and Rescue Operations with UAV Imagery. *Remote Sensing* **2017**, *9*, 100, doi:10.3390/rs9020100.

48. Wang, H.; Zhang, L.; Luo, H.; He, J.; Cheung, R.W.M. AI-Powered Landslide Susceptibility Assessment in Hong Kong. *Engineering Geology* **2021**, *288*, 106103, doi:10.1016/j.enggeo.2021.106103.

49. Murray, J.; Sargent, I.; Holland, D.; Gardiner, A.; Dionysopoulou, K.; Coupland, S.; Hare, J.; Zhang, C.; Atkinson, P.M. opportunities for machine learning and artificial intelligence in national mapping agencies: enhancing ordnance survey workflow. *Int. Arch. Photogramm. Remote Sens. Spatial Inf. Sci.* **2020**, *XLIII-B5-2020*, 185–189, doi:10.5194/isprs-archives-XLIII-B5-2020-185-2020.

50. Centraal Bureau voor de Statistiek StatLine - Renewable electricity; production and capacity Available online: https://opendata.cbs.nl/#/CBS/en/dataset/82610ENG/table (accessed on 3 June 2021).

51. MEA Climate Policy - Climate Change - Government.Nl Available online: https://www.government.nl/topics/climate-change/climate-policy (accessed on 3 June 2019).

52. RES Nationaal Programma Regionale Energiestrategie Available online: https://www.regionale-energiestrategie.nl/default.aspx (accessed on 8 June 2021).

53. Centraal Bureau voor de Statistiek Slim zonnestroom in kaart brengen Available online: https://www.cbs.nl/nl-nl/onze-diensten/innovatie/project/slim-zonnestroom-in-kaart-brengen (accessed on 3 June 2019).

54. Stowell, D.; Kelly, J.; Tanner, D.; Taylor, J.; Jones, E.; Geddes, J.; Chalstrey, E. A Harmonised, High-Coverage, Open Dataset of Solar Photovoltaic Installations in the UK. *Sci Data* **2020**, *7*, 394, doi:10.1038/s41597-020-00739-0.

55. Malof, J.M.; Bradbury, K.; Collins, L.M.; Newell, R.G. Automatic Detection of Solar Photovoltaic Arrays in High Resolution Aerial Imagery. *Applied Energy* **2016**, *183*, 229–240, doi:10.1016/j.apenergy.2016.08.191.

56. Jilge, M.; Heiden, U.; Habermeyer, M.; Mende, A.; Juergens, C. Detecting Unknown Artificial Urban Surface Materials Based on Spectral Dissimilarity Analysis. **2017**, 20.

57. Malof, J.M.; Collins, L.; Bradbury, K. A Deep Convolutional Neural Network, with Pre-Training, for Solar Photovoltaic Array Detection in Aerial Imagery. *2017 IEEE International Geoscience and Remote Sensing Symposium (IGARSS)* **2017**, doi:10.1109/IGARSS.2017.8127092.

58. Puttemans, S.; van Ranst, W.; Goedeme, T. Detection of Photovoltaic Installations in RGB Aerial Imaging: A Comparative Study. In Proceedings of the GEOBIA 2016 : Solutions and Synergies; University of Twente Faculty of Geo-Information and Earth Observation (ITC): Enschede, Netherlands, September 15 2016.

59. Salamanca, S.; Merchán, P.; García, I. On the Detection of Solar Panels by Image Processing Techniques.; July 2017; p. 7.

60. Osinga, D. *Deep Learning Cookbook: Practical Recipes to Get Started Quickly*; First Edition.; O'Reilly: Beijing, Boston, Farnham, Sebastopol, Tokyo, 2018; ISBN 978-1-4919-9584-6.

61. Patterson, J.; Gibson, A. *Deep Learning: A Practitioner's Approach*; First edition.; O'Reilly: Sebastopol, CA, 2017; ISBN 978-1-4919-1425-0.

62. Yuan, J.; Yang, H.-H.L.; Omitaomu, O.A.; Bhaduri, B.L. Large-Scale Solar Panel Mapping from Aerial Images Using Deep Convolutional Networks. In Proceedings of the 2016 IEEE International Conference on Big Data (Big Data); IEEE: Washington DC,USA, December 2016; pp. 2703–2708.

63. Camilo, J.; Wang, R.; Collins, L.M.; Bradbury, K.; Malof, J.M. Application of a Semantic Segmentation Convolutional Neural Network for Accurate Automatic Detection and Mapping of Solar Photovoltaic Arrays in Aerial Imagery. *arXiv preprint arXiv:1801.04018* **2018**.

64. Castello, R.; Roquette, S.; Esguerra, M.; Guerra, A.; Scartezzini, J.-L. Deep Learning in the Built Environment: Automatic Detection of Rooftop Solar Panels Using

Convolutional Neural Networks. *J. Phys.: Conf. Ser.* **2019**, *1343*, 012034, doi:10.1088/1742-6596/1343/1/012034.

65. Hou, X.; Wang, B.; Hu, W.; Yin, L.; Wu, H. SolarNet: A Deep Learning Framework to Map Solar Power Plants in China from Satellite Imagery. *arXiv preprint arXiv:1912.03685* **2019**.

66. Yu, J.; Wang, Z.; Majumdar, A.; Rajagopal, R. DeepSolar: A Machine Learning Framework to Efficiently Construct a Solar Deployment Database in the United States. *Joule* **2018**, *2*, 2605–2617, doi:10.1016/j.joule.2018.11.021.

67. De Jong, T.; Bromuri, S.; Chang, X.; Debusschere, M.; Rosenski, N.; Schartner, C.; Strauch, K.; Boehmer, M.; Curier, L. Monitoring Spatial Sustainable Development: Semi-Automated Analysis of Satellite and Aerial Images for Energy Transition and Sustainability Indicators. *arXiv:2009.05738 [cs]* **2020**.

68. Wu, A.N.; Biljecki, F. Roofpedia: Automatic Mapping of Green and Solar Roofs for an Open Roofscape Registry and Evaluation of Urban Sustainability. *Landscape and Urban Planning* **2021**, *214*, 104167, doi:10.1016/j.landurbplan.2021.104167.

69. Janowicz, K.; Gao, S.; McKenzie, G.; Hu, Y.; Bhaduri, B. GeoAI: Spatially Explicit Artificial Intelligence Techniques for Geographic Knowledge Discovery and Beyond. *International Journal of Geographical Information Science* **2020**, *34*, 625–636, doi:10.1080/13658816.2019.1684500.

70. Beeldmateriaal Nederland Aerial Imagery Available online: https://www.beeldmateriaal.nl/voorjaarsvlucht (accessed on 23 August 2021).

71. Haala, N. Multiray Photogrammetry and Dense Image Matching. *Photogrammetric Week 2011* **2011**, 185–195.

72. Haala, N.; Cavegn, S. High density aerial image matching: state-of-the-art and future prospects. *Int. Arch. Photogramm. Remote Sens. Spatial Inf. Sci.* **2016**, *XLI-B4*, 625–630, doi:10.5194/isprs-archives-XLI-B4-625-2016.

73. Wenzel, K.; Rothermel, M.; Haala, N.; Fritsch, D. SURE-The Ifp Software for Dense Image Matching. *Photogrammetric Week 2013* **2013**, 59–70.

74. Het Kadaster Over BAG - Kadaster.Nl Available online: https://www.kadaster.nl /zakelijk/registraties/basisregistraties/bag/over-bag (accessed on 20 June 2021).

75. Het Kadaster TOPNL - Land Registry.Nl Available online: https://www.kadaster.nl /zakelijk/producten/geo-informatie/topnl (accessed on 20 June 2021).

76. Iglovikov, V.; Shvets, A. TernausNet: U-Net with VGG11 Encoder Pre-Trained on ImageNet for Image Segmentation. *arXiv:1801.05746 [cs]* **2018**.

77. Iglovikov, V. *Ternaus/TernausNet*; 2021;

78. Maxwell, A.E.; Warner, T.A.; Guillén, L.A. Accuracy Assessment in Convolutional Neural Network-Based Deep Learning Remote Sensing Studies—Part 1: Literature Review. *Remote Sensing* **2021**, *13*, 2450, doi:10.3390/rs13132450.

79. Sokolova, M.; Lapalme, G. A Systematic Analysis of Performance Measures for Classification Tasks. *Information Processing & Management* **2009**, *45*, 427–437, doi:10.1016/j.ipm.2009.03.002.

80. Docker Overview Available online: https://docs.docker.com/get-started/overview/ (accessed on 23 June 2021).

81. Tamram Introduction to Azure Storage - Cloud Storage on Azure Available online: https://docs.microsoft.com/en-us/azure/storage/common/storage-introduction (accessed on 23 June 2021).

82. Centraal Bureau voor de Statistiek; Het Kadaster Verkenning samenhang regionale zonnestroomcijfers Available online: https://www.cbs.nl/nl-nl/achtergrond/2021/04/verkenning-samenhang-regionale-zonnestroomcijfers (accessed on 20 May 2021).

83. Olson, C.L.; Luxembourg, S.L.; Sark, W. van; Sinke, W.C. Is Grid Parity an Indicator for PV Market Expansion in the Netherlands? *Solar Energy* **2014**, *2013*, 2012.

84. Alsema, E.A.; Van Brummelen, M. *Less CO2 by Means of Photovoltaic Energy (PV)*; Netherlands, 1992; p. 93;.

85. Bergsma, G. *Het Potentieel van PV Op Daken En Gevels in Nederland.*; Centrum voor energiebesparing en schone technologie: Delft, 1997;

86. de Noord, M.; Beurskens, L.W.M.; de Vries, H.J. *"Potentials and Costs for Renewable Electricity Generation," ECN, Petten, February, 2004*; ECN: Petten, 2004;

87. Krekel, N.R.; Berdowski, P.A.; Dieren *Duurzame Energie: Een Toekomstverkenning.*; Krekel van der Woerd Wouterse: Rotterdam, 1987;

88. Lemmens, J.; van der Burgt, J.; Bosma, T.; van den Wijngaart, R.; van Bemmel, B.; Koelemeijer, R. *Het potentieel van zonnestroom in de gebouwde omgeving van Nederland*; DNV GL, 2014;

89. CBS CBS StatLine - Energy Consumption Private Dwellings; Type of Dwelling and Regions Available online: http://statline.cbs.nl/Statweb/publication/?DM=SLEN&PA=81528ENG&D1=7&D2=0,2,13,33,74,149,327,380,447&D3=a&LA=EN&HDR=T&STB=G1,G2&VW=T.

90. KEMA *Nationaal Actieplan Zonnestroom*; 2012;

91. Zonatlas GA NAAR DE ZONATLAS | Zonatlas Apeldoorn Available online: http://www.zonatlas.nl/apeldoorn/ontdek-de-zonatlas/.

92. Izquierdo, S.; Rodrigues, M.; Fueyo, N. A Method for Estimating the Geographical Distribution of the Available Roof Surface Area for Large-Scale Photovoltaic Energy-Potential Evaluations. *Solar Energy* **2008**, *82*, 929–939, doi:10.1016/j.solener.2008.03.007.

93. Bergamasco, L.; Asinari, P. Scalable Methodology for the Photovoltaic Solar Energy Potential Assessment Based on Available Roof Surface Area: Application to Piedmont Region (Italy). *Solar Energy* **2011**, *85*, 1041–1055, doi:10.1016/j.solener.2011.02.022.

94. Šúri, M.; Hofierka, J. A New GIS-Based Solar Radiation Model and Its Application to Photovoltaic Assessments. *Transactions in GIS* **2004**, *8*, 175–190, doi:10.1111/j.1467-9671.2004.00174.x.

95. Hofierka, J.; Kaňuk, J. Assessment of Photovoltaic Potential in Urban Areas Using Open-Source Solar Radiation Tools. *Renewable Energy* **2009**, *34*, 2206–2214, doi:10.1016/j.renene.2009.02.021.

96. Karteris, M.; Slini, T.; Papadopoulos, a. M. Urban Solar Energy Potential in Greece: A Statistical Calculation Model of Suitable Built Roof Areas for Photovoltaics. *Energy and Buildings* **2013**, *62*, 459–468, doi:10.1016/j.enbuild.2013.03.033.

97. Kodysh, J.B.; Omitaomu, O. a.; Bhaduri, B.L.; Neish, B.S. Methodology for Estimating Solar Potential on Multiple Building Rooftops for Photovoltaic Systems. *Sustainable Cities and Society* **2013**, *8*, 31–41, doi:10.1016/j.scs.2013.01.002.

98. Redweik, P.; Catita, C.; Brito, M. Solar Energy Potential on Roofs and Facades in an Urban Landscape. *Solar Energy* **2013**, *97*, 332–341, doi:10.1016/j.solener.2013.08.036.

99. Fu, P.; Rich, P.M. Design and Implementation of the Solar Analyst: An ArcView Extension for Modeling Solar Radiation at Landscape Scales. In Proceedings of the Proceedings of the 19th annual ESRI user conference, San Diego, USA; 1999.

100. Nederland, A.H. AHN - Actueel Hoogtebestand Nederland - Homepage Available online: http://www.ahn.nl/index.html.

101. Chaves, A.; Bahill, T.A. Locating Sites for Photovoltaic Solar Available online: http://www.esri.com/news/arcuser/1010/solarsiting.html.

102. Fu, P.; Rich, P.M. Design and Implementation of the Solar Analyst: An ArcView Extension for Modeling Solar Radiation at Landscape Scales. *19th Annual ESRI User Conference* **1999**, 1–24.

103. van Sark, W.; Segaar, P.; Gerrissen, P.; Esmeijer, K.; Moraitis, P.; van den Donker, M.; Emsbroek, G.; Segers, R.; Bosselaar, L. *Opbrengst van Zonnestroomsystemen in Nederland*; 2014;

104. Šúri, M.; Huld, T.A.; Dunlop, E.D.; Ossenbrink, H.A. Potential of Solar Electricity Generation in the European Union Member States and Candidate Countries. *Solar Energy* **2007**, *81*, 1295–1305, doi:10.1016/j.solener.2006.12.007.

105. Araya-Muñoz, D.; Carvajal, D.; Sáez-Carreño, A.; Bensaid, S.; Soto-Márquez, E. Assessing the Solar Potential of Roofs in Valparaíso (Chile). *Energy and Buildings* **2014**, *69*, 62–73, doi:10.1016/j.enbuild.2013.10.014.

106. Chow, A.; Fung, A.; Li, S. GIS Modeling of Solar Neighborhood Potential at a Fine Spatiotemporal Resolution. *Buildings* **2014**, *4*, 195–206, doi:10.3390/buildings4020195.

107. Redweik, P.; Catita, C.; Brito, M. Solar Energy Potential on Roofs and Facades in an Urban Landscape. *Solar Energy* **2013**, *97*, 332–341, doi:10.1016/j.solener.2013.08.036.

108. Litjens, G.B.M.A.; Kausika, B.B.; Worrell, E.; van Sark, W.G.J.H.M. A Spatio-Temporal City-Scale Assessment of Residential Photovoltaic Power Integration Scenarios. *Solar Energy* **2018**, *174*, 1185–1197, doi:10.1016/j.solener.2018.09.055.

109. Izquierdo, S.; Rodrigues, M.; Fueyo, N. A Method for Estimating the Geographical Distribution of the Available Roof Surface Area for Large-Scale Photovoltaic Energy-Potential Evaluations. *Solar Energy* **2008**, *82*, 929–939, doi:10.1016/j.solener.2008.03.007.

110. Kausika, B.B.; Dolla, O.; van Sark, W.G.J.H.M. Assessment of Policy Based Residential Solar PV Potential Using GIS-Based Multicriteria Decision Analysis: A Case Study of Apeldoorn, The Netherlands. *Energy Procedia* **2017**, *134*, 110–120, doi:10.1016/j.egypro.2017.09.544.

111. Santos, T.; Gomes, N.; Freire, S.; Brito, M.C.; Santos, L.; Tenedório, J.A. Applications of Solar Mapping in the Urban Environment. *Applied Geography* **2014**, *51*, 48–57, doi:10.1016/j.apgeog.2014.03.008.

112. Ineichen, P. Validation of Models That Estimate the Clear Sky Global and Beam Solar Irradiance. *Solar Energy* **2016**, *132*, 332–344, doi:10.1016/j.solener.2016.03.017.

113. Gueymard, C.A. Clear-Sky Irradiance Predictions for Solar Resource Mapping and Large-Scale Applications: Improved Validation Methodology and Detailed Performance Analysis of 18 Broadband Radiative Models. *Solar Energy* **2012**, *86*, 2145–2169, doi:10.1016/j.solener.2011.11.011.

114. Wiginton, L.K.; Nguyen, H.T.; Pearce, J.M. Quantifying Rooftop Solar Photovoltaic Potential for Regional Renewable Energy Policy. *Computers, Environment and Urban Systems* **2010**, *34*, 345–357, doi:10.1016/j.compenvurbsys.2010.01.001.

115. Bergamasco, L.; Asinari, P. Scalable Methodology for the Photovoltaic Solar Energy Potential Assessment Based on Available Roof Surface Area: Application to Piedmont Region (Italy). *Solar Energy* **2011**, *85*, 1041–1055, doi:10.1016/j.solener.2011.02.022.

116. Choi, Y.; Rayl, J.; Tammineedi, C.; Brownson, J.R.S. PV Analyst: Coupling ArcGIS with TRNSYS to Assess Distributed Photovoltaic Potential in Urban Areas. *Solar Energy* **2011**, *85*, 2924–2939, doi:10.1016/j.solener.2011.08.034.

117. Lee, M.; Hong, T.; Jeong, J.; Jeong, K. Development of a Rooftop Solar Photovoltaic Rating System Considering the Technical and Economic Suitability Criteria at the Building Level. *Energy* **2018**, *160*, 213–224, doi:10.1016/j.energy.2018.07.020.

118. Nguyen, H.T.; Pearce, J.M. Estimating Potential Photovoltaic Yield with r.Sun and the Open Source Geographical Resources Analysis Support System. *Solar Energy* **2010**, *84*, 831–843, doi:10.1016/j.solener.2010.02.009.

119. Melius, J.; Margolis, R.; Ong, S. Estimating Rooftop Suitability for PV: A Review of Methods, Patents, and Validation Techniques. **2013**.

120. Freitas, S.; Catita, C.; Redweik, P.; Brito, M.C. Modelling Solar Potential in the Urban Environment: State-of-the-Art Review. *Renewable and Sustainable Energy Reviews* **2015**, *41*, 915–931, doi:10.1016/j.rser.2014.08.060.

121. Lukač, N.; Špelič, D.; Štumberger, G.; Žalik, B. Optimisation for Large-Scale Photovoltaic Arrays' Placement Based on Light Detection And Ranging Data. *Applied Energy* **2020**, *263*, 114592, doi:10.1016/j.apenergy.2020.114592.

122. Brito, M.C.; Gomes, N.; Santos, T.; Tenedório, J.A. Photovoltaic Potential in a Lisbon Suburb Using LiDAR Data. *Solar Energy* **2012**, *86*, 283–288, doi:10.1016/j.solener.2011.09.031.

123. Gergelova, M.B.; Kuzevicova, Z.; Labant, S.; Kuzevic, S.; Bobikova, D.; Mizak, J. Roof's Potential and Suitability for PV Systems Based on LiDAR: A Case Study of Komárno, Slovakia. *Sustainability* **2020**, *12*, 10018, doi:10.3390/su122310018.

124. Li, Z.; Zhang, Z.; Davey, K. Estimating Geographical PV Potential Using LiDAR Data for Buildings in Downtown San Francisco. *Transactions in GIS* **2015**, *19*, 930–963, doi:10.1111/tgis.12140.

125. Jakubiec, J.A.; Reinhart, C.F. A Method for Predicting City-Wide Electricity Gains from Photovoltaic Panels Based on LiDAR and GIS Data Combined with Hourly Daysim Simulations. *Solar Energy* **2013**, *93*, 127–143, doi:10.1016/j.solener.2013.03.022.

126. Šúri, M.; Hofierka, J. A New GIS-Based Solar Radiation Model and Its Application to Photovoltaic Assessments. *Transactions in GIS* **2004**, *8*, 175–190.

127. About ArcGIS | Mapping & Analytics Software and Services Available online: https://www.esri.com/en-us/arcgis/about-arcgis/overview (accessed on 22 February 2021).

128. Fu, P.; Rich, P.M. Design and Implementation of the Solar Analyst: An ArcView Extension for Modeling Solar Radiation at Landscape Scales. In Proceedings of the Proceedings of the Nineteenth Annual ESRI User Conference; 1999; pp. 1–31.

129. Ramirez Camargo, L.; Zink, R.; Dorner, W. SPATIOTEMPORAL MODELING FOR ASSESSING COMPLEMENTARITY OF RENEWABLE ENERGY SOURCES IN DISTRIBUTED ENERGY SYSTEMS. *ISPRS Annals of Photogrammetry, Remote Sensing and Spatial Information Sciences* **2015**, *II-4/W2*, 147–154, doi:10.5194/isprsannals-II-4-W2-147-2015.

130. ESRI How Solar Radiation Is Calculated—ArcGIS Pro | Documentation Available online: https://pro.arcgis.com/en/pro-app/latest/tool-reference/spatial-analyst/how-solar-radiation-is-calculated.htm (accessed on 8 February 2021).

131. Huang, S.; Fu, P. Modeling Small Areas Is a Big Challenge Available online: http://www.esri.com/news/arcuser/0309/solar.html (accessed on 22 February 2021).

132. Australian Photovoltaic Institute • APVI Solar Maps Available online: http://pv-map.apvi.org.au (accessed on 24 May 2018).

133. Copper, J.K.; Bruce, A. Validation of Methods Used in the APVI Solar Potential Tool.; 2014.

134. Gilman, P.; Dobos, A. *System Advisor Model, SAM 2011.12.2: General Description*; NREL, 2012;

135. Rich, P.M.; Dubayah, R.; Hetrick, W.A.; Saving, S.C. Using Viewshed Models to Calculate Intercepted Solar Radiation: Applications in Ecology. American Society for Photogrammetry and Remote Sensing Technical Papers. In Proceedings of the American Society of Photogrammetry and Remote Sensing; 1994; pp. 524–529.

136. Fu, P. A Geometric Solar Radiation Model with Applications in Landscape Ecology., Department of Geography, University of Kansas: Lawrence, Kansas, USA., 2000.

137. Fu, P.; Rich, P.M. A Geometric Solar Radiation Model with Applications in Agriculture and Forestry. *Computers and Electronics in Agriculture* **2002**, *37*, 25–35, doi:10.1016/S0168-1699(02)00115-1.

138. Fu, P.; Rich, P.M. *The Solar Analyst 1.0 Manual*; Helios Environmental Modeling Institute (HEMI): USA, 2000;

139. KNMI - Koninklijk Nederlands Meteorologisch Instituut Available online: https://www.knmi.nl/home (accessed on 8 February 2021).

140. Velds, C.A.; Hoeven, P.C.T. van der *Zonnestraling in Nederland*; Thieme ; KNMI: Baarn; De Bilt, 1992; ISBN 978-90-5210-140-8.

141. Kausika, B.B.; Moraitis, P.; van Sark, W. Visualization of Operational Performance of Grid-Connected PV Systems in Selected European Countries. *Energies* **2018**, *11*, 1330, doi:10.3390/en11061330.

142. König-Langlo, G.; Sieger, R.; Schmithüsen, H.; Bücker, A.; Richter, F.; Dutton, E.G. *The Baseline Surface Radiation Network and Its World Radiation Monitoring Centre at the Alfred Wegener Institute.*; Germany, 2013; p. 30;.

143. Driemel, A.; Augustine, J.; Behrens, K.; Colle, S.; Cox, C.; Cuevas-Agulló, E.; Denn, F.M.; Duprat, T.; Fukuda, M.; Grobe, H.; et al. Baseline Surface Radiation Network (BSRN): Structure and Data Description (1992–2017). *Earth System Science Data* **2018**, *10*, 1491–1501, doi:https://doi.org/10.5194/essd-10-1491-2018.

144. Knap, W. Basic and Other Measurements of Radiation at Station Cabauw (2020-03) 2020.

145. Home | AHN Available online: https://www.ahn.nl/ (accessed on 22 February 2021).

146. NASA/METI/AIST/Japan Spacesystems And U.S./Japan ASTER Science Team ASTER DEM Product 2001.

147. NASA/METI/AIST/Japan Spacesystems And U.S./Japan ASTER Science Team ASTER Global Digital Elevation Model V003 2019.

148. ESRI What Is ArcPy?—ArcGIS Pro | Documentation Available online: https://pro.arcgis.com/en/pro-app/latest/arcpy/get-started/what-is-arcpy-.htm (accessed on 8 February 2021).

149. van Tiggelen, J. *Assimilation of Satellite Data and In-Situ Data for the Improvement of Global Radiation Maps in the Netherlands*; Royal Netherlands Meteorological Institute (KNMI), 2014;

150. van Heerwaarden, C.C.; Mol, W.B.; Veerman, M.A.; Benedict, I.; Heusinkveld, B.G.; Knap, W.H.; Kazadzis, S.; Kouremeti, N.; Fiedler, S. Record High Solar Irradiance in Western Europe during First COVID-19 Lockdown Largely Due to Unusual Weather. *Commun Earth Environ* **2021**, *2*, 37, doi:10.1038/s43247-021-00110-0.

151. Isabel Santiago; David Trillo Montero; Juan Luna Rodríguez; Isabel Moreno Garcia; Emilio Palacios Garcia Graphical Diagnosis of Performances in Photovoltaic Systems: A Case Study in Southern Spain. *Energies* **2017**, *10*, 1964, doi:10.3390/en10121964.

152. Mayer, D.; Wald, L.; Poissant, Y.; Pelland, S. *Performance Prediction of Grid-Connected Photovoltaic Systems Using Remote Sensing*; International Energy Agency, Report IEA-PVPS T2-07:2008, 2008;

153. Nordmann, T.; Clavadetscher, L.; van Sark, W.; Green, M. *Analysis of Long-Term Performance of PV Systems*; International Energy Agency, 2014;

154. Jahn, U.; Nasse, W. Operational Performance of Grid-Connected PV Systems on Buildings in Germany. *Progress in Photovoltaics: Research and Applications* **2004**, *12*, 441–448, doi:10.1002/pip.550.

155. Huld, T.; Suri, M.; Dunlop, E. A GIS-Based System for Performance Assessment of Solar Energy Systems over Large Geographical Regions. In Proceedings of the Proceeding of Solar 2006 Conference; American Solar Energy Society, 2006.

156. Stegner, C.; Dalsass, M.; Luchscheider, P.; Brabec, C.J. Monitoring and Assessment of PV Generation Based on a Combination of Smart Metering and Thermographic Measurement. *Solar Energy* **2018**, *163*, 16–24, doi:10.1016/j.solener.2018.01.070.

157. Drews, A.; de Keizer, A.C.; Beyer, H.G.; Lorenz, E.; Betcke, J.; van Sark, W.G.J.H.M.; Heydenreich, W.; Wiemken, E.; Stettler, S.; Toggweiler, P.; et al. Monitoring and Remote Failure Detection of Grid-Connected PV Systems Based on Satellite Observations. *Solar Energy* **2007**, *81*, 548–564, doi:10.1016/j.solener.2006.06.019.

158. Mau, S.; Jahn, U. Performance Analysis of Grid-Connected PV Systems. *Proceedings of the 21st EUPVSEC* **2006**, 2676–2680.

159. Moraitis, P.; van Sark, W.G.J.H.M. Operational Performance of Grid-Connected PV Systems.; IEEE, June 2014; pp. 1953–1956.

160. Moraitis, P.; Kausika, B.B.; van Sark, W.G.J.H.M. Visualization of Operational Performance of Grid-Connected PV Systems in Selected European Countries. In Proceedings of the Proceedings of the 42nd IEEE PVSC; IEEE, 2015; pp. 1–3.

161. Solar Log GmbH Available online: https://www.solar-log.com/en/ (accessed on 15 April 2018).

162. SMA Solar Technology AG - Inverter & Photovoltaics Solutions | SMA Solar Available online: https://www.sma.de/en/ (accessed on 15 April 2018).

163. Moraitis, P. Review of the Operational Performance of Grid Connected PV Systems. Master thesis, 2014.

164. Olmo, F.J.; Vida, J.; Foyo, I.; Castro-Diez, Y.; Alados-Arboledas, L. Prediction of Global Irradiance on Inclined Surfaces from Horizontal Global Irradiance. *Energy* **1999**, *24*, 689–704, doi:10.1016/S0360-5442(99)00025-0.

165. IEC 61724 *Photovoltaic System Performance Monitoring—Guidelines for Measurement, Data Exchange and Analysis*; 1998;

166. Tsafarakis, O.; Sinapis, K.; van Sark, W.G.J.H.M. PV System Performance Evaluation by Clustering Production Data to Normal and Non-Normal Operation. *Energies* **2018**, *11*, 977, doi:10.3390/en11040977.

167. Burrough, P.A.; McDonnell, R.A.; Lloyd, C.D. *Principles of Geographical Information Systems*; OUP Oxford, 2015; ISBN 978-0-19-874284-5.

168. What Is GIS? | Geographic Information System Mapping Technology Available online: https://www.esri.com/en-us/what-is-gis/overview (accessed on 15 April 2018).

169. ArcGIS Platform Available online: http://www.esri.com/software/arcgis (accessed on 13 June 2016).

170. Fouad, M.M.; Shihata, L.A.; Morgan, E.I. An Integrated Review of Factors Influencing the Perfomance of Photovoltaic Panels. *Renewable and Sustainable Energy Reviews* **2017**, *80*, 1499–1511.

171. Reich Nils H.; Mueller Bjoern; Armbruster Alfons; Sark Wilfried G. J. H. M.; Kiefer Klaus; Reise Christian Performance Ratio Revisited: Is PR > 90% Realistic? *Progress in Photovoltaics: Research and Applications* **2012**, *20*, 717–726, doi:10.1002/pip.1219.

172. Müller Björn; Hardt Laura; Armbruster Alfons; Kiefer Klaus; Reise Christian Yield Predictions for Photovoltaic Power Plants: Empirical Validation, Recent Advances and Remaining Uncertainties. *Progress in Photovoltaics: Research and Applications* **2015**, *24*, 570–583, doi:10.1002/pip.2616.

173. Tsafarakis, O.; Moraitis, P.; Kausika, B.B.; Velde, H. van der; Hart, S. 't; Vries, A. de; Rijk, P. de; Jong, M.M. de; Leeuwen, H.-P. van; Sark, W. van Three Years Experience in a Dutch Public Awareness Campaign on Photovoltaic System Performance. *IET Renewable Power Generation* **2017**, doi:10.1049/iet-rpg.2016.1037.

174. EU (European Union) 20 20 by 2020: Europe's Climate Change Opportunity. President of the European Commission. Available online: http://europa.eu/rapid/press-release_SPEECH-08-34_en.htm (accessed on 4 August 2016).

175. VROM *Nieuwe energie voor het klimaat - Werkprogramma schoon en zuinig*; Ministy of VROM: The Hague, 2007;

176. Graziano, M.; Gillingham, K. Spatial Patterns of Solar Photovoltaic System Adoption: The Influence of Neighbors and the Built Environment. *Journal of Economic Geography* **2015**, *15*, 815–839, doi:10.1093/jeg/lbu036.

177. PV-magazine *pv magazine*. 2014,.

178. PV-Tech Netherlands Connects over 600MW of PV to Grid by Lucy Woods Available online: http://www.pv-tech.org/news/holland_connects_over_600mw_of_pv_to_grid (accessed on 4 August 2016).

179. Centraal Bureau voor de Statistiek CBS StatLine - Renewable Electricity; Production Capacity Available online: http://statline.cbs.nl/Statweb/publication/?DM=SLNL&PA=82610ned&D1=a&D2=5&D3=23-24&VW=T (accessed on 4 August 2016).

180. SER Summary of Energy Agreement for Sustainable Growth Available online: http://www.ser.nl/~/media/files/internet/talen/engels/2013/energy-agreement-sustainable-growth-summary.ashx (accessed on 4 August 2016).

181. Hägerstrand, T. *The Propagation of Innovation Waves.*; Royal University of Lund: Lund,Sweden, 1952;

182. Rogers, E.M. Diffusion of Innovations. *New York* **1995**, 12.

183. Bass, F.M. A New Product Growth for Model Consumer Durables. *Management science* **1969**, *15*, 215–227.

184. Webber, M. Brown,L.A.1981:Innovation Diffusion: A New Perspective. London: Methuen. *Prog Hum Geogr* **2006**, *30*, 487–489, doi:10.1191/0309132506ph620xx.

185. Rai, V.; Beck, A.L. Public Perceptions and Information Gaps in Solar Energy in Texas. *Environmental Research Letters* **2015**, *10*, 074011, doi:10.1088/1748-9326/10/7/074011.

186. Dietz, T. Narrowing the US Energy Efficiency Gap. *Proceedings of the National Academy of Sciences* **2010**, *107*, 16007–16008.

187. Thaler, R.H.; Sunstein, C.R. *Nudge: Improving Decisions about Health, Wealth, and Happiness.*; Yale University Press, 2008;

188. Rai, V.; Robinson, S.A. Effective Information Channels for Reducing Costs of Environmentally-Friendly Technologies: Evidence from Residential PV Markets. *Environmental Research Letters* **2013**, *8*, 014044.

189. Noll, D.; Dawes, C.; Rai, V. Solar Community Organizations and Active Peer Effects in the Adoption of Residential PV. *Energy Policy* **2014**, *67*, 330–343.

190. Rode, J.; Weber, A. Does Localized Imitation Drive Technology Adoption? A Case Study on Rooftop Photovoltaic Systems in Germany. *Journal of Environmental Economics and Management* **2016**, *78*, 38–48, doi:10.1016/j.jeem.2016.02.001.

191. Bollinger, B.; Gillingham, K. Peer Effects in the Diffusion of Solar Photovoltaic Panels. *Marketing Science* **2012**, *31*, 900–912.

192. Richter, L.-L. Social Effects in the Diffusion of Solar Photovoltaic Technology in the UK. **2013**.

193. Zhang, H.; Vorobeychik, Y.; Letchford, J.; Lakkaraju, K. Data-Driven Agent-Based Modeling, with Application to Rooftop Solar Adoption. In Proceedings of the Proceedings of the 2015 International Conference on Autonomous Agents and Multiagent Systems; International Foundation for Autonomous Agents and Multiagent Systems, 2015; pp. 513–521.

194. Malczewski, J. GIS-based Multicriteria Decision Analysis: A Survey of the Literature. *International Journal of Geographical Information Science* **2006**, *20*, 703–726, doi:10.1080/13658810600661508.

195. Kumar, A.; Dash, M.K. *Fuzzy Optimization and Multi-Criteria Decision Making in Digital Marketing*; IGI Global, 2015; ISBN 978-1-4666-8809-4.

196. Tiwari, M.K.; Banerjee, R. A Decision Support System for the Selection of a Casting Process Using Analytic Hierarchy Process. *Production planning & control* **2001**, *12*, 689–694.

197. Saaty, T.L.; Vargas, L.G. *Models, Methods, Concepts & Applications of the Analytic Hierarchy Process*; Springer Science & Business Media, 2012; Vol. 175;.

198. Kausika, B.B.; Dolla, O.; Folkerts, W.; Siebenga, B.; Hermans, P.; van Sark, W. Bottom-up Analysis of the Solar Photovoltaic Potential for a City in the Netherlands: A Working Model for Calculating the Potential Using High Resolution LiDAR Data. In Proceedings of the Smart Cities and Green ICT Systems (SMARTGREENS), 2015 International Conference on; IEEE, 2015; pp. 1–7.

199. van Sark, W.; Bosselaar, L.; Gerrissen, P.; Esmeijer, K.B.D.; Moraitis, P.; van den Donker, M.; Emsbroek, G.; others Update of the Dutch PV Specific Yield for Determination of PV Contribution to Renewable Energy Production: 25% More Energy! *Proceedings of the 29th EUR-PSEC* **2014**, 4095–4097.

200. Acuto, M. Give Cities a Seat at the Top Table. *Nature* **2016**, *537*, 611–613, doi:10.1038/537611a.

201. Louwen, A.; Sark, W.G.J.H.M.; Faaij, A.P.C.; Schropp, R.E.I. Re-Assessment of Net Energy Production and Greenhouse Gas Emissions Avoidance after 40 Years of Photovoltaics Development. *Nat. Commun* **2016**, *7*, 13728, doi:https://doi.org/10.1038/ncomms13728.

202. Schmidt, O.; Hawkes, A.; Gambhir, A.; Staffell, I. The Future Cost of Electrical Energy Storage Based on Experience Rates. *Nat. Energy* **2017**, *2*, 17110, doi:10.1038/nenergy.2017.110.

203. Hoogvliet, T.; Litjens, G.; Sark, W. Provision of Regulating- and Reserve Power by Electric Vehicle Owners in the Dutch Market. *Appl. Energy* **2017**, *190*, 1008–1019, doi:10.1016/j.apenergy.2017.01.006.

204. Nykvist, B.; Nilsson, M. Rapidly Falling Costs of Battery Packs for Electric Vehicles. *Nat. Climate Change* **2015**, *5*, 329–332, doi:10.1038/nclimate2564.

205. Hawkins, T.R.; Singh, B.; Majeau-Bettez, G.; Strømman, A.H. Comparative Environmental Life Cycle Assessment of Conventional and Electric Vehicles. *J. Indus. Ecol* **2012**, *17*, 53–64, doi:10.1111/j.1530-9290.2012.00532.x.

206. Ajanovic, A.; Haas, R. Driving with the Sun: Why Environmentally Benign Electric Vehicles Must Plug in at Renewables. *Sol. Energy* **2015**, *121*, 169–180, doi:https://doi.org/10.

207. Sijm, J.; Gockel, P.; Joode, J.; Westering, W.; Musterd, M. *The Demand for Flexibility of the Power System in the Netherlands, 2015-2050, Report of Phase 1 of the Flexnet Project*; ECN & Alliander, 2017;

208. Mwasilu, F.; Justo, J.J.; Kim, E.-K.; Do, T.D.; Jung, J.-W. Electric Vehicles and Smart Grid Interaction: A Review on Vehicle to Grid and Renewable Energy Sources Integration. *Renew. Sustain. Energy Rev* **2014**, *34*, 501–516, doi:10.1016/j.

209. European Commission *Best Practices on Renewable Energy Self-Consumption Accompanying*; European Commission: Brussels, 2015;

210. Freitas, S.; Reinhart, C.; Brito, M. Minimizing Storage Needs for Large Scale Photovoltaics in the Urban Environment. *Sol. Energy* **2018**, *159*, 375–389, doi:https://doi.org/10.

211. Luthander, R.; Widén, J.; Nilsson, D.; Palm, J. Photovoltaic Self-Consumption in Buildings: A Review. *Appl. Energy* **2015**, *142*, 80–94, doi:10.1016/j.apenergy.

212. Defaix, P.; Sark, W.; Worrell, E.; Visser, E. Technical Potential for Photovoltaics on Buildings in the EU-27. *Sol. Energy* **2012**, *86*, 2644–2653, doi:10.1016/j.solener.2012.06.007.

213. Hofierka, J.; Kaňuk, J. Assessment of Photovoltaic Potential in Urban Areas Using Open-Source Solar Radiation Tools. *Renewable Energy* **2009**, *34*, 2206–2214, doi:10.1016/j.renene.2009.02.021.

214. Mainzer, K.; Fath, K.; McKenna, R.; Stengel, J.; Fichtner, W.; Schultmann, F. A High-Resolution Determination of the Technical Potential for Residential-Roof-Mounted Photovoltaic Systems in Germany. *Sol. Energy* **2014**, *105*, 715–731, doi:https://doi.org/10.

215. Rodríguez, L.R.; Duminil, E.; Ramos, J.S.; Eicker, U. Assessment of the photovoltaic potential at urban level based on 3d city models: a case study and new methodological approach. *Sol. Energy* **2017**, *146*, 264–275, doi:10.1016/j.solener.2017.

216. Assouline, D.; Mohajeri, N.; Scartezzini, J.-L. Large-Scale Rooftop Solar Photovoltaic Technical Potential Estimation Using Random Forests. *Appl. Energy* **2018**, *217*, 189–211, doi:10.1016/j.apenergy.2018.02.118.

217. Molin, A.; Schneider, S.; Rohdin, P.; Moshfegh, B. Assessing a Regional Building Applied PV Potential – Spatial and Dynamic Analysis of Supply and Load Matching. *Renew. Energy* **2016**, *91*, 261–274, doi:10.1016/j.renene.2016.01.084.

218. Wegertseder, P.; Lund, P.; Mikkola, J.; Alvarado, R.G. Combining Solar Resource Mapping and Energy System Integration Methods for Realistic Valuation of Urban Solar Energy Potential. *Sol. Energy* **2016**, *135*, 325–336, doi:10.1016/j.solener.2016.

219. Bottaccioli, L.; Estebsari, A.; Patti, E.; Pons, E.; Acquaviva, A. A Novel Integrated Real-Time Simulation Platform for Assessing Photovoltaic Penetration Impacts in Smart Grids. *Energy Proc* **2017**, *111*, 780–789, doi:10.1016/j.egypro.2017.03.240.

220. Camargo, L.R.; Zink, R.; Dorner, W.; Stoeglehner, G. Spatio-temporal modeling of roof-top photovoltaic panels for improved technical potential assessment and electricity peak load offsetting at the municipal scale. *Comput., Environ. Urban Syst* **2015**, *52*, 58–69, doi:10.1016/j.compenvurbsys.2015.03.002.

221. Mu, Y.; Wu, J.; Jenkins, N.; Jia, H.; Wang, C. A Spatial–Temporal Model for Grid Impact Analysis of Plug-in Electric Vehicles. *Appl. Energy* **2014**, *114*, 456–465, doi:10.1016/j.apenergy.2013.10.006.

222. Yamagata, Y.; Seya, H. Community-Based Resilient Electricity Sharing: Optimal Spatial Clustering. In Proceedings of the 2013 43rd Annual IEEE/IFIP Conference on Dependable Systems and Networks Workshop (DSN-W). IEEE; 2013.

223. ArcGIS, E.S.R.I. Spatial Analyst 2017.

224. Andrews, R.W.; Stein, J.S.; Hansen, C.; Riley, D. Introduction to the Open Source PV LIB for Python Photovoltaic System Modelling Package. In Proceedings of the 2014 IEEE 40th Photovoltaic Specialist Conference (PVSC). IEEE; 2014.

225. Panasonic Panasonic HIP-225HDE1 2015, Available online: http://www.technosun.com/eu/products/solar-module-SANYO-HIP-225HDE1.php.

226. Enphase Energy, Enphase M215 2015, Available online: https://www.enphase.com/sites/default/files/M215_DS_EN_60Hz.pdf

227. Jordan, D.C.; Kurtz, S.R.; VanSant, K.; Newmiller, J. Compendium of photovoltaic degradation rates. *Prog. Photovolt.: Res. Appl* **2016**, *24*, 978–989, doi:https://doi.org/10.

228. Centraal Bureau voor de Statistiek. *Wijk- en buurtkaart* **2016**.

229. Liander N.V Liander Open data 2016.

230. Stedin Holding N.V. Stedin Verbruiksgegevens, 2016 Available online: https://www.stedin.net/zakelijk/open-data/verbruiksgegevens.

231. Gerdes, J.; Marbus, S.; Boelhouwer, M. *Energietrends 2016*; 2016;

232. Centraal Bureau Statistiek Verkeersprestaties personenauto's, leeftijd uitgebreid, brandstof Available online: http://statline.cbs.nl/StatWeb/publication/?VW=T&DM=&PA=83702NED&D1=a&D2=0&D3=a&D4=a&HD=171009-0949&HDR=T,G3&STB=G1,G2.

233. Munkhammar, J.; Bishop, J.D.; Sarralde, J.J.; Tian, W.; Choudhary, R. Household Electricity Use, Electric Vehicle Home-Charging and Distributed Photovoltaic Power Production in the City of Westminster. *Energy Build* **2015**, *86*, 439–448, doi:https://doi.org/10.

234. Kam, M.; Sark, W. Smart Charging of Electric Vehicles with Photovoltaic Power and Vehicle-to-Grid Technology in a Microgrid; a Case Study. *Appl. Energy* **2015**, *152*, 20–30, doi:10.1016/j.apenergy.2015.04.092.

235. Litjens, G.; Worrell, E.; Sark, W. Assessment of Forecasting Methods on Performance of Photovoltaic-Battery Systems. *Appl. Energy* **2018**, *221*, 358–373, doi:10.1016/j.apenergy.2018.03.154.

236. Hoppmann, J.; Volland, J.; Schmidt, T.S.; Hoffmann, V.H. The Economic Viability of Battery Storage for Residential Solar Photovoltaic Systems – a Review and a Simulation Model. *Renew. Sustain. Energy Rev* **2014**, *39*, 1101–1118, doi:https://doi.org/10.1016/ j.rser.2014.07.068.

237. S.M.A.Solar Technology AG Sunny Boy Storage 2.5 Available online: https://www.sma.de/en/products/battery-inverters/sunny-boy-storage-25.html#Downloads-236248.

238. Tesla Motors Tesla Motors, Inc. Powerwall Product Homepage Available online: http://www.teslamotors.com/nl_NL/powerwall.

239. Truong, C.; Naumann, M.; Karl, R.; Müller, M.; Jossen, A.; Hesse, H. Economics of Residential Photovoltaic Battery Systems in Germany: The Case of Tesla's Powerwall. *Batteries* **2016**, *2*, 14, doi:10.3390/batteries2020014.

240. Litjens, G.; Worrell, E.; Sark, W. Economic Benefits of Combining Self-Consumption Enhancement with Frequency Restoration Reserves Provision by Photovoltaic-Battery Systems. *Appl. Energy* **2018**, *223*, 172–187, doi:10.1016/j.

241. Masson, G.; Kaizuka, I. *Trends 2017 in Photovoltaic Applications*; International Energy Agency; Photovoltaic Power Systems Programme, 2017;

242. Wild-Scholten, M.M. Energy payback time and carbon footprint of commercial photovoltaic systems. *Sol. Energy Mater. Sol. Cells* **2013**, *119*, 296–305, doi:https://doi.org/10.

243. Peters, J.F.; Baumann, M.; Zimmermann, B.; Braun, J.; Weil, M. The Environmental Impact of Li-Ion Batteries and the Role of Key Parameters – a Review. *Renew. Sustain. Energy Rev* **2017**, *67*, 491–506, doi:10.1016/j.rser.2016.08.039.

244. Sociaal-Economische Raad *The Agreement on Energy for Sustainable Growth*; 2015;

245. Centraal Bureau voor de Statistiek Rendementen en CO2-emissie elektriciteitsproductie 2016 2018.

246. Schram, W.L.; Lampropoulos, I.; Sark, W.G. Photovoltaic Systems Coupled with Batteries That Are Optimally Sized for Household Self-Consumption: Assessment of Peak Shaving Potential. *Appl. Energy* **2018**, *223*, 69–81, doi:10.1016/j.apenergy.

247. Litjens, G.; Worrell, E.; Sark, W. Influence of demand patterns on the optimal orientation of photovoltaic systems. *Sol. Energy* **2017**, *155*, 1002–1014, doi:https://doi.org/10.

248. Catita, C.; Redweik, P.; Pereira, J.; Brito, M.C. Extending Solar Potential Analysis in Buildings to Vertical Facades. *Computers & Geosciences* **2014**, *66*, 1–12, doi:10.1016/j.cageo.2014.01.002.

249. Sinapis, K.; Tzikas, C.; Litjens, G.; Donker, M.; Folkerts, W.; Sark, W.; Smets, A. A Comprehensive Study on Partial Shading Response of C-Si Modules and Yield Modeling of String Inverter and Module Level Power Electronics. *Sol. Energy* **2016**, *135*, 731–741, doi:10.1016/j.solener.2016.06.050.

250. Lake, A.; Rezaie, B.; Beyerlein, S. Review of District Heating and Cooling Systems for a Sustainable Future. *Renew. Sustain. Energy Rev* **2017**, *67*, 417–425, doi:https://doi.org/10.

251. Kruitwagen, L.; Story, K.T.; Friedrich, J.; Byers, L.; Skillman, S.; Hepburn, C. A Global Inventory of Photovoltaic Solar Energy Generating Units. *Nature* **2021**, *598*, 604–610, doi:10.1038/s41586-021-03957-7.

252. Kausika, B.B.; Moshrefzadeh, M.; Kolbe, T.H.; Sark, W.V. 3D Solar Potential Modelling and Analysis: A Case Study for the City of Utrecht. In Proceedings of the 32nd European Photovoltaic Solar Energy Conference; 2016.

253. Poggi, F.; Firmino, A.; Amado, M. Shaping Energy Transition at Municipal Scale: A Net-Zero Energy Scenario-Based Approach. *Land Use Policy* **2020**, *99*, 104955, doi:10.1016/j.landusepol.2020.104955.

254. Alhamwi, A.; Medjroubi, W.; Vogt, T.; Agert, C. GIS-Based Urban Energy Systems Models and Tools: Introducing a Model for the Optimisation of Flexibilisation Technologies in Urban Areas. *Applied Energy* **2017**, *191*, 1–9, doi:10.1016/j.apenergy.2017.01.048.

255. Ali, U.; Shamsi, M.H.; Bohacek, M.; Purcell, K.; Hoare, C.; Mangina, E.; O'Donnell, J. A Data-Driven Approach for Multi-Scale GIS-Based Building Energy Modeling for Analysis, Planning and Support Decision Making. *Applied Energy* **2020**, *279*, 115834, doi:10.1016/j.apenergy.2020.115834.

256. García-Ballano, C.J.; Ruiz-Varona, A.; Casas-Villarreal, L. Parametric-Based and Automatized GIS Application to Calculate Energy Savings of the Building Envelope in Rehabilitated Nearly Zero Energy Buildings (NZEB). Case Study of Zaragoza, Spain. *Energy and Buildings* **2020**, *215*, 109922, doi:10.1016/j.enbuild.2020.109922.

257. Pedro, J. Integrating GIS Spatial Dimension into BREEAM Communities Sustainability Assessment to Support Urban Planning Policies, Lisbon Case Study. *Land Use Policy* **2019**, 11.

258. Pick, J.B.; Perry, M.; Rosales, J. Application of GIS to Support Regional Policy for Development of Renewable Energy in Southern California: An Exploratory Case Study Analysis. 37.

259. Dong, E.; Du, H.; Gardner, L. An Interactive Web-Based Dashboard to Track COVID-19 in Real Time. *The Lancet Infectious Diseases* **2020**, *20*, 533–534, doi:10.1016/S1473-3099(20)30120-1.

260. Madakam, S.; Ramaswamy, R.; Tripathi, S. Internet of Things (IoT): A Literature Review. *JCC* **2015**, *03*, 164–173, doi:10.4236/jcc.2015.35021.

261. Lehner, H.; Dorffner, L. Digital GeoTwin Vienna: Towards a Digital Twin City as Geodata Hub. *PFG* **2020**, *88*, 63–75, doi:10.1007/s41064-020-00101-4.

262. Hansen, T. Building a National Spatial Data Infrastructure.; Kehl, Germany.

263. OGC, "Open Geospatial Consortium." https://www.ogc.org/ (accessed Feb. 14, 2021).

264. Biljecki, F.; Ledoux, H.; Stoter, J. An Improved LOD Specification for 3D Building Models. *Computers, Environment and Urban Systems* **2016**, *59*, 25–37, doi:10.1016/j.compenvurbsys.2016.04.005.

Acknowledgements

"No man is an island" and rightly said so. This work wouldn't have been completed without collaboration and support. This dissertation is a journey with many breaks (expected and unexpected), loads of conversations, excited discussions, love and support from family and friends. I thoroughly enjoyed research at Utrecht university and am learning a lot at the Kadaster.

I extend my sincerest gratitude to my supervisor and promoter Wilfried van Sark, for being and bearing with me throughout my long PhD journey. Thank you for your constant support and motivation without which this would not have been possible. I always feel recharged after a conversation with you, my head buzzing with inspiration and ideas.

I started my career at Utrecht university and am happy to have shared memorable moments with my colleagues. A call out to all my colleagues at Copernicus institute who already graduated and are ready to graduate. I really enjoyed working with you all. The PV- Smart Grids team with Atse, Boudewijn. E, Anne, Boudewijn. P, Geert, Panos, Ody, Ioannis, Takek, Wouter, Sara and Nick where I enjoyed many stimulating conversations and working together with you. Ana and Thuy for being good friends and providing support outside of work. Aisha, Siham and Finona, I really enjoyed the funny moments in your office. I am grateful for all the conversations during the coffee breaks and lovely summer lunches and walks with you all.

Special thanks to the management at Kadaster who facilitated in finishing my thesis and to my colleagues at the Geo Expertise Centre. Vincent I really appreciate our exchanges and so call PhD race, it reminded me of my days at the university. Iris, Vera, Diede, Peter and Ditmar thank you for the flexibility, freedom and taking things off my plate especially when I needed time to focus on our paper. Special thanks to Vera for going the extra mile in helping me with my thesis translations and

helping me settle in the organization explaining things in English when the Dutch meetings went too fast.

Finally, but the most importantly, I owe this to my family. Amma, Papa, and my dear sisters who've always been my pillars of strength and never-ending love. To my dear husband Swagath for his encouragement, push and love. Although, his incessant trails to wake me up early in the mornings failed, his constant reminders helped to the finish line. Dhruv, my little star, who can take my stress away with a smile and help me to unwind and focus, I love you. I hope to have contributed to a better future for you.

Cheers to the heart that didn't give out and the mind that didn't give up!

About the Author

Bhavya Kausika was born on April 30th, 1989, in Visakhapatnam, India. She obtained her Bachelor of Engineering degree in Geoinformatics from Andhra University in 2011. She then started Masters in Geo-information and Earth Observation Science in a collaboration program from Indian Institute of Remote sensing and ITC, Twente. She graduated with her master's thesis titled "Polarimetric modelling of Lunar Surface for scattering information retrieval using Mini-SAR Data of Chandrayaan-1" in 2013.

In August 2013, she started working as a researcher at the Copernicus institute of sustainable development, Utrecht University. There, she worked on the TKI project "Advanced Solar monitoring" and helped in the initiation of a follow-up project "Advanced Scenario Management". From 2018, she started working as a GIS specialist at the Kadaster, The Netherlands, where she has been part of a team creating innovative geospatial data and techniques. She finds integrating Remote sensing and Earth observation techniques with energy studies challenging and hopes to work closely with governments to develop geo-spatial methods to provide reliable data for sustainable energy transition.

Journal publications

1. Kausika, B.B.; Nijmeijer, D.; Reimerink, I.; Brouwer, P.; Liem, V. GeoAI for Detection of Solar Photovoltaic Installations in the Netherlands. *Energy and AI* **2021**, *6*, 100111, doi:10.1016/j.egyai.2021.100111.

2. Kausika, B.B.; van Sark, W. Calibration and Validation of ArcGIS Solar Radiation Tool for Photovoltaic Potential Determination in the Netherlands. *Energies* **2021**, *14*, 1865, doi:10.3390/en14071865.

3. Litjens, G.B.M.A.; Kausika, B.B.; Worrell, E.; van Sark, W.G.J.H.M. A Spatio-Temporal City-Scale Assessment of Residential Photovoltaic Power Integration Scenarios. *Solar Energy* **2018**, *174*, 1185–1197, doi:10.1016/j.solener.2018.09.055.

4. Kausika, B.B.; Moraitis, P.; van Sark, W. Visualization of Operational Performance of Grid-Connected PV Systems in Selected European Countries. *Energies* **2018**, *11*, 1330, doi:10.3390/en11061330.

5. Moraitis, P.; Kausika, B.; Nortier, N.; van Sark, W. Urban Environment and Solar PV Performance: The Case of the Netherlands. *Energies* **2018**, *11*, 1333, doi:10.3390/en11061333.

6. Tsafarakis, O.; Moraitis, P.; Kausika, B.B.; Velde, H. van der; Hart, S. 't; Vries, A. de; Rijk, P. de; Jong, M.M. de; Leeuwen, H.-P. van; Sark, W. van Three Years Experience in a Dutch Public Awareness Campaign on Photovoltaic System Performance. *IET Renewable Power Generation* **2017**, doi:10.1049/iet-rpg.2016.1037.

7. Kausika, B.B.; Dolla, O.; van Sark, W.G.J.H.M. Assessment of Policy Based Residential Solar PV Potential Using GIS-Based Multicriteria Decision Analysis: A Case Study of Apeldoorn, The Netherlands. *Energy Procedia* **2017**, *134*, 110–120, doi:10.1016/j.egypro.2017.09.544.

Conference publications

1. Litjens, G.; Kausika, B.B.; Worrell, E.; van Sark, W. Spatial Analysis of Residential Combined Photovoltaic and Battery Potential: Case Study Utrecht, the Netherlands. In Proceedings of the 2017 IEEE 44th Photovoltaic Specialist Conference (PVSC); IEEE: Washington, DC, June 2017; pp. 3014–3019 (poster).

2. Kausika, B.B.; Moshrefzadeh, M.; Kolbe, T.H.; Sark, W.V. 3D Solar Potential Modelling and Analysis: A Case Study for the City of Utrecht. In Proceedings of the 32nd European Photovoltaic Solar Energy Conference; 2016.

3. Kausika, B.B.; Dolla, O.; Folkerts, W.; Siebenga, B.; Hermans, P.; Sark, W.G.J.H.M. Bottom-up Analysis of the Solar Photovoltaic Potential for a City in the Netherlands - A Working Model for Calculating the Potential Using High Resolution LiDAR Data. In Proceedings of the Proceedings of the 4th International Conference on Smart Cities and Green ICT Systems; SCITEPRESS - Science and Technology Publications, 2015.

4. Moraitis, P.; Kausika, B.B.; van Sark, W.G.J.H.M. Visualization of Operational Performance of Grid-Connected PV Systems in Selected European Countries. In Proceedings of the Proceedings of the 42nd IEEE PVSC; IEEE, 2015; pp. 1-3.